Instituto Tecnológico de Buenos Aires

Doctoral Thesis

Simulation & Control in Type 1 Diabetes

Author:
Patricio H. Colmegna

Adviser:
Ricardo S. Sánchez Peña, Ph.D.

Jury Members:
Dr. Hernán De Battista
Dr. Jorge Bondía Company
Dr. Marta Basualdo

A thesis submitted in fulfilment of the requirements for the degree of
Doctor del Instituto Tecnológico de Buenos Aires
in the field of Engineering

Buenos Aires, Argentina
2015

Patricio H. Colmegna: Simulation & Control in Type 1 Diabetes. *A thesis submitted in fulfilment of the requirements for the degree of* ***Doctor del Instituto Tecnológico de Buenos Aires*** *in the field of Engineering.*

Buenos Aires, Argentina

This research was supported by Program PRH No. 71 (PICT 290 and PFDT) of the Ministry of Science, Technology and Innovation of Argentina, and since August 2013 by Nuria (Argentina) and Cellex (Spain) Foundations.

A todos los que confiaron en mí...

"Nuestras horas son minutos cuando esperamos saber, y siglos cuando sabemos lo que se puede aprender."

"Our hours are minutes when we hope to know, and centuries when we know what can be learned."

Antonio Machado

INSTITUTO TECNOLÓGICO DE BUENOS AIRES

Abstract

Departamento de Matemática

Centro de Sistemas y Control

Doctor en Ingeniería

Simulation & Control in Type 1 Diabetes

by Patricio H. Colmegna

The study of Type 1 Diabetes has grown exponentially over the years. Thus, a huge number of scientific articles that are focused on this disease can be found. In this thesis, two issues are mainly addressed.

Firstly, the most relevant mathematical models that describe the insulin-glucose dynamics are analysed. Through that analysis, the main features of these models are presented, and their advantages and disadvantages are described. Also, several inconsistencies that appear in previous works are pointed out.

On the other hand, different control algorithms that are aimed towards maintaining the glucose levels in a safe region are studied. The main challenge is to obtain a controller that achieves safe blood glucose control, despite issues like actuator saturation, measurement noise and high inter- and intra-subject variability. Due to the fact that an artificial pancreas scheme involves glucose measurement and insulin infusion through the subcutaneous route, there are delays that make the control problem even more challenging. In addition, in order to minimise the patient self-management of his/her disease, it is assumed that meals are unannounced, i.e., the controller does not receive any warning related to meal times or meal sizes either.

Based on the latter, strategies that involve techniques like $\mathcal{H}_\infty$, and switching of linear parameter varying systems are proposed. For each strategy, the advantages and drawbacks are analysed, and closed-loop performance indices are presented. Furthermore, tests on the complete *in silico* adult cohort of the UVA/Padova metabolic simulator, which has been accepted by the Food and Drug Administration in lieu of animal trials, are included for validation purposes.

INSTITUTO TECNOLÓGICO DE BUENOS AIRES

Resumen

Departamento de Matemática

Centro de Sistemas y Control

Doctor en Ingeniería

Simulation & Control in Type 1 Diabetes

por Patricio H. Colmegna

El estudio de la Diabetes Tipo 1 ha crecido de manera exponencial a lo largo de los años. Así, un basto número de artículos científicos que se centran en esta enfermedad pueden ser hallados. En esta tesis dos cuestiones son abordadas principalmente.

En primer lugar, los modelos matemáticos más relevantes que describen la dinámica insulina-glucosa son analizados. A través de ese análisis, las principales características de estos modelos son presentadas, y sus ventajas y desventajas, descritas. Además, ciertas inconsistencias presentes en la literatura son indicadas.

Por otro lado, diferentes algoritmos de control destinados a mantener la concentración de glucosa dentro de límites seguros son estudiados. El principal desafío es obtener un controlador que alcance un control adecuado de glucosa en sangre, a pesar de cuestiones como la saturación en la actuación, el ruido de medición y la gran variabilidad inter e intrapaciente. Debido a que un esquema de páncreas artificial involucra la medición de glucosa y la inyección de insulina a través de la ruta subcutánea, también existen retardos temporales que hacen al problema de control aún más desafiante. Además, con el fin de minimizar la participación del paciente en el control de su enfermedad, se asume que no existen anuncios de comidas, es decir, que al controlador no se le advierte ni los horarios ni la cantidad de carbohidratos de las mismas.

En base a esto último, estrategias que involucran técnicas como $\mathcal{H}_\infty$ y la conmutación de sistemas lineales de parámetros variantes son estudiadas. Para cada estrategia, sus fortalezas y debilidades son analizadas, e índices de performance a lazo cerrado son presentados. Además, pruebas sobre la base de datos completa de adultos *in silico* del simulador metabólico de UVA/Padova, el cual es aceptado por la Food and Drug Administration en reemplazo de pruebas en animales, son incluidas para validar los algoritmos de control.

Acknowledgements

No duty is more urgent than that of returning thanks.

James Allen

It is difficult to list all the people who have helped me to get to this point. While some of them have been direct participants, others have collaborated perhaps without realising it.

Firstly, I wish to thank my family for its support, and for helping me to never give up despite difficulties. I also wish to thank my girlfriend that with her company makes my life much more better. My friends have been really important as well, helping me to go off duty at opportune moments. Actually, this achievement would have been impossible without all of them.

I am also indebted to Ricardo Sánchez Peña for his guidance, for tolerating my mistakes and for offering me his friendship. In addition, I would like to mention my colleagues Demián García Violini, Alejandro Ghersin and Ignacio Más who, as well as sharing their friendship with me, have helped me to enhance my technical knowledge. Furthermore, I would like to thank Susana Otero who has kindly assisted me with all the administrative issues that researchers seem to never know how to solve.

On the other hand, I would like to mention all the members of *The Doyle Group* that have welcomed and treated me wonderfully during my stay at the University of California, Santa Barbara (UCSB). I wish to especially thank Ravi Gondhalekar, Eyal Dassau and Francis Doyle III with whom I have worked.

Finally, I cannot miss the opportunity of thanking the following institutes that supported this research:

- The *Agencia Nacional de Promoción Científica y Tecnológica* (ANPyCT), of the Argentinian Federal Government, through a PFDT (Proyectos de Formación de Doctores en Áreas Tecnológicas) doctoral fellowship from the PRH (Programa de Recursos Humanos) No. 71.
- Nuria (Argentina) and Cellex (Spain) Foundations, through the financial support of the project: "*Control Automático de Diabetes Mellitus Tipo 1*" since August 2013.

- The Buenos Aires Institute of Technology (ITBA).
- The University of Quilmes (UNQ).

Agradecimientos

No hay deber más urgente que el de saber ser agradecido.

James Allen

Es difícil enumerar a todas aquellas personas que me han ayudado a llegar hasta este punto. Mientras que algunas han sido partícipes directas, otras han colaborado quizás sin darse cuenta.

En primer lugar, quiero agradecer a mi familia por su respaldo y por ayudarme a nunca bajar los brazos a pesar de las dificultades. Además quiero agradecer a mi novia, quien con su compañía hace que mi vida sea mucho mejor. Mis amigos también han sido muy importantes, ayudándome a desconectarme de los problemas en los momentos oportunos. De hecho, sin todos ellos este logro hubiese sido imposible.

Asimismo, estoy en deuda con Ricardo Sánchez Peña por guiarme durante mi tesis, por tolerar mis errores y por ofrecerme su amistad. Me gustaría mencionar también a mis colegas Demián García Violini, Alejandro Ghersin e Ignacio Más, quienes, además de ofrecerme su amistad, me han ayudado a enriquecerme técnicamente. También quisiera agradecer a Susana Otero, quien gentilmente me ha ayudado en todas aquellas cuestiones administrativas que los investigadores pareciera nunca sabemos resolver.

Por otro lado, quisiera mencionar a los integrantes del grupo de Francis Doyle III ("*The Doyle Group*"), quienes durante mi estadía en la Universidad de California, Santa Bárbara (UCSB) me han recibido y tratado excelentemente. Especialmente, quiero agradecer a Ravi Gondhalekar, Eyal Dassau y Francis Doyle III con quienes he trabajado en colaboración.

Por último, no quiero perder la oportunidad de agradecer a las siguientes instituciones que apoyaron esta investigación:

- La Agencia Nacional de Promoción Científica y Tecnológica (ANPyCT) del Ministerio de Ciencia y Tecnología e Innovación Productiva de Argentina, a través de una beca doctoral PFDT (Proyectos de Formación de Doctores en Áreas Tecnológicas) que forma parte del PRH (Programa de Recursos Humanos) No. 71.
- Las fundaciones Nuria (Argentina) y Cellex (España), a través del financiamiento del proyecto "Control Automático de Diabetes Mellitus Tipo 1" desde agosto del 2013.

- El Instituto Tecnológico de Buenos Aires (ITBA).
- La Universidad Nacional de Quilmes (UNQ).

Contents

List of Figures

List of Tables

Abbreviations

ADP	**A**denosine **D**i**P**hosphate
APP	**A**rtificial **P**ancreas **P**roject
ATP	**A**denosine **T**ri**P**hosphate
BW	**B**ody **W**eight
CAD	**C**oronary **H**eart **D**isease
CF	**C**orrection **F**actor
CGM	**C**ontinuous **G**lucose **M**onitoring
CR	**C**arbohydrate **R**atio
CSII	**C**ontinuous **S**ubcutaneous **I**nsulin **I**nfusion
CV	**C**oefficient of **V**ariation
CVGA	**C**ontrol **V**ariability **G**rid **A**nalysis
DCCT	**D**iabetes **C**ontrol and **C**omplications **T**rial
DREAM	**D**iabetes Wi**RE**less **A**rtificial **P**ancreas **C**onsortiu**M**
EGP	**E**ndogenous **G**lucose **P**roduction
FDA	**F**ood and **D**rug **A**dministration
FIR	**F**inite **I**mpulse **R**esponse
GIP	**G**lucose-Dependent **I**nsulinotropic **P**eptide
GLP-1	**G**lucagon-**L**ike **P**eptide-1
GLUT-1	**G**lucose **T**ransporter-1
GLUT-2	**G**lucose **T**ransporter-2
HbA$_{1c}$	**G**lycated **H**aemoglobin
HBGI	**H**igh **B**lood **G**lucose **I**ndex
HD	**H**yperglycaemia **D**etection
IFL	**I**nsulin **F**eedback **L**oop
IIT	**I**ntensive **I**nsulin **T**herapy

IOB	**I**nsulin **O**n **B**oard
JDRF	**J**uvenile **D**iabetes **R**esearch **F**oundation
$\mathbf{K_{ATP}}$	**ATP**-Dependent $\mathbf{K^+}$
LBGI	**L**ow **B**lood **G**lucose **I**ndex
LMI	**L**inear **M**atrix **I**nequality
LPV	**L**inear **P**arameter-**V**arying
LTI	**L**inear **T**ime **I**nvariant
MDI	**M**ultiple **D**aily **I**njections
MPC	**M**odel **P**redictive **C**ontrol
NPH	**N**eutral **P**rotamine **H**agedorn
NSF	**N**oise-**S**pike **F**ilter
OB	**O**ptimal **B**olus
OBT	**O**ptimal **B**olus **T**reatment
ODE	**O**rdinary **D**ifferential **E**quations
PID	**P**roportional **I**ntegral **D**erivative
PVD	**P**eripheral **V**ascular **D**isease
ROC	**R**ate of **C**hange
SGF	**S**avitzky-**G**olay **F**ilter
SM	**S**afety **M**echanism
SMBG	**S**elf-**M**onitoring of **B**lood **G**lucose
SQLF	**S**ingle **Q**uadratic **L**yapunov **F**unction
SSG	**S**witching **S**ignal **G**enerator
T1DM	**T**ype 1 **D**iabetes **M**ellitus
T2DM	**T**ype 2 **D**iabetes **M**ellitus
TDI	**T**otal **D**aily **I**nsulin
UC	**U**nfalsified **C**ontrol
UKPDS	**U**nited **K**ingdom **P**rospective **D**iabetes **S**tudy
ZOH	**Z**ero **O**rder **H**old

Chapter 1

Introduction

1.1 Motivation

Diabetes is one of the most challenging health problems. Scientific evidence reflects an increasing number of cases of diabetes throughout the world, a continued growth in economic burden to both patients and health care systems worldwide, and the existence of several complications that are associated with this disease.

An automatic blood glucose control in insulin dependent patients can improve their life quality, reducing the extremely demanding self-management plan that they need to follow. In addition, this solution can also reduce the health complications associated with this disease, and therefore, the health expenditure on their treatment.

1.2 Diabetes

1.2.1 Diagnosis and Types

Diabetes is a chronic disease that represents one of the main health problems in the world. The criteria for its diagnosis is presented in [9], and it is summarised here in Fig. 1.1.

The majority of cases of diabetes can be classified into two broad categories:

- **Type 1:** Although it usually appears before age 35, it can be developed at any age. It is an autoimmune disease which is characterised by the destruction of the pancreatic

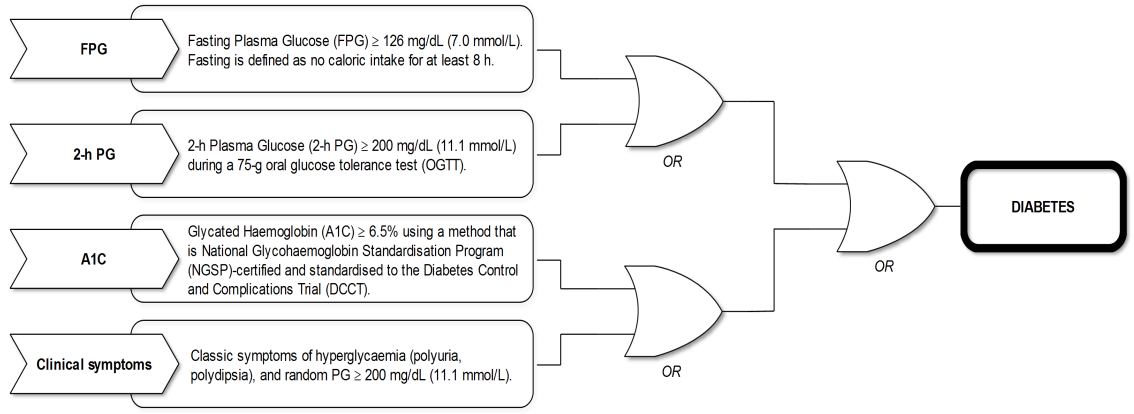

FIGURE 1.1: Diagnostic criteria of diabetes.

β-cells and consequently, insulin deficiency. Therefore, an insulin dependent treatment is essential from the beginning of the disease to prevent dehydration, ketoacidosis, and death.

- **Type 2:** It usually appears after age 35-40, but an increasing number of adolescents and young adults have been developing this disease mainly due to limited physical activity. The capacity to produce insulin does not completely disappear, but the body increases its resistance to it. Patients with Type 2 Diabetes Mellitus (T2DM) are usually treated with oral sulfonlyureas that increase the cell sensitivity to the insulin produced by the pancreas. However, in some cases insulin therapy is often required to reduce the risks of hyperglycaemia.

Nevertheless, there are other forms of diabetes that cannot be clearly classified as type 1 or type 2. For example,

- **Latent Autoimmune Diabetes in the Adult (LADA):** Although it is an autoimmune type of diabetes that is initially non-insulin-requiring, it can progress to insulin dependency at an adult age [10].
- **Monogenic forms of diabetes:** The two main forms are:
  - **Maturity Onset Diabetes in the Young (MODY):** It is a genetically based form of diabetes characterised by impaired insulin secretion at an early age, generally before age 25 [11].

  - **Neonatal Diabetes Mellitus (NDM):** It occurs in the first six months of age, and has a low incidence rate (1 in 100000-500000 newborns). There are two forms: transient and permanent (PNMD), which involves insulin therapy throughout patient's life [12].

- **Gestational Diabetes Mellitus (GDM):** It is diagnosed during pregnancy, and nearly 7% of all pregnancies are affected by this form of diabetes [13].

1.2.2 Statistics and Projections

The International Diabetes Federation (IDF) is an umbrella organisation that has been promoting diabetes research since 1950. Through high-quality studies, the IDF confirms that there is an increasing number of people with diabetes, and that the burden of diabetes in health care costs is enormous. The main estimates that are presented in the sixth edition of the IDF Diabetes Atlas [1] are summarised in Fig. 1.2.

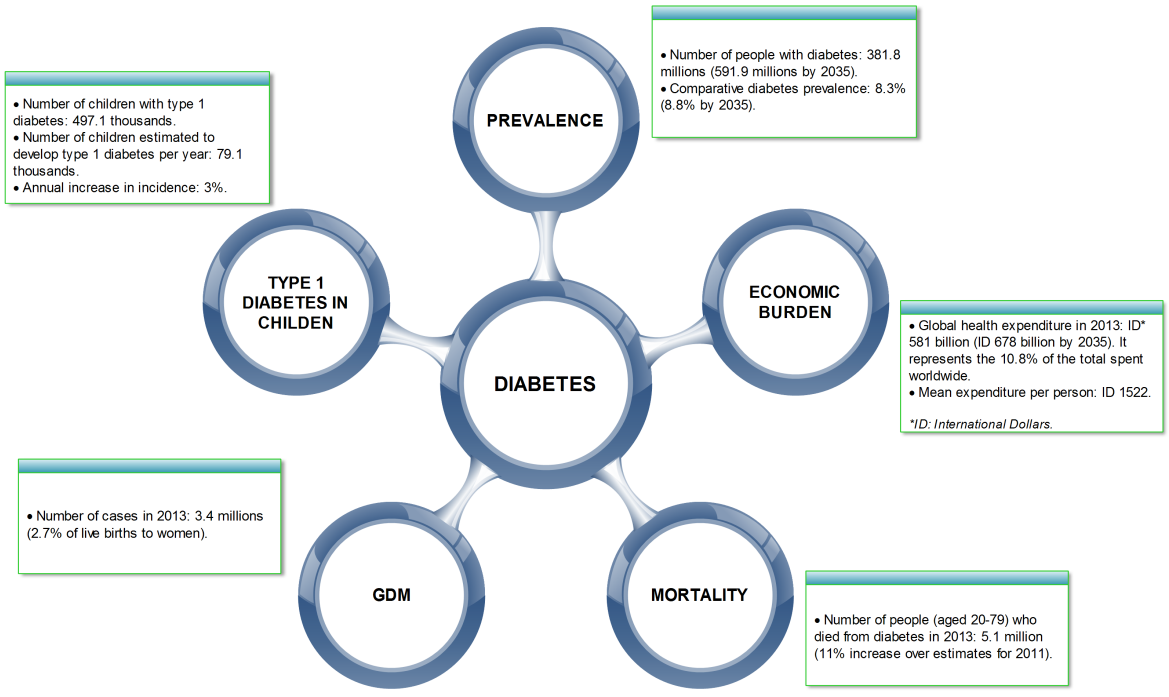

FIGURE 1.2: Global estimates. Source: The sixth edition of the IDF Diabetes Atlas [1].

Some of the most relevant collaborative projects that aim to study the incidence and complications of diabetes in different regions using standardised protocols are the SEARCH for Diabetes in Youth study, the Diabetes Mondiale (DIAMOND) study and the Europe

and Diabetes (EURODIAB) study. As recent estimates from IDF, their registries confirm that the incidence of diabetes is increasing worldwide [14–19].

Regarding T1DM, the average annual increase in incidence in children aged ≤ 14 for the period 1990-1999 was 2.8% [18]. In that study, which was performed by the DIAMOND Project Group, 114 populations in 112 centres in 57 countries all over the world were analysed. The EURODIAB Study Group shows in [19] that the overall annual increase was 3.9% in 17 European countries during 1989-2003, and it is predicted that prevalent cases aged ≤ 15 will rise by 70% in 2020. Registries obtained by the SEARCH study, which monitors diabetes among children and young adults in the United States, present similar statistics. For example, in [17] a 21.1% increase in T1DM was estimated for the period 2001-2009.

As mentioned above, the economic burden of diabetes is huge. Although the health expenditure on diabetes is estimated in several works (see [20,21] for a survey), the difference between the costs of type 1 and type 2 diabetes is not always distinguished. In [22], that difference is presented, showing that indirect costs associated with T1DM in the U.S. represent over 25% of the total diabetes costs in that country. Therefore, considering that just a 5% to 10% of individuals diagnosed with diabetes represent those with T1DM, it can be concluded that there is a vast difference between the economic impact of both types.

1.2.3 Complications

There are several complications associated with diabetes (see Fig. 1.3). A complete description of them can be found in [23–25]. It is well-known that they are related to the persistence of high levels of blood glucose, and that high Glycated Haemoglobin (HbA_{1c}) levels, as well as longer duration of diabetes, increase the risk of developing them.

Basically, diabetes complications can be divided into two major groups:

- **Macrovascular complications:** Coronary Heart Disease (CAD), Peripheral Vascular Disease (PVD), and cerebrovascular disease are the three major types. They are caused predominantly by the development of atherosclerosis that either tightens or shrinks the diameter of the large vessels, such as veins and arteries.

- **Microvascular complications:** Retinopathy, nephropathy, and neuropathy (chronic sensorimotor distal symmetric polyneuropathy and autonomic neuropathies) are the most common types. They affect small vessels, such as capillaries.

As mentioned above, diabetes is associated with an increased risk of both macro- and microvascular complications. For example, in [26] it is estimated that a woman of 20 to 29 years old with T1DM is 45 times more likely to die of ischaemic heart disease than a woman of similar age without diabetes. Regarding microvascular diseases, in the Wisconsin Epidemiologic Study of Diabetic Retinopathy, 86% of blindness was attributable to diabetic retinopathy in the younger-onset group [27]. But fortunately, it has been shown in several surveys that intensive diabetes treatment has beneficial effects on the risk of both complications. For example, in [28] it is shown that intensive therapy reduces the early stages of microvascular complications by 35–76% compared with conventional therapy. In addition, intensive treatment reduces the risk of any cardiovascular disease event by 42% according to [29].

1.2.4 Physiological Regulation of Blood Glucose Levels

The energy obtained via the oxidation of carbohydrates, fats and proteins is used to transform Adenosine Diphosphate (ADP) into Adenosine Triphosphate (ATP). ATP is known as the *molecular unit of currency*, because it is used in muscle contraction, protein and DNA synthesis, and in every physiological process that needs energy. The production of ATP involves different mechanisms such as glycolysis, the Krebs cycle, dehydrogenation, decarboxylation, and the chemiosmotic mechanism. For each molecule of glucose, 38 molecules of ATP are generated as a result of the previous processes, giving a total efficiency of energy transfer of 66%.

In order to achieve good energy balance, the blood concentration of different molecules that are used as energy source has to be regulated. In normal subjects, that process is mainly performed by the pancreas, which is an organ located in the abdomen, and has the following functions:

- Contributes to maintain glucose homeostasis via the secretion of hormones from the islets of Langerhans (endocrine function).

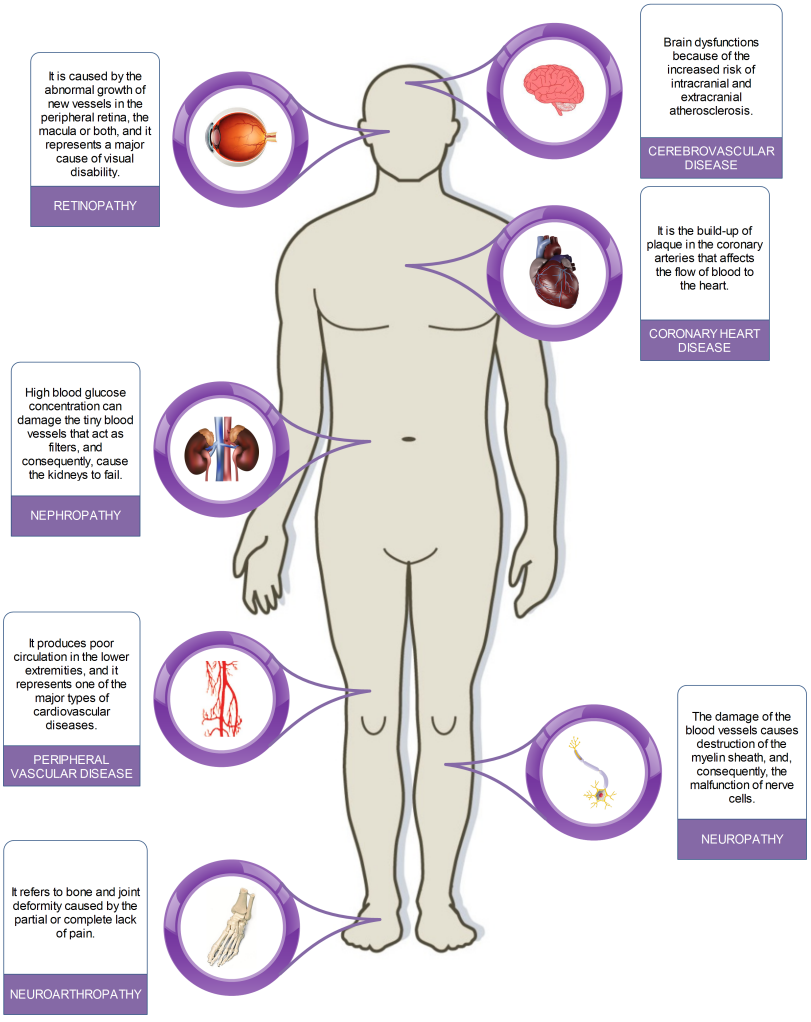

FIGURE 1.3: The main health complications associated with diabetes.

- Digestion as it releases pancreatic juices from the acinar cells into the duodenum (exocrine function).

The pancreas has approximately one million islets of Langerhans of diameter 0.3 mm that are organised around small capillaries into which they release different hormones. Each islet is made up of β-, α-, δ-, and PP-cells that release insulin and amylin, glucagon, somatostatin and pancreatic polypeptide, respectively. Although the endocrine component represents just 1% of the total mass of the pancreas, it has an essential role in regulating the blood glucose. The most important hormones are insulin and glucagon. While insulin lowers blood glucose concentration, glucagon has the opposite effect. A schematic of the feedback control of the blood glucose level is depicted in Fig. 1.4.

After meals, blood glucose concentration increases, and as a consequence, the secretion of insulin starts to increase as well. The stimulation of insulin secretion begins via the release of the incretin hormones Glucagon-like Peptide-1 (GLP-1) and Glucose-dependent Insulinotropic Peptide (GIP) from the L-cells of the small intestine [30, 31]. However, the main effect on insulin secretory response is produced by the glucose-sensing mechanism of pancreatic β-cells [32]. Glucose transport into β-cells is facilitated by high capacity, low affinity Glucose Transporter-2 (GLUT-2) [33]. Once glucose molecules are inside the cell, they are used to produce ATP by cellular respiration. ATP inhibits the activity of ATP-dependent K^+ channels, inducing plasma membrane depolarisation. Consequently, voltage-dependent Ca^{2+} channels are opened, letting calcium enter into the cell, and triggering exocytosis of insulin granules.

On the other hand, glucose is transported into α-cells by low-capacity/high-affinity glucose transporters called Glucose Transporter-1 (GLUT-1). At low glucose levels, the ATP/ADP ratio is low as well. As a result of the moderate activity of ATP-dependent K^+ channels, T-type Ca^{2+} channels are opened, depolarising the plasma membrane, and activating N-type Ca^{2+} channels. Finally, the entrance of calcium stimulates glucagon granule exocytosis [34].

The main effects of both insulin and glucagon are presented in Table 1.1. As shown in that table, they have opposite effects on the blood glucose level and nutrient metabolism. Insulin enhances glucose uptake in peripheral tissues by the expression of glucose transporters from intracellular membrane compartments to the cell surface [35]. In addition, it stimulates glucose storage as glycogen (glycogenesis) in the liver. By contrast, glucagon promotes gluconeogenesis that is the synthesis of glucose from amino and fatty acids, and glycogenolysis that is the breakdown of glycogen to glucose. Due to the fact that the most important actions of insulin and glucagon occur in the liver, the latter has a major role in glucose homeostasis, reducing glucose level fluctuations. In summary, while insulin induces an anabolic state, stimulating glucose disappearance, glucagon promotes a catabolic state, stimulating glucose appearance. As a result of this counterregulatory response, hypo- and hyperglycaemia rarely occur in normal subjects.

Although insulin and glucagon are the most important hormones, there are others that are also involved in blood glucose regulation. For example:

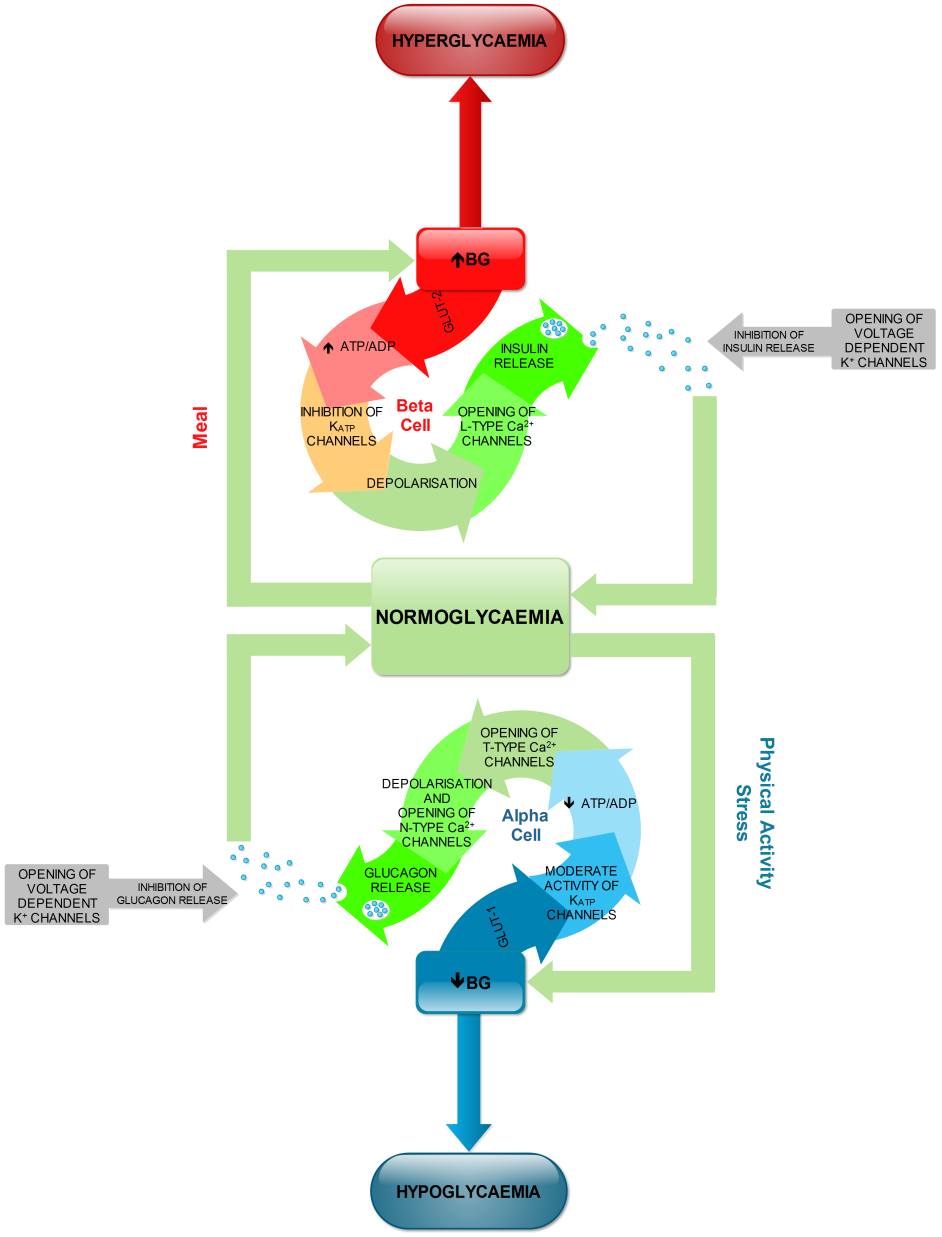

FIGURE 1.4: Glucose homeostasis.

- Amylin, which is cosecreted with insulin by pancreatic β-cells, suppresses glucagon secretion and regulates gastric emptying [36].
- Somatostatin, which is secreted by pancreatic δ-cells, inhibits insulin and glucagon secretion [37].
- Growth hormone, cortisol, norepinephrine and epinephrine increase blood glucose concentration by, for example, decreasing glucose uptake.

Insulin	Glucagon
Increases glucose uptake and metabolism by insulin-sensitive cells.	Stimulates gluconeogenesis and glycogenolysis.
Promotes glycogenesis in skeletal muscle and liver.	Inhibits glycogenesis and glycolysis.
Inhibits glucose production via glycogenolysis and gluconeogenesis.	Promotes lipolysis that increases non-esterified fatty acids and glycerol from adipocytes.
Promotes lipogenesis and therefore, triglyceride synthesis and storage.	Increases amino acid transport into hepatocytes for gluconeogenesis.
Increases amino acid transport into cells, and synthesis of new proteins.	Promotes hepatic ketogenesis.
Inhibits glucagon secretion from pancreatic α-cells.	Stimulates insulin secretion from pancreatic β-cells.

TABLE 1.1: Insulin and glucagon effects on glycaemia and nutrient metabolism.

1.2.5 Diabetes Management: An Overview

Diabetes detection and treatment is a long-standing objective. A timeline that includes some important events in the evolution of diabetes management is depicted in Fig. 1.5.

It is believed that the first documented sign of this condition is presented in an Egyptian papyrus that dates from around 1550 BC. That papyrus, which is also known as the Ebers papyrus in honour of its discoverer, the Egyptologist and novelist Georg Moritz Ebers, mentions people with urine disorders [38]. Since then, more accurate clinical descriptions have been performed, allowing great progress in detecting the disease. One of the first attempts to identify people with diabetes was performed by Tomas Willis, who noted that the urine of people with diabetes was sweet. From that point onwards, various chemical tests were developed, such as the reagent strip presented by Jules Maumené, which turned into black colour when sugar was presented in urine [39]. However, there was not any successful long-term treatment until the discovery of insulin in 1921 by Frederick Banting and his research group at the University of Toronto. The benefits of such a discovery soon arose, because Leonard Thompson, aged 14, became the first person to be successfully treated with insulin injections the very next year.

The early insulins came from bovine and porcine pancreata, and therefore, they had

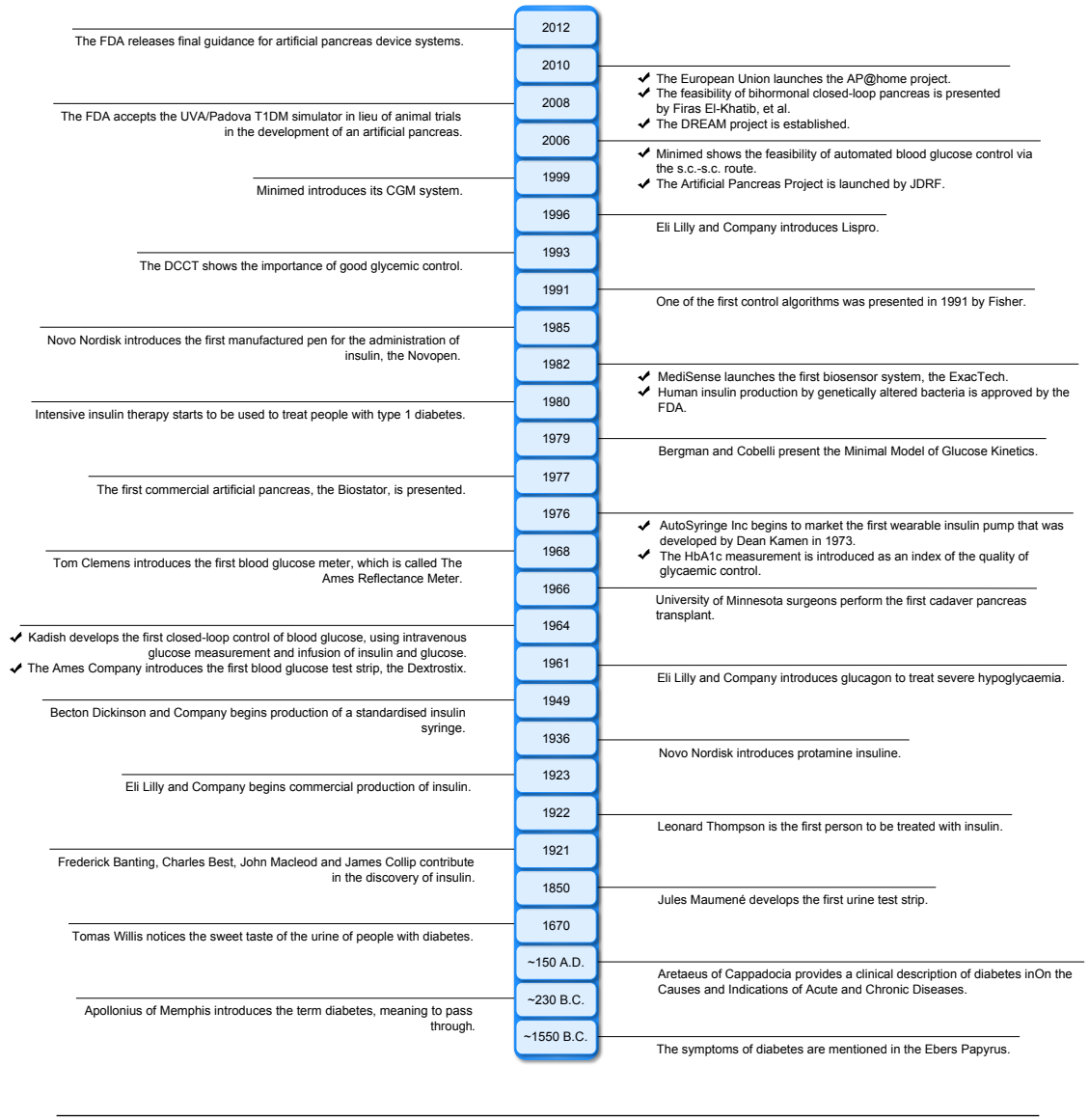

FIGURE 1.5: Evolution of diabetes detection and treatment.

several limitations, such as immunological reactions, lipodystrophy[1], and a short duration of action. In order to develop slower-acting insulins, protamine was added to the insulin molecule along with zinc, allowing the introduction of the first protamine insulin by Novo Nordisk in 1936. This insulin form was later modified to form crystals of protamine and insulin, producing the well-known intermediate-acting Neutral Protamine Hagedorn (NPH) insulin. A step further was achieved when recombinant DNA technology started to be used for human insulin production. This technique, which was approved by the Food and Drug Administration (FDA) in 1982, made it possible to insert the human insulin gene into a bacterial plasmid to produce (regular) human insulin. Then, scientists were able to change

[1]Lipodystrophy is the result of insulin stimulation of fat cell growth.

the onset, peak and duration of insulin action by modifying the structure of the insulin molecule, obtaining rapid- and long-acting insulins. Thus, physiologic insulin patterns, which are characterised by continuous basal release with superimposed surges of insulin after meals [24], could be mimicked more closely by insulin therapy using Multiple Daily Injections (MDI). Different insulin preparations and regimens are presented in Fig. 1.6 and Table 1.2.

After recognising several limitations in the use of urine testing as diabetes monitoring, scientists were focused on developing different blood glucose meters. The latter ones can be classified as follows [39].

- **First generation meters:** They were characterised by the use of dry reagents. The first strip (the Dextrostix), which utilised the glucose oxidase/peroxidase reaction to change its colour depending on the blood glucose value, was introduced by the Ames Company in 1964 [40].

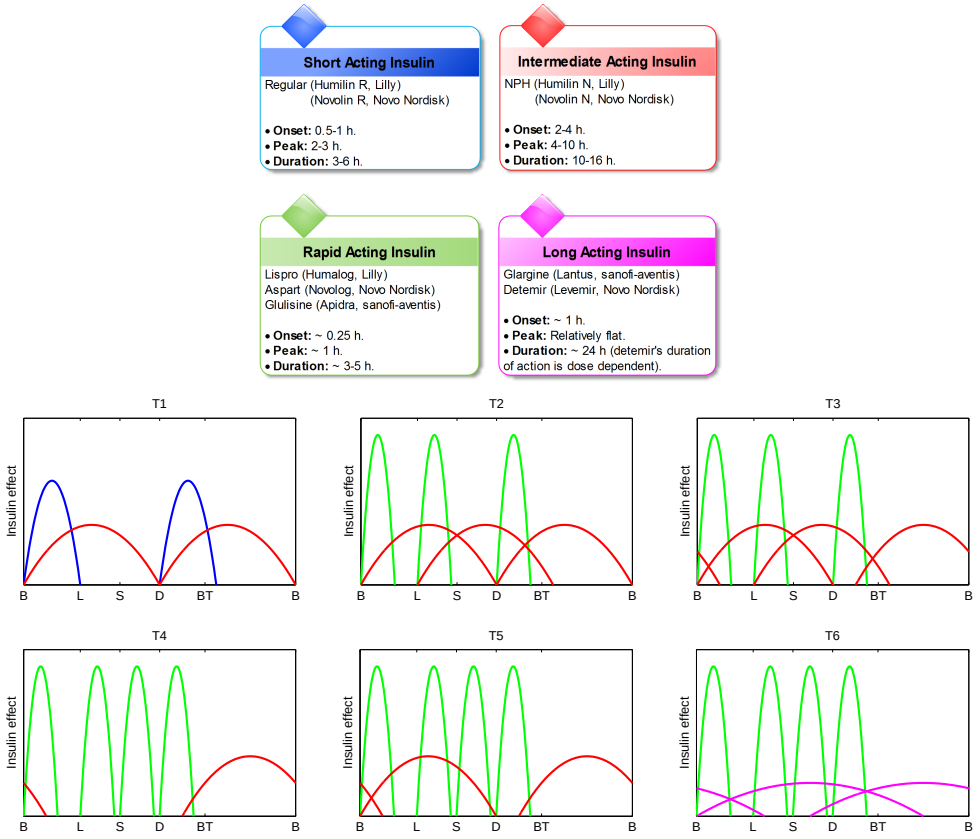

FIGURE 1.6: Insulin preparations and regimens using MDI. B, breakfast; L, lunch; S, snack; D, dinner; BT, bedtime.

T1	**T2**
Two injections of short- or rapid-acting insulin mixed with intermediate-acting insulin. **Pros:** Few number of insulin injections. **Cons:** Difficulty in achieving good glycaemic control (possible nocturnal hypoglycaemia), and limited flexibility to changes in meals and exercise.	Three injections of rapid-acting insulin mixed with intermediate-acting insulin. **Pros:** Improves glycaemic control between lunch and late dinner. **Cons:** Difficulty in achieving good glycaemic control.
T3	**T4**
Three mixed insulin injections before meals, and one injection of intermediate-acting insulin at bedtime. **Pros:** Improves glycaemic control during the night. **Cons:** Demands one more insulin injection than T2.	Rapid-acting insulin injections before meals, and one injection of intermediate-acting insulin at bedtime. **Pros:** Improves glycaemic control during meals. **Cons:** Possible lack of insulin during the last hours before the next meal.
T5	**T6**
Rapid-acting insulin injections before meals, and two injections of intermediate-acting insulin at breakfast and bedtime. **Pros:** Improves glycaemic control during the afternoon. **Cons:** Possible lack of insulin during the last hours before dinner. A third NPH injection at lunch may be necessary.	Rapid-acting insulin injections before meals combined with injections of long-acting basal insulin every 12 (detemir) or 24 (glargine) h. **Pros:** Offers flexibility in meals, and mimics normal insulin secretion.

TABLE 1.2: Insulin regimens using MDI.

- **Second generation meters:** A modified sampling method to reduce the operator participation was one of the main adjustments included in these monitors. The One-Touch meter, which was launched in 1987, was the first device to have these features.
- **Third generation meters:** An amperometric enzyme method was employed to produce a current proportional to the blood glucose concentration, giving rise to the ExacTech, which was introduced in 1987 by MediSense.

In 1976 the HbA_{1c} measurement was introduced as a marker for monitoring the glycaemic control in patients with diabetes [41]. Although it is still widely accepted in clinical practice and research, it only reflects blood glucose average with a temporal resolution of approximately 2-3 months. The latter means that only long-term changes can be detected, ignoring rapid blood glucose variations, such as hypoglycaemic episodes [42].

Blood glucose meters appeared as a solution to that problem. Therefore, they have been continuously evolving in size, functionality, and accuracy in order to be in accordance with recommendations made by the American Diabetes Association (ADA). These improvements allowed for frequent (5 readings per day) and accurate blood glucose measurements, introducing the Self-monitoring of Blood Glucose (SMBG) as a key element in diabetes management [43].

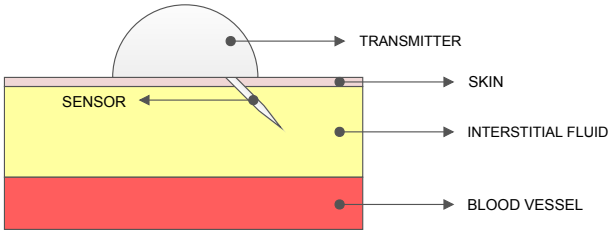

FIGURE 1.7: Measuring glucose levels in the interstitial fluid.

A major change came with the emergence of CGM devices in the 1990s. They include a glucose sensor, a transmitter attached to the sensor, and a receiver. The tiny sensor is inserted under the skin (see Fig. 1.7), and measures the glucose level in the interstitial fluid by means of the glucose oxidase enzyme. After a chain chemical reaction, an electrical signal is generated, and then relayed wirelessly to the receiver in order to display the result approximately every 5 min.

The main disadvantage of this system is that glucose is measured in the interstitium. Therefore, there is an inherent time lag due to glucose diffusion from blood to the interstitial compartment that cannot be eliminated, although a few calibrations with capillary glucose are needed each day. Despite those drawbacks, several works enhance the benefits of CGM in improving metabolic control [44, 45], and new generations of CGMs are rapidly evolving to achieve more reliable glucose measurements.

Insulin delivery devices have experienced several changes since the appearance of the first reusable needles and large glass syringes [46]. Most of those changes have been caused by

various adverse issues associated with the use of syringes, such as social and psychological problems. However, it was not until 1976 that the first wearable insulin pump was introduced by Dean Kamen, giving rise to the Continuous Subcutaneous Insulin Infusion (CSII) therapy [47]. Regarding MDI, it underwent a significant change with the launch of the first insulin pen in 1985. Since then, both CSII pumps and insulin pens have been increasing their accuracy, and including new features. These improvements not only have enhanced patients' quality of life, but also their adherence to Insulin Intensive Therapy (IIT) regimens, which in accordance with the Diabetes Control and Complications (DCCT) and the United Kingdom Prospective Diabetes Study (UKPDS) have beneficial effects on diabetes management [48–50]. However, *there is no such thing as a free lunch*, and IIT is also associated with an increased risk of hypoglycaemia [51].

Implantable pumps into the peritoneal cavity represent another suitable alternative for delivering insulin [52–54]. Their use leads to more physiological plasma insulin profiles, reducing hypoglycaemic events, and restoring glucagon response to hypoglycaemia and exercise [55, 56]. Despite these benefits, they are not widely used because they are invasive and expensive. CSII devices are also costly, but they are far less invasive than implantable pumps. Therefore, both CSII and MDI are still the main options for IIT.

Due to the fact that a T1DM patient is dependent on insulin injections and self-monitoring of blood glucose throughout his/her life, the self-management of this disease is extremely demanding and does not reliably lead to effective glycaemic control. Consequently, the problem of automatically controlling the blood glucose level in T1DM patients is a long standing problem [57–61]. Since the first closed-loop results [62–64], the feasibility of different routes of glucose sensing and insulin infusion have been tested. Although each system has pros and cons [65], the minimally invasive subcutaneous-subcutaneous route is the most widely used nowadays. Thus, an artificial pancreas consists of a CSII pump, a CGM and a control algorithm which closes the loop (see Fig. 1.8). In order to develop fully automated devices, different systems that allow the communication between the components have been implemented for clinical trials [66–68]. Some examples of currently available CGMs and CSII pumps are presented in Table 1.3.

CGM		CSII pump	
Model	**Manufacturer**	**Model**	**Manufacturer**
FreeStyle Navigator®	Abbott Diabetes Care	Paradigm 522/722	Medtronic
Dexcom G4	Dexcom	Accu-Chek® combo	Roche Diagnostics
Guardian® REAL-Time	Medtronic	OneTouch® Ping®	Animas Corporation
Enlite™	Medtronic	DANA Diabecare IISG	Sooil Development
		Amigo®	Nipro Diagnostics
		OmniPod®	Insulet
		T-Slim	Tandem Diabetes Care

TABLE 1.3: Currently available CGMs and CSII pumps.

A few models based upon Ordinary Differential Equations (ODE) have been used for simulation and control design purposes [5,58,69–71]. Among the initial ones we can mention Sorensen's 19th order model [2] and Bergman's 3rd order model [72, 73]. A remarkable event regarding simulation models came with the acceptance of the UVA/Padova metabolic simulator by FDA in lieu of animals trials [74, 75].

One of the first control algorithms was presented in 1991 by Fisher [76] and was based on [73]. Since then, a variety of MPC strategies and Proportional Integral Derivative (PID) controllers have been extensively tested both *in silico* and also in clinical trials [8, 77–82]. Furthermore, other control techniques like adaptive control [83], LPV control [84], $\mathcal{H}_\infty$ control [85–87] and even fuzzy logic theory [88,89] have also been considered. However, both LPV and also $\mathcal{H}_\infty$ control have not been tested in clinical trials yet. Regarding bihormonal approaches, the feasibility of safe blood glucose control with subcutaneous delivery of both insulin and glucagon has been demonstrated in several works [90–92]. In addition, the use of pramlintide to delay gastric emptying and reduce the magnitude of postprandial blood glucose excursions has also been studied [93].

Many of these works have been conducted as part of international projects. Some of these projects are the Artificial Pancreas Project (APP) launched by the Juvenile Diabetes Research Foundation (JDRF) in 2005, the AP@Home Consortium launched by the European Commission in 2010, and the Diabetes wiREless Artificial Pancreas ConsortiuM (DREAM) that was established by 3 diabetes centres in Slovenia, Germany and Israel in 2010.

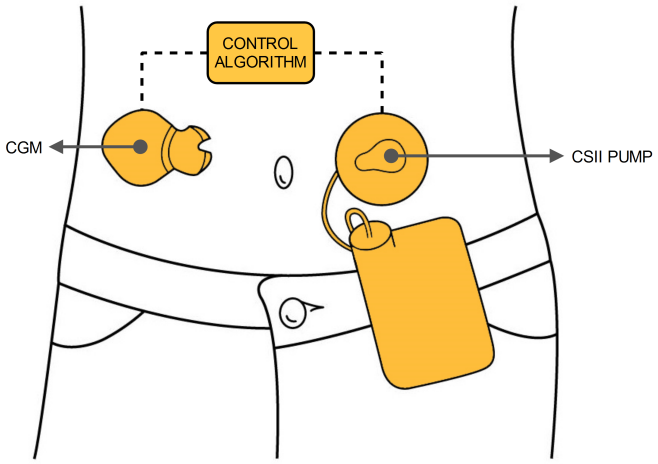

FIGURE 1.8: Closed-loop insulin delivery system.

1.3 Objetives

This thesis aims to design glucose controllers for T1DM, using techniques that are not widely employed in this area. In particular, a special focus is put on the following aspects:

- **State of the art:** Reporting the main advances regarding the development of an artificial pancreas, and analysing the limitations that are involved in its implementation.
- **Simulation models:** Comparing the three main models, and presenting their advantages and disadvantages for controller design and simulation purposes.
- **Controller design:** Synthesising controllers using $\mathcal{H}_\infty$ and LPV techniques.
- ***In silico* validation:** Rigorously testing the proposed control strategies on the complete *in silico* adult cohort of the UVA/Padova metabolic simulator, which has been accepted by the FDA in lieu of animal trials.

1.4 Contributions

Some results that appear in this thesis have been presented previously in the following publications:

Conference Articles

1. Colmegna P., Sánchez Peña R., "Insulin Dependent Diabetes Mellitus Control", in *Actas XIV Reunión de Trabajo en Procesamiento de la Información y Control*, Oro Verde, Entre Ríos, 2011, pp. 13-7. Selected for special issue of Latin American Applied Research.

2. Colmegna P., Sánchez Peña R., "Simulators of Diabetes Mellitus Dynamics", in *Actas XXIII Congreso Argentino de Control Automático*, Buenos Aires, 2012.

3. Colmegna P., Sánchez Peña R., "Personalized Glucose Control Based on Patient Identification", in *Actas XV Reunión de Trabajo en Procesamiento de la Información y Control*, San Carlos de Bariloche, Río Negro, 2013, pp. 397-402.

4. Colmegna P., Sánchez Peña R., "Linear Parameter-Varying Control to Minimize Risks in Type 1 Diabetes", *19th IFAC World Congress*, Cape Town, South Africa, 2014, pp. 9523-7.

Journal Articles

1. Colmegna P. and Sánchez Peña R., "Insulin Dependent Diabetes Mellitus Control", *Latin American Applied Research*, vol. 43, no. 3, pp. 243-8, 2013.

2. Colmegna P. and Sánchez Peña R., "Analysis of three T1DM simulation models for evaluating robust closed-loop controllers", *Computer Methods and Programs in Biomedicine*, vol. 113, no. 1, pp. 371-82, 2014.

3. Sánchez Peña R., Colmegna P. and Bianchi F., "Unfalsified control based on the $\mathcal{H}_\infty$ controller parameterisation", *International Journal of Systems Science*, 2014, doi: 10.1080/00207721.2013.879251.

4. Colmegna P., Sánchez Peña R., Gondhalekar R., Dassau E. and F. Doyle III, "Reducing Risks in Type 1 Diabetes Using $\mathcal{H}_\infty$ control", *IEEE Transactions on Biomedical Engineering*, 2014, doi: 10.1109/TBME.2014.2336772.

There is also a paper in preparation (Colmegna P., Sánchez Peña R., Gondhalekar R., Dassau E. and F. Doyle III, "Switched LPV Glucose Control in Type 1 Diabetes", *IEEE Transactions on Biomedical Engineering*) related to the contents presented in Chapter 5.

Conference Poster

1. Colmegna P. and Sánchez Peña R., "Time-Varying Controllers for Type 1 Diabetes", *6th International Conference on Advanced Technologies & Treatments for Diabetes*, Paris, 2013.

The paper "*Unfalsified control based on the $\mathcal{H}_\infty$ controller parameterisation*" represents the theoretical framework to continue the works [84, 94]. In that sense, an approach to that framework is presented in the aforementioned conference poster. However, the unfalsified control concept was not further studied in this research, because the difficulty of its implementation for the management of blood glucose levels in T1DM patients when some practical issues, such as CGM noise, were included.

1.5 Organisation

This thesis is organised as follows. In Chapter 2, the three main models that describe the glucose-insulin behaviour are presented, pointing out several errors that appear in the literature. In addition, a comparison of those models from the control point of view is included. In Chapter 3, the problem of closing the loop is addressed. For that purpose, closed-loop controllers that regulate the blood glucose concentration are designed via $\mathcal{H}_\infty$ control theory, considering different sources of uncertainty. In the following chapters, the UVA/Padova metabolic simulator is selected to design and test the controllers, due to the fact that the complete version of that simulator has been accepted by the FDA in lieu of animal trials. In Chapter 4, a control scheme that is composed of an $\mathcal{H}_\infty$ controller, an Insulin Feedback Loop (IFL), and a Safety Mechanism (SM) is designed, and later tested on the complete *in silico* adult cohort of the UVA/Padova metabolic simulator. In order to replace the action of the IFL and the SM, a switching robust LPV controller that includes a hyperglycaemia detection algorithm is designed in Chapter 5. As in Chapter 4, tests on the complete UVA/Padova metabolic simulator are performed. Final conclusions and future work are presented in Chapter 6.

Chapter 2

Simulation Models in Type 1 Diabetes

2.1 Motivation

In order to design an automatic controller that may connect a glucose monitor and an insulin pump, a model of the underlying dynamics is generally necessary. To verify the effectiveness of the controller before clinical tests, several *in silico* evaluations should be performed. To this end, a more elaborate dynamic model which includes not only the glucose-insulin behaviour, but also many other practical issues (insulin pump constraints, glucose monitor errors, interstitial-plasma delays) should be implemented as a simulator.

As mentioned previously in Chapter 1, a few models based on ODE have been used for simulation and control design purposes. Many of them are instrumental for patient analysis, like the AIDA freeware available at **http://www.2aida.org/aida/intro.htm** [95], while others are also used for automatic controller design and testing.

The objective of this chapter is to compare the three main models which are used in controller (closed-loop) testing: Sorensen's 19th. order model [2], the model developed by the Universities of Virginia and Padova (UVA/Padova) [74] and the Cambridge model [8]. The two latter ones have been implemented in the form of simulators as well. As a byproduct of this research, several errors in the literature have been found, and are pointed out in order to help the practitioner when programming these models [96].

I wish to thank Dr. Jorge Bondía and Dr. Germán Campetelli for their helpful comments and suggestions which have enhanced the quality of this chapter. I am also grateful to Prof. Hovorka's group in Cambridge for allowing me to use their simulator. Finally, I also wish to thank Dr. Wilinska, who answered all my questions so patiently.

2.2 Sorensen's Model

Sorensen's mathematical model is an explanatory physiological mechanism of the glucose metabolism and its regulation by insulin and glucagon in a normal average man. It considers that three models interact: glucose, insulin and glucagon. With respect to the glucose and insulin models, the body is divided into six compartments: brain, representing the central nervous system; lungs; gut; kidneys; and muscular skeleton and adipose tissue (periphery). As for the glucagon model, a simple one-compartment is employed. As shown in Fig. 2.1, each compartment is composed of three well-mixed spaces[1]: blood capillary, fed by the arterial blood and evacuated by the venous one; interstitial; and intracellular.

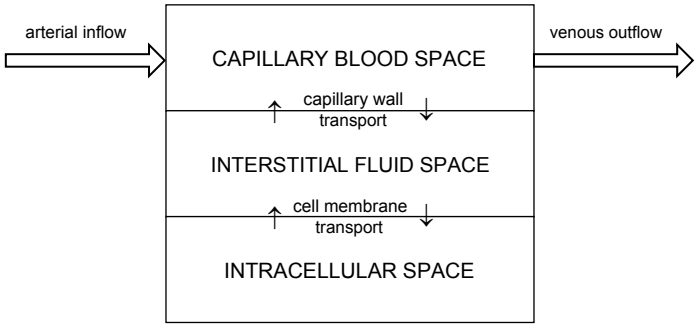

FIGURE 2.1: Representation of a generic compartment. Adapted from [2].

The glucose and insulin model schemes are presented in Figs. 2.2 and 2.3, respectively. Note that the number of spaces of each compartment can be reduced to two or to one, depending on the permeability of both the cell membrane and the capillary wall.

In order to obtain a mathematical representation, a mass balance is performed in each physiological compartment, including any metabolic source and sink which add or remove mass. Regarding metabolic processes, they are represented by hyperbolic tangent functions which are fitted to clinical data. As a consequence, twelve nonlinear ODE are obtained for

[1]The solute concentration is assumed to be uniform.

the glucose (three associated with non-dimensional variables) and glucagon dynamics, and seven linear ones for the insulin. It is important to note that the linearity in the insulin model is obtained when T1DM is considered, i.e. when the pancreatic insulin release rate (Γ_{PIR}) is set to zero. This assumption not only induces linearity, but also decouples the insulin dynamics from the others. In addition, normal basal state concentrations are assumed to create a patient that is effectively controlled through the use of intravenous insulin delivery (Γ_{IVI}).

The equations for the glucose dynamics are:

$$\dot{G}_B^C = \left(G_H^C - G_B^C\right)\frac{q_B}{v_B^C} - \left(G_B^C - G_B^T\right)\frac{v_B^T}{T_B v_B^C} \tag{2.1}$$

$$\dot{G}_B^T = \left(G_B^C - G_B^T\right)\frac{1}{T_B} - \frac{\Gamma_{BU}}{v_B^T} \tag{2.2}$$

$$\dot{G}_H^C = \left(G_B^C q_B + G_L^C q_L + G_K^C q_K + G_P^C q_P - G_H^C q_H - \Gamma_{RBCU}\right)\frac{1}{v_H^C} \tag{2.3}$$

$$\dot{G}_S^C = \left(G_H^C - G_S^C\right)\frac{q_S}{v_S^C} + \frac{\Gamma_{meal}}{v_S^C} - \frac{\Gamma_{SU}}{v_S^C} \tag{2.4}$$

$$\dot{G}_L^C = \left(G_H^C q_A + G_S^C q_S - G_L^C q_L\right)\frac{1}{v_L^C} + \frac{\Gamma_{HGP}}{v_L^C} - \frac{\Gamma_{HGU}}{v_L^C} \tag{2.5}$$

$$\dot{G}_K^C = \left(G_H^C - G_K^C\right)\frac{q_K}{v_K^C} - \frac{\Gamma_{KE}}{v_K^C} \tag{2.6}$$

$$\dot{G}_P^C = \left(G_H^C - G_P^C\right)\frac{q_P}{v_P^C} + \left(G_P^T - G_P^C\right)\frac{v_P^T}{T_P^G v_P^C} \tag{2.7}$$

$$\dot{G}_P^T = \left(G_P^C - G_P^T\right)\frac{1}{T_P^G} - \frac{\Gamma_{PGU}}{v_P^T}. \tag{2.8}$$

Equations for insulin dynamics are:

$$\dot{I}_B^C = \left(I_H^C - I_B^C\right)\frac{Q_B}{V_B^C} \tag{2.9}$$

$$\dot{I}_H^C = \left(I_B^C Q_B + I_L^C Q_L + I_K^C Q_K + I_P^C Q_P - I_H^C Q_H + \Gamma_{IVI}\right)\frac{1}{V_H^C} \tag{2.10}$$

$$\dot{I}_S^C = \left(I_H^C - I_S^C\right)\frac{Q_S}{V_S^C} \tag{2.11}$$

$$\dot{I}_L^C = \left(I_H^C Q_A + I_S^C Q_S - I_L^C Q_L\right)\frac{1}{V_L^C} + \frac{\Gamma_{PIR}}{V_L^C} - \frac{\Gamma_{LC}}{V_L^C} \tag{2.12}$$

$$\dot{I}_K^C = \left(I_H^C - I_K^C\right)\frac{Q_K}{V_K^C} - \frac{\Gamma_{KC}}{V_K^C} \tag{2.13}$$

$$\dot{I}_P^C = \left(I_H^C - I_P^C\right)\frac{Q_P}{V_P^C} + \left(I_P^T - I_P^C\right)\frac{V_P^T}{T_P^I V_P^C} \tag{2.14}$$

$$\dot{I}_P^T = \left(I_P^C - I_P^T\right)\frac{1}{T_P^I} + \frac{\Gamma_{SIA}}{V_P^T} - \frac{\Gamma_{PC}}{V_P^T} \tag{2.15}$$

and the remaining four equations of Sorensen's model are given by:

$$\dot{N} = \left(\Gamma_{PNR} - N\right)\frac{F_{PNC}}{V_N} \tag{2.16}$$

$$\dot{A}_{IHGP} = \frac{1}{25}\left\{1.2088 - 1.138\tanh\left[1.1669\left(\frac{I_L^C}{21.43} - 0.8885\right)\right] - A_{IHGP}\right\} \tag{2.17}$$

$$\dot{A}_{NHGP} = \frac{1}{65}\left[\frac{2.7\tanh\left(0.388N\right) - 1}{2} - A_{NHGP}\right] \tag{2.18}$$

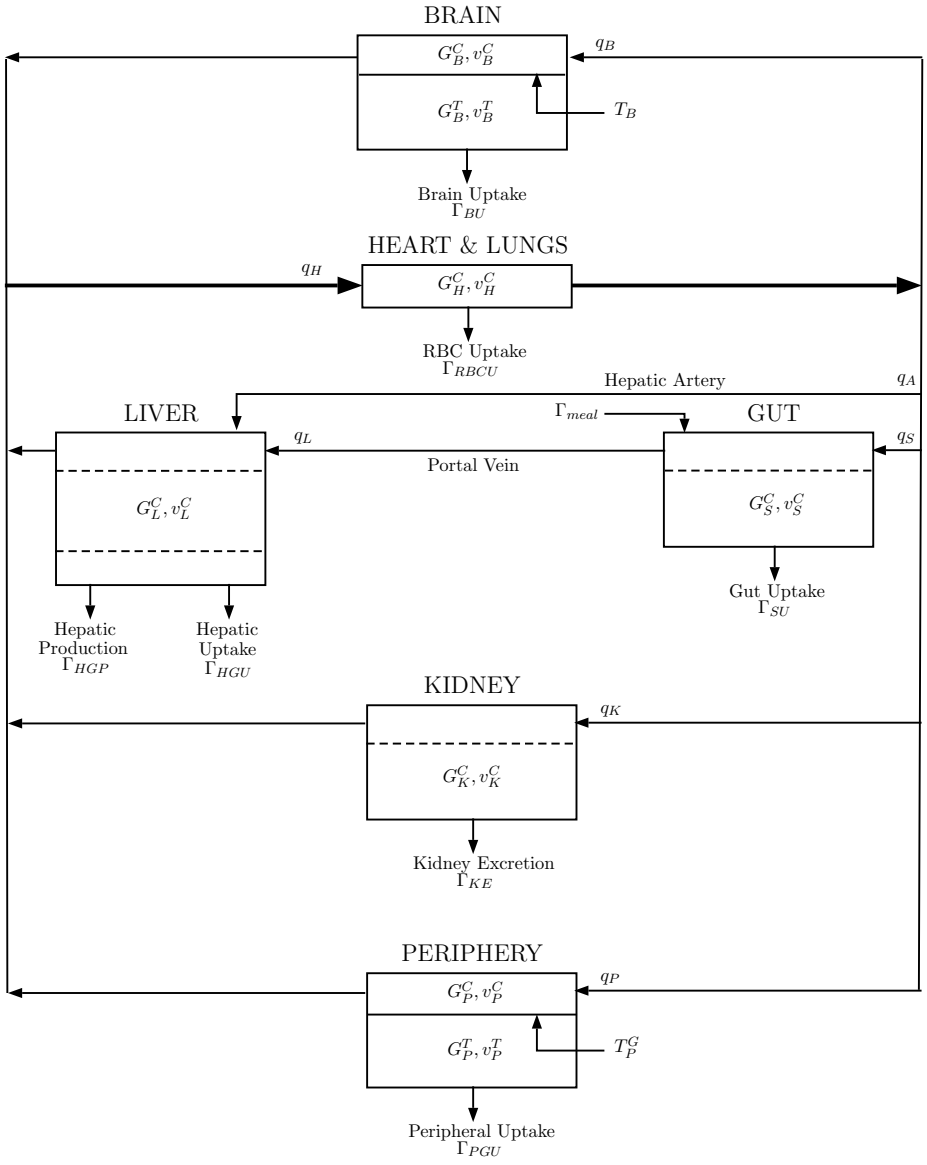

FIGURE 2.2: Block diagram of Sorensen's glucose model. Adapted from [2].

$$\dot{A}_{IHGU} = \frac{1}{25}\left[2\tanh\left(0.549\frac{I_L^C}{21.43}\right) - A_{IHGU}\right]. \tag{2.19}$$

The Γ_i parameters which appear in the equations are as follows: $\Gamma_{BU} = 70$, $\Gamma_{RBCU} = 10$, $\Gamma_{SU} = 20$, $\Gamma_{PIR} = 0$, $\Gamma_{LC} = F_{LC}\left(I_H^C Q_A + I_S^C Q_S + \Gamma_{PIR}\right)$ and

$$\Gamma_{HGU} = 20A_{IHGU}\left\{5.6648 + 5.6589\tanh\left[2.4375\left(\frac{G_L^C}{101} - 1.48\right)\right]\right\} \tag{2.20}$$

$$\Gamma_{HGP} = 155A_{IHGP}\left[2.7\tanh\left(0.388N\right) - A_{NHGP}\right] \times \left\{1.425 - 1.406\tanh\left[0.1699\left(\frac{G_L^C}{101} - 0.4969\right)\right]\right\} \tag{2.21}$$

$$\Gamma_{PGU} = \frac{35G_P^T}{86.81}\left\{7.035 + 6.51623\tanh\left[0.33827\left(\frac{I_P^T}{5.304} - 5.82113\right)\right]\right\}$$

$$\Gamma_{PNR} = \left\{1.3102 - 0.61016\tanh\left[1.0571\left(\frac{I_H^C}{15.15} - 0.46981\right)\right]\right\} \times \left\{2.9285 - 2.095\tanh\left[4.18\left(\frac{G_H^C}{91.89} - 0.6191\right)\right]\right\} \tag{2.22}$$

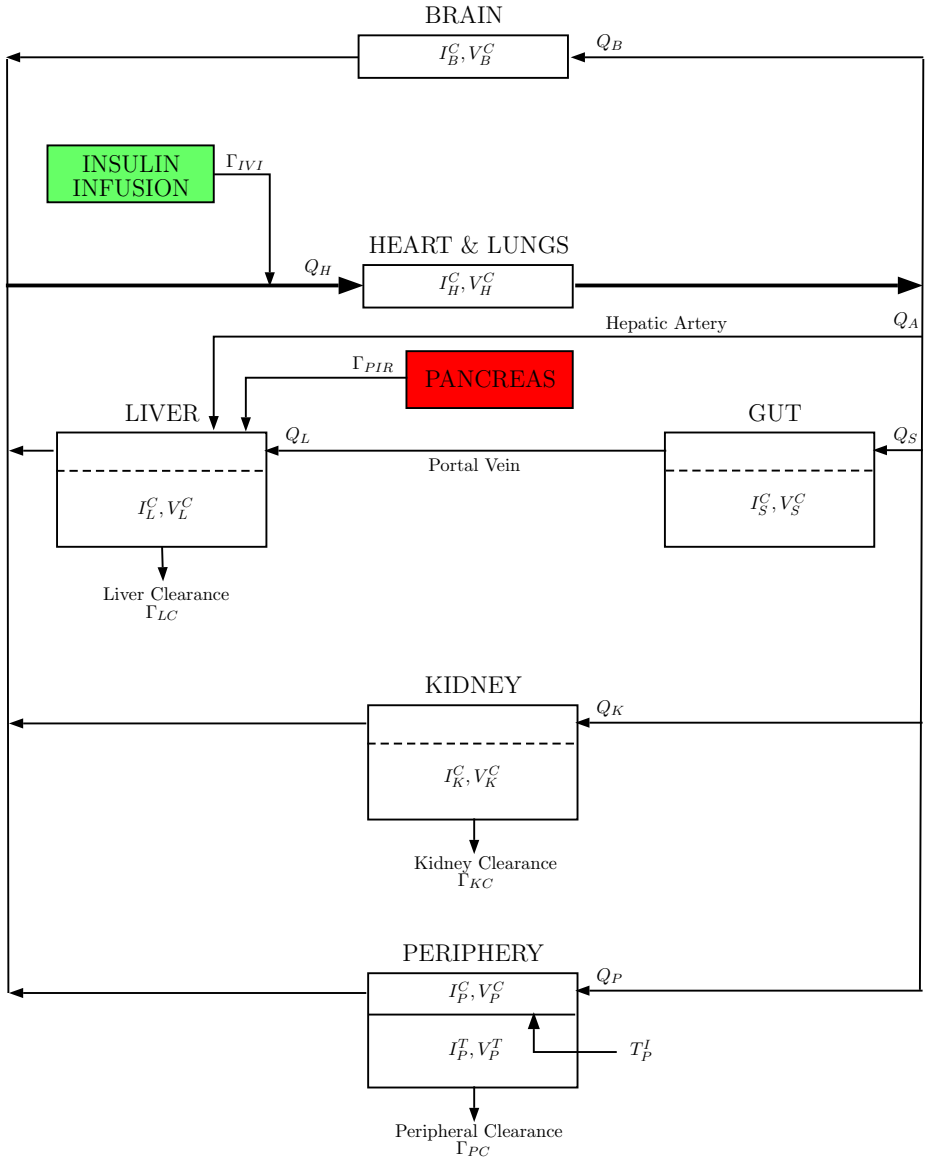

FIGURE 2.3: Block diagram of Sorensen's insulin model. The red and green blocks represent the inputs that are removed and included, respectively, from the normal model to create a T1DM one. Adapted from [2].

$$\Gamma_{PC} = \frac{I_P^T}{\frac{1-F_{PC}}{Q_P F_{PC}} - \frac{T_P^I}{V_P^T}} \tag{2.23}$$

$$\Gamma_{KC} = F_{KC} I_H^C Q_K \tag{2.24}$$

$$\Gamma_{KE} = \begin{cases} 71\left\{1 + \tanh\left[0.11\left(G_K^C - 460\right)\right]\right\} & \text{if } \mathrm{G_K^C} < 460\,\frac{\mathrm{mg}}{\mathrm{dl}} \\ 0.872 G_K^C - 330 & \text{if } \mathrm{G_K^C} \geq 460\,\frac{\mathrm{mg}}{\mathrm{dl}} \end{cases} \tag{2.25}$$

The indices and the model variable and parameter notation in the above equations, which are the same used in [87, 97], are presented in Tables 2.1 and 2.2, respectively. Parameters values are given in Table 2.3.

Indices		
A: Hepatic artery.	B: Brain.	BU: Brain uptake.
C: Capillary space.	G: Glucose.	H: Heart and lungs.
HGP: Hepatic glucose production.	HGU: Hepatic glucose uptake.	I: Insulin.
IHGP: Insulin effect on HGP.	IHGU: Insulin effect on HGU.	IVI: Intravenous insulin infusion.
K: Kidney.	KC: Kidney clearance.	KE: Kidney excretion.
L: Liver.	LC: Liver clearance.	N: Glucagon.
NHGP: Glucagon effect on HGP.	P: Periphery (muscle/adipose tissue).	PC: Peripheral clearance.
PC: Peripheral clearance.	PGU: Peripheral glucose uptake.	PIR: Pancreatic insulin release.
PNC: Pancreatic glucagon clearance.	PNR: Pancreatic glucagon release.	RBCU: Red blood cell uptake.
S: Gut.	SIA: Insulin absorption into blood stream from subcutaneous depot.	SU: Gut uptake.
T: Tissue.		

TABLE 2.1: Indices used in Sorensen's model.

Variable/Parameter	**Unit**
A: Auxiliary equation state.	dimensionless
F: Fractional clearance.	I, dimensionless; N, [L/min]
G: Glucose concentration.	[mg/dl]
I: Insulin concentration.	[mU/l]
N: Glucagon concentration (normalised).	dimensionless
Q: Vascular plasma flow rate.	[L/min]
q: Vascular blood flow rate.	[dl/min]
T: Transcapillary diffusion time constant.	[min]
V: Volume.	[l]
v: Volume.	[dl]
Γ: Metabolic source or sink rate	G, [mg/min]; I, [mU/min]; N, dimensionless

TABLE 2.2: Variables and parameters used in Sorensen's model.

Glucose			**Insulin**			**Glucagon and Γ**		
[dL]	[dL/min]	[min]	[L]	[L/min]	[min]	[L]	[L/min]	dimensionless
$v_B^C = 3.5$	$q_B = 5.9$	$T_B = 2.1$	$V_B^C = 0.26$	$Q_B = 0.45$	$T_P^I = 20$	$V_N = 9.93$	$F_{PNC} = 0.91$	$F_{LC} = 0.4$
$v_B^T = 4.5$	$q_H = 43.7$	$T_P^G = 5.0$	$V_H^C = 0.99$	$Q_H = 3.12$				$F_{KC} = 0.3$
$v_H^C = 13.8$	$q_A = 2.5$		$V_S^C = 0.94$	$Q_A = 0.18$				$F_{PC} = 0.15$
$v_L^C = 25.1$	$q_L = 12.6$		$V_L^C = 1.14$	$Q_L = 0.90$				
$v_S^C = 11.2$	$q_S = 10.1$		$V_K^C = 0.51$	$Q_S = 0.72$				
$v_K^C = 6.6$	$q_K = 10.1$		$V_P^C = 0.74$	$Q_K = 0.72$				
$v_P^C = 10.4$	$q_P = 15.1$		$V_P^T = 6.74$	$Q_P = 1.05$				
$v_P^T = 67.4$								

TABLE 2.3: Parameter values for Sorensen's model.

The glucose absorption model is presented in the original work [2] in Section IV. However, in this analysis, it is considered that Γ_{meal} is defined by the model introduced in [95], which is used by several other authors [87,97–99], as well as in the AIDA simulator. Model equations

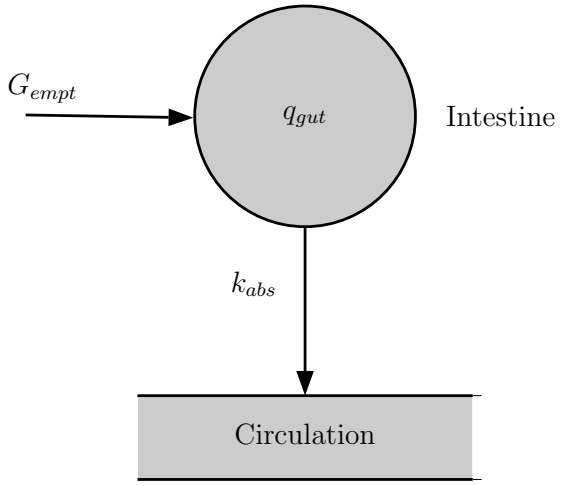

FIGURE 2.4: Lehmann and Deutsch's glucose absorption model. Adapted from [3].

are as follows:

$$\dot{q}_{gut}(t) = -k_{abs} q_{gut}(t) + G_{empt}(t) \tag{2.26}$$

$$\Gamma_{meal}(t) = k_{abs} q_{gut}(t) \tag{2.27}$$

$$T_{max} = [D - V_{max}(T_{up} + T_{down})]/V_{max} \tag{2.28}$$

$$G_{empt}(t) = \begin{cases} \frac{V_{max}}{T_{up}} t, & t < T_{up} \\ V_{max}, & T_{up} \leq t < T_{up} + T_{max} \\ V_{max} - \frac{V_{max}}{T_{down}}(t - T_{up} - T_{max}), & T_{up} + T_{max} \leq t < T_{up} + T_{max} + T_{down} \\ 0, & \text{otherwise} \end{cases} \tag{2.29}$$

where q_{gut} is the amount of glucose in the intestine, k_{abs} is the rate constant for glucose absorption from the gut, G_{empt} is the rate of gastric emptying, V_{max} is the maximum velocity of gastric emptying, D is the ingested glucose dose in mg, and T_{max}, T_{up} and T_{down} are the duration of staying, rising, and dropping periods of G_{empt}, respectively. A schematic of this model is depicted in Fig. 2.4, and parameters values are presented in Table 2.4. Thus, this model assumes that gastric emptying is a trapezoidal time-limited signal with a maximum of 360 mg/min, which inputs a first order filter $1/(60s + 1)$ in order to represent the intestinal absorption. This results in signal Γ_{meal} illustrated in Fig. 2.5 with $T_{up} = T_{down} = 15$ min.

Parameter	**Value**
k_{abs}	$1/60$ min^{-1}
T_{up} and T_{down}	$\begin{cases} 30 \text{ min (default)} & \text{if } D \geq 10^3 \text{ mg} \\ 2D/V_{max} & \text{otherwise} \end{cases}$
V_{max}	360 mg/min

TABLE 2.4: Parameter values for Lehmann and Deutsch's glucose absorption model.

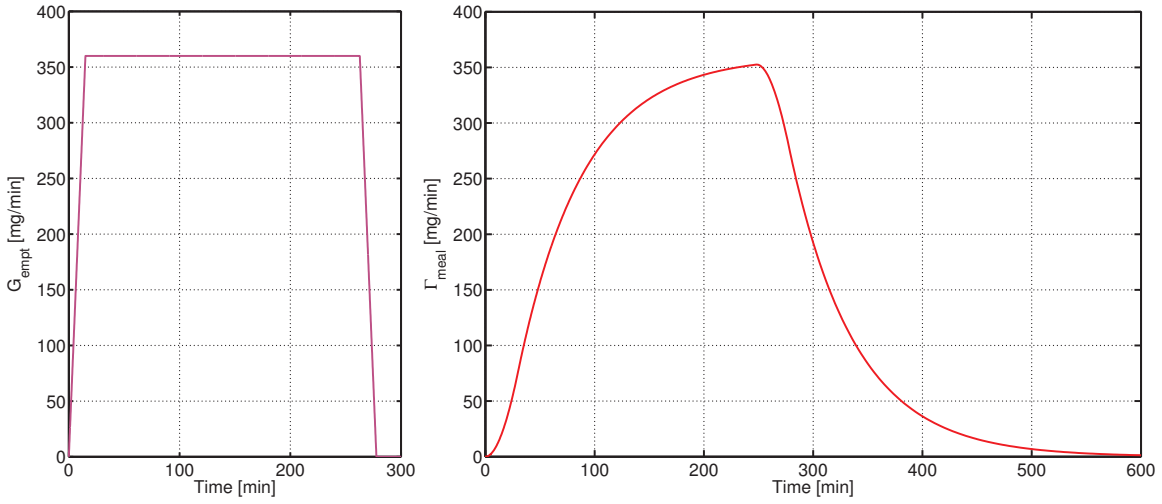

FIGURE 2.5: Glucose emptying as a function of time.

A close analysis of the dynamic equations indicates several inconsistencies with respect to the models presented in previous works (see also [85, 96]). For example in [98], variable A_{IHGU} is confused with A_{IHGP} in Eqn. (2.21). In the same work, there are no parenthesis in Eqn. (2.17) and there are numerical differences in Eqn. (2.25). Also in Eqn. (2.23) the denominator should read $\frac{T_P^I}{V_P^T}$ instead of $\frac{1}{T_P^I V_P^T}$. These last three errors are also present in [87]. In Eqn. (2.15) of [86], instead of V_P^C we find V_P^T, which does not allow its simplification. All these can always be interpreted as typing errors. Nevertheless, there is a common error in all of these works and also in [71] which concerns equation (2.24). The variable which should be there is not I_K^C, but I_H^C instead. This error already appears in the original work [2] in the section where the complete model is presented (pages 213-222), but the correct variable can be identified through the analysis of page 134 over Γ_{KC}, where the article [100] is referenced. The latter can be also ratified by the programming instructions of the model in [2] on page 535.

2.3 UVA/Padova's Model/Simulator

This model is presented in [6] and describes the relation between plasma glucose and insulin concentrations, and glucose and insulin fluxes. To this end, it divides the body into two subsystems: glucose and insulin, each divided into two compartments. The parameter adjustment is based on experiments over 204 normal subjects in order to obtain a non-diabetic model (a T2DM model is also obtained with another database).

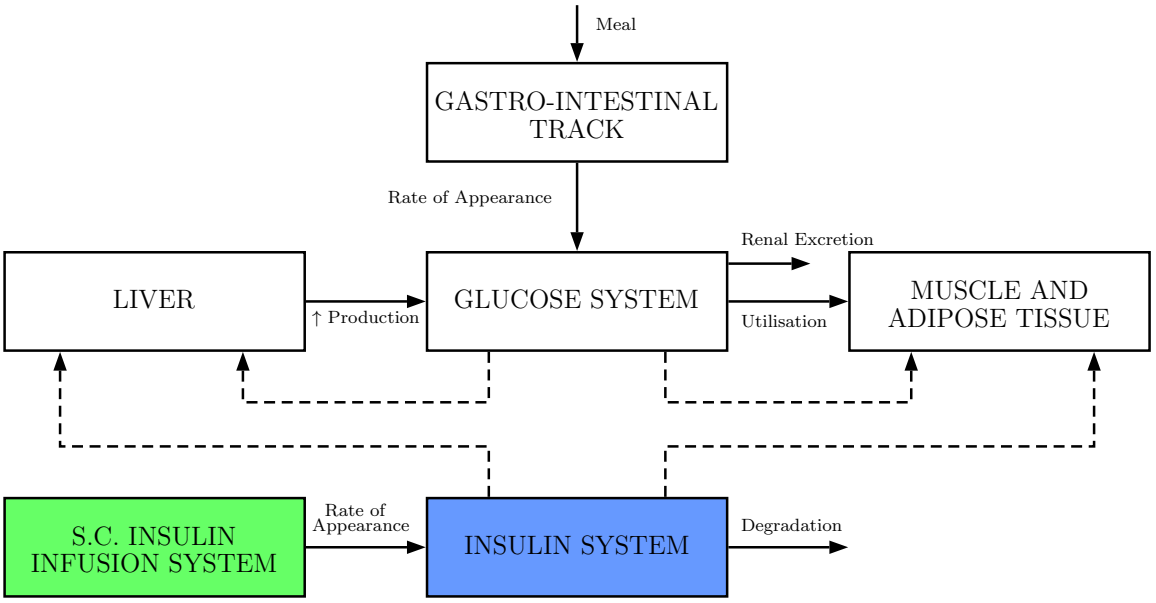

FIGURE 2.6: Scheme of the UVA/Padova glucose-insulin system. The green and blue blocks represent the unit processes that has been included and modified, respectively, regarding the system presented in [4]. Adapted from [5].

The Glucose Insulin Model (GIM) simulator [4], which has been developed by researchers of the universities of Virginia and Padova, adapts the previous non-diabetic model in order to simulate a type 1 diabetic subject which includes a model of subcutaneous insulin kinetics, and a higher endogenous glucose production as shown in Fig. 2.6. The complete model equations used in GIM are as follows.

Glucose subsystem (Fig. 2.7):

$$\dot{G}_p(t) = EGP(t) + Ra(t) - U_{ii}(t) - E(t) - k_1 G_p(t) + k_2 G_t(t) \tag{2.30}$$

$$\dot{G}_t(t) = -U_{id}(t) + k_1 G_p(t) - k_2 G_t(t) \tag{2.31}$$

$$G(t) = \frac{G_p(t)}{V_G} \tag{2.32}$$

$$EGP(t) = k_{p1} - k_{p2} G_p(t) - k_{p3} I_d(t) \tag{2.33}$$

$$U_{ii}(t) = F_{cns} \tag{2.34}$$

$$U_{id}(t) = \frac{V_m(X) G_t(t)}{K_{m0} + G_t(t)} \tag{2.35}$$

$$E(t) = \begin{cases} k_{e1}\left[G_p(t) - k_{e2}\right], & G_p(t) > k_{e2} \\ 0, & G_p(t) \leq k_{e2} \end{cases} \tag{2.36}$$

Insulin subsystem (Fig. 2.8):

$$\dot{I}_\ell(t) = -\left(m_1 + m_3\right) I_\ell(t) + m_2 I_p(t) \tag{2.37}$$

$$\dot{I}_p(t) = -(m_2 + m_4) I_p(t) + m_1 I_\ell(t) + R_i(t) \tag{2.38}$$

$$I(t) = \frac{I_p(t)}{V_I} \tag{2.39}$$

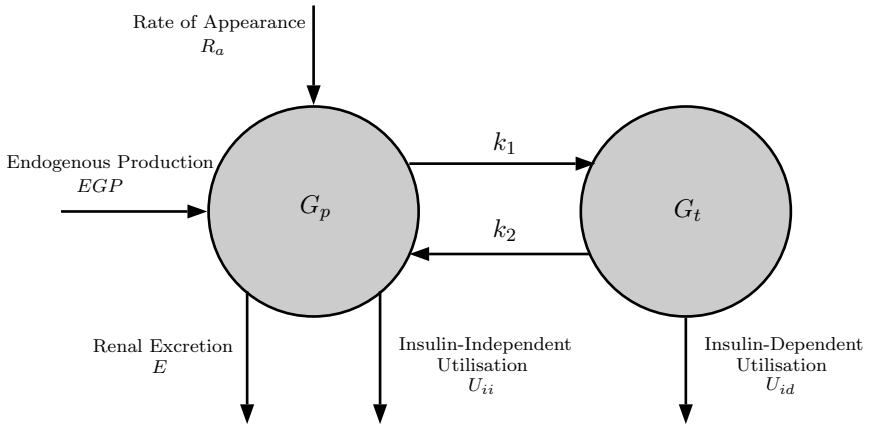

FIGURE 2.7: Block diagram of the UVA/Padova glucose model. Adapted from [6].

$$m_3 = \frac{HE_b m_1}{1 - HE_b} \tag{2.40}$$

$$\dot{I}_1(t) = -k_i \left(I_1 - I\right)(t) \tag{2.41}$$

$$\dot{I}_d(t) = -k_i \left(I_d - I_1\right)(t) \tag{2.42}$$

$$V_{m0} = \frac{(EGP_b - F_{cns})(K_{m0} + G_{tb})}{G_{tb}} \tag{2.43}$$

$$V_m(X) = V_{m0} + V_{mx} X(t) \tag{2.44}$$

$$\dot{X}(t) = -p_{2U} X(t) + p_{2U} \left[I(t) - I_b\right] \tag{2.45}$$

$$\dot{I}_{sc1} = -(k_d + k_{a1}) I_{sc1}(t) + IIR(t) \tag{2.46}$$

$$\dot{I}_{sc2} = k_d I_{sc1}(t) - k_{a2} I_{sc2}(t) \tag{2.47}$$

$$R_i(t) = k_{a1} I_{sc1}(t) + k_{a2} I_{sc2}(t). \tag{2.48}$$

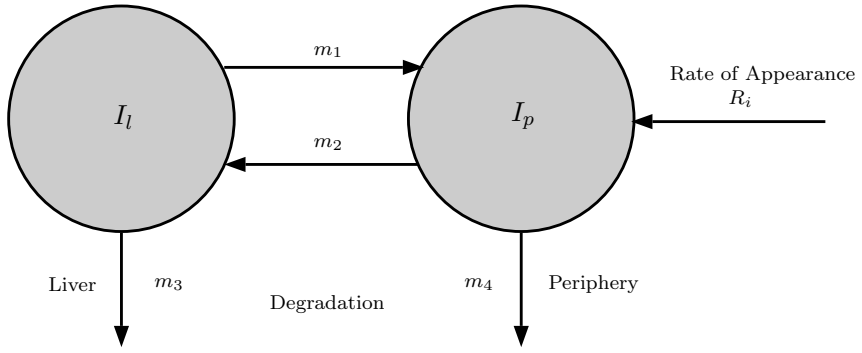

FIGURE 2.8: Block diagram of the UVA/Padova insulin model. Adapted from [6].

Note that suffix b denotes basal state. The model notation is reported in Table 2.5.

Variable/Parameter	**Unit**
G_p: Glucose mass in plasma and rapidly equilibrating tissues.	[mg/kg]
G_t: Glucose mass in slowly equilibrating tissues.	[mg/kg]
G: Plasma glucose concentration.	[mg/dl]
EGP: Endogenous glucose production.	[mg/kg/min]
k_{p1}: Extrapolated EGP at zero glucose and insulin.	[mg/kg/min]
k_{p2}: Liver glucose effectiveness.	$[\text{min}^{-1}]$
k_{p3}: Parameter governing amplitude of insulin action on the liver.	[mg/kg/min] per [pmol/l]
Ra: Glucose rate of appearance in plasma.	[mg/kg/min]
E: Renal excretion.	[mg/kg/min]
k_{e1}: Glomerular filtration rate.	$[\text{min}^{-1}]$
k_{e2}: Renal threshold of glucose.	[mg/kg]
U_{ii} and U_{id}: Insulin independent and dependent glucose utilisations.	[mg/kg/min]
$V_m(X)$: Parameter from the Michaelis Menten equation.	[mg/kg/min]
K_{m0}: Parameter from the Michaelis Menten equation.	[mg/kg]
p_{2U}: Rate constant of insulin action on the peripheral glucose utilisation.	$[\text{min}^{-1}]$
F_{cns}: Glucose uptake by the brain and erythrocytes.	[mg/kg/min]
k_1 and k_2: Rate parameters.	$[\text{min}^{-1}]$
V_G: Distribution volume of glucose.	[dl/kg]
I_p: Insulin mass in plasma	[pmol/kg]
I_l: Insulin mass in liver.	[pmol/kg]
I: Plasma insulin concentration.	[pmol/l]
V_I: Distribution volume of insulin.	[l/kg]
HE: Hepatic extraction of insulin.	dimensionless
m_1, m_2, m_3 and m_4: Rate parameters	min^{-1}
I_d: Delayed insulin signal.	[pmol/l]
I_1: Insulin signal associated with I_d.	[pmol/l]
k_i: Rate parameter accounting for delay between insulin signal and insulin action.	$[\text{min}^{-1}]$
R_i: Rate of appearance of insulin in plasma.	[pmol/kg/min]
k_d, k_{a1} and k_{a2}: Rate parameters accounting for subcutaneous insulin kinetics.	$[\text{min}^{-1}]$
X: Insulin in the interstitial fluid.	[pmol/l]

TABLE 2.5: Variables and parameters used in the UVA/Padova glucose-insulin system.

The glucose absorption model is presented in [3]. As shown in Fig. 2.9, it consists of three compartments, two for the stomach, and the other for the gut. The key feature of this model is that the gastric emptying rate (k_{empt}) is described more realistically, because it depends nonlinearly on the amount of glucose in the stomach (Q_{sto}) as shown in the following equations:

$$Q_{sto}(t) = Q_{sto1}(t) + Q_{sto2}(t) \tag{2.49}$$

$$\dot{Q}_{sto1}(t) = -k_{gri}Q_{sto1}(t) + D\delta(t) \tag{2.50}$$

$$\dot{Q}_{sto2}(t) = -k_{empt}(Q_{sto})Q_{sto2}(t) + k_{gri}Q_{sto1}(t) \tag{2.51}$$

$$\dot{Q}_{gut}(t) = -k_{abs}Q_{gut}(t) + k_{empt}(Q_{sto})Q_{sto2}(t) \tag{2.52}$$

$$k_{empt}(Q_{sto}) = k_{min} + \frac{k_{max} - k_{min}}{2}\left\{\tanh\left[\alpha\left(Q_{sto} - bD\right)\right] - \tanh\left[\beta\left(Q_{sto} - cD\right)\right] + 2\right\} \tag{2.53}$$

$$\alpha = \frac{5}{2D(1-b)}, \quad \beta = \frac{5}{2Dc} \tag{2.54}$$

$$Ra(t) = \frac{fk_{abs}Q_{gut}}{BW}. \tag{2.55}$$

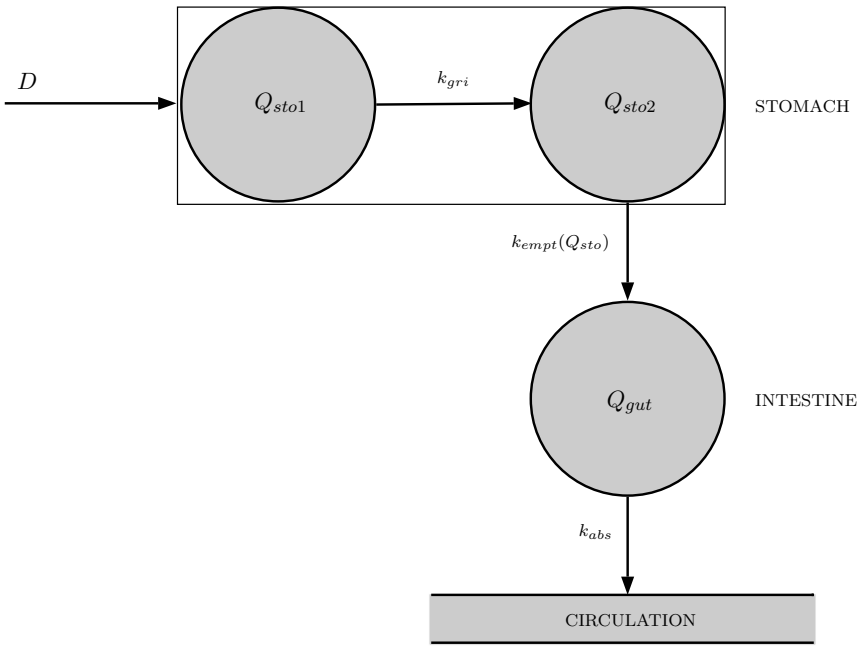

FIGURE 2.9: Block diagram of the UVA/Padova glucose absorption model. Adapted from [3].

Variable/Parameter	**Unit**
Q_{sto}: Total amount of glucose in the stomach.	[mg]
Q_{sto1}: Amount of glucose in the stomach (solid phase).	[mg]
Q_{sto2}: Amount of glucose in the stomach (triturated phase).	[mg]
D: Ingested glucose dose.	[mg]
k_{gri}: Rate of grinding.	$[\text{min}^{-1}]$
k_{abs}: Rate of intestinal absorption.	$[\text{min}^{-1}]$
k_{empt}: Rate of gastric emptying.	$[\text{min}^{-1}]$
k_{max}: Maximum rate of gastric emptying.	$[\text{min}^{-1}]$
k_{min}: Minimum rate of gastric emptying.	$[\text{min}^{-1}]$
b: Percentage of the dose for which k_{empt} decreases to $(k_{max} - k_{min})/2$.	dimensionless
c: Percentage of the dose for which k_{empt} is back to $(k_{max} - k_{min})/2$.	dimensionless
f: Fraction of the intestinal absorption which appears in plasma.	dimensionless
BW: Body weight.	[kg]

TABLE 2.6: Variables and parameters used in the UVA/Padova glucose absorption model.

In Eqn. 2.50, $\delta(t)$ is the impulse function in order to set an initial condition D. The complete definition of variables is presented in Table 2.6.

The UVA/Padova metabolic simulator v2.10, which is based on the previous model, is presented in [74]. It is equipped with 300 *in silico*[2] patients (100 adults, 100 adolescents, 100 children) whose parameters have been randomly generated, and as mentioned in Chapter 1, it is accepted by the FDA in lieu of animal trials. Its distributed version can be obtained

[2] A *in silico* patient denotes a synthetic subject which has been designed by combining different parameters in the simulator.

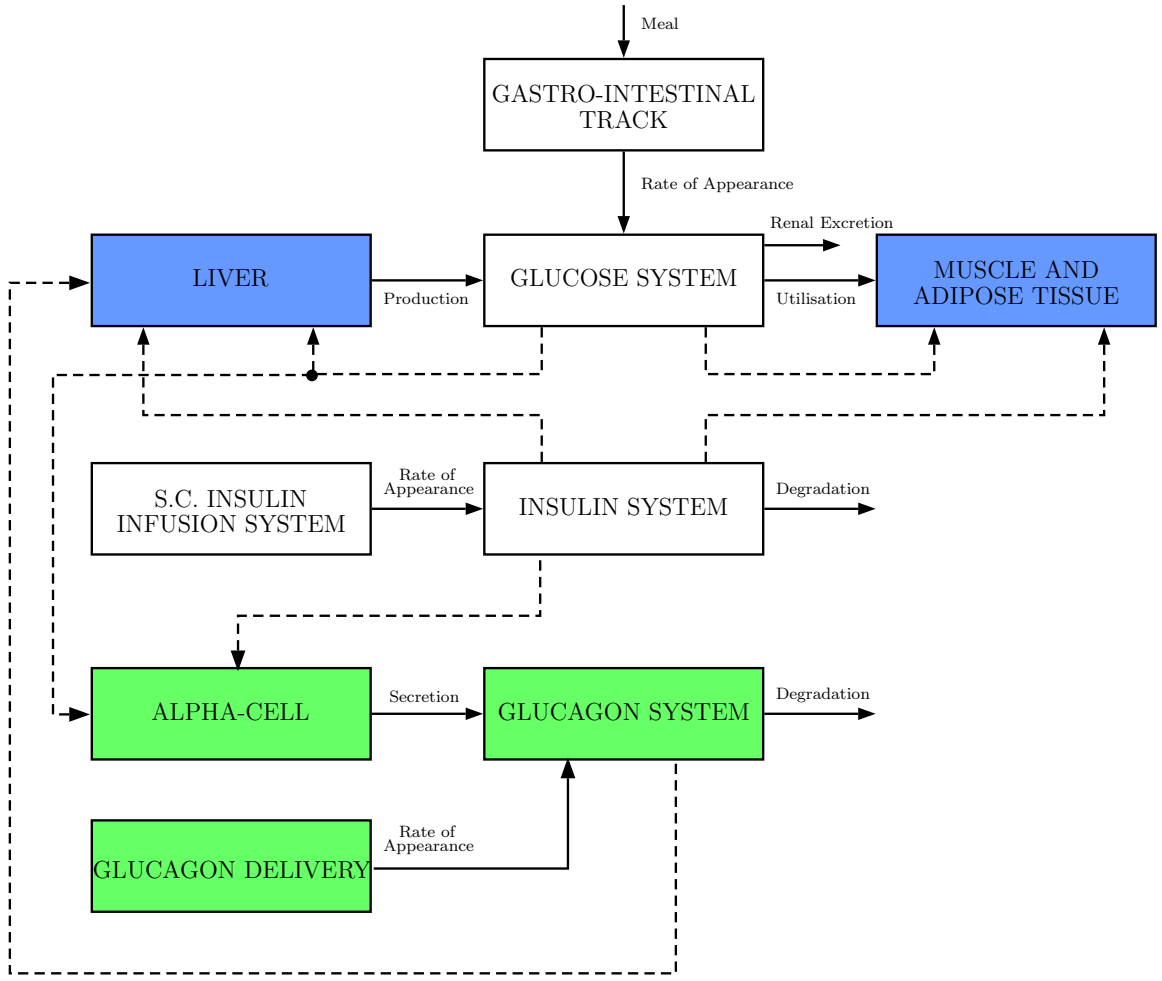

FIGURE 2.10: Scheme of the new UVA/Padova glucose-insulin system. The green and blue blocks represent the unit processes that has been included and modified, respectively, with respect to the system presented in [6]. Adapted from [7].

through the Epsilon Group, enhanced by models of insulin pumps and glucose monitors, both considered subcutaneous. The aforementioned distributed version has a reduced cohort of 30 *in silico* patients (10 adults, 10 adolescents, 10 children).

One of the main problems of this model is in describing glucose kinetics during hypoglycaemic events. Therefore, a new version of the UVA/Padova metabolic simulator (version 3.2 for future reference) has been developed [7]. As shown in Fig. 2.10, it includes various improvements with respect to the previous one that can be summarised as follows.

- It incorporates the following one-compartment model that accounts for the glucagon counterregulatory response:

$$\dot{H}(t) = nH(t) + SR_H(t) \tag{2.56}$$

$$SR_H(t) = SR_H^s(t) + SR_H^d(t) \tag{2.57}$$

$$\dot{SR}_H^s(t) = \begin{cases} -\rho\left[SR_H^s(t) - \max\left(\sigma_2\left[G_{th} - G(t)\right] + SR_H^b, 0\right)\right] & \text{if } G(t) \geq G_b \\ -\rho\left[SR_H^s(t) - \max\left(\dfrac{\sigma\left[G_{th} - G(t)\right]}{I(t)+1} + SR_H^b, 0\right)\right] & \text{if } G(t) < G_b \end{cases} \tag{2.58}$$

$$SR_H^d(t) = \delta \cdot \max\left(-\frac{dG(t)}{dt}, 0\right) \tag{2.59}$$

where $H(t)$ is the plasma glucagon concentration, $SR_H(t)$ is the glucagon secretion, n is the clearance rate, $1/\rho$ is the delay between static glucagon secretion and plasma glucose, G_{th} is a given glucose threshold, σ and σ_2 denote the alpha-cell responsivity to the glucose level, and δ, the alpha-cell responsivity to the glucose rate of change.

- It modifies Eqn. 2.33 to include the effect of glucagon on EGP:

$$EGP(t) = k_{p1} - k_{p2}G_p(t) - k_{p3}I_d(t) + \psi X^H(t) \tag{2.60}$$

$$\dot{X}^H(t) = -k_H X^H(t) + k_H \max\left[(H(t) - H_b), 0\right] \tag{2.61}$$

where $X^H(t)$ is the delayed glucagon action on EGP, ψ is the liver responsivity to glucagon, and $1/k_H$ is the delay between glucagon concentration and action.

- It reformulates Eqn. 2.35 in order to reflect how insulin action increases when blood glucose decreases under a certain threshold:

$$U_{id}(t) = \frac{[V_{m0} + V_{mx}X(t)(1 + r_1 \cdot risk)]G_t(t)}{K_{m0} + G_t(t)} \tag{2.62}$$

$$risk = \begin{cases} 0 & \text{if } G \geq G_b \\ 10[f(G)]^2 & \text{if } G_{th} \leq G < G_b \\ 10[f(G_th)]^2 & \text{if } G < G_{th} \end{cases} \tag{2.63}$$

$$f(G) = log\left(\frac{G}{G_b}\right)^{r_2} \tag{2.64}$$

with r_1 and r_2 model parameters. This modification is of great importance from a control standpoint, because it makes the new *in silico* patients more sensitive to insulin, and therefore, more difficult to control.

- It includes the following two-compartment model for subcutaneous glucagon transport:

$$\dot{H}_{sc1}(t) = -(k_{h1} + k_{h2})H_{sc1}(t) + H_{inf}(t) \tag{2.65}$$

$$\dot{H}_{sc2}(t) = k_{h1}H_{sc1}(t) - k_{h3}H_{sc2}(t) \tag{2.66}$$

$$Ra_H(t) = k_{h3}H_{sc2}(t) \tag{2.67}$$

where H_{sc1} and H_{sc2} are the glucagon concentrations in the first and second compartment, respectively, k_{h1}, k_{h2}, and k_{h3} are rate parameters, and H_{inf} is the glucagon infusion rate. Although stable glucagon formulation does not currently exist [101], there is some progress with respect to that issue [102, 103].

- It considers the duration of T1DM to generate its new subject cohort. In addition, it presents more realistic patients' parameters, and *a priori* clinical information.

This updated version with the full FDA-accepted cohort of 300 patients will be considered in the next chapters for validation purposes.

2.4 Cambridge's Model/Simulator

This model has been developed by the group directed by Prof. Hovorka in Cambridge (see [8, 104, 105]). It is focused on the effect of insulin in glucose distribution, disposal, and endogenous production, with subcutaneous insulin delivery and CGM. To this end, and as shown in Fig. 2.11, it has five submodels that describe the glucose kinetics in T1DM as follows.

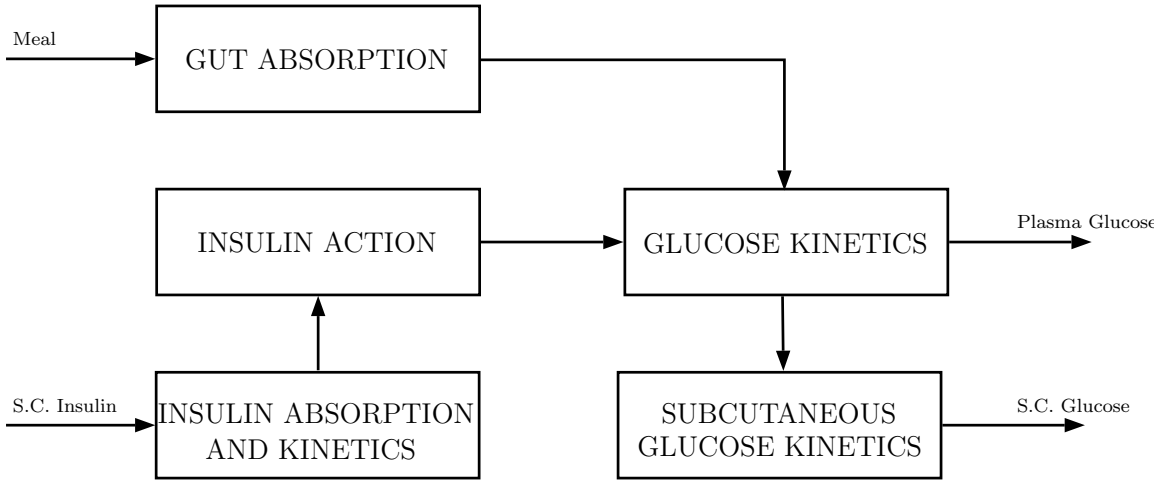

FIGURE 2.11: Block diagram of Cambridge's model. Adapted from [8].

Insulin action submodel (see Fig. 2.12):

$$\dot{x}_1(t) = -k_{b1}x_1(t) + S_{IT}k_{b1}I(t) \tag{2.68}$$

$$\dot{x}_2(t) = -k_{b2}x_2(t) + S_{ID}k_{b2}I(t) \tag{2.69}$$

$$\dot{x}_3(t) = -k_{b3}x_3(t) + S_{IE}k_{b3}I(t) \tag{2.70}$$

with $S_{IT} = \frac{k_{a1}}{k_{b1}}$, $S_{ID} = \frac{k_{a2}}{k_{b2}}$, and $S_{IE} = \frac{k_{a3}}{k_{b3}}$ the insulin sensitivities for transport, disposal, and endogenous production, respectively.

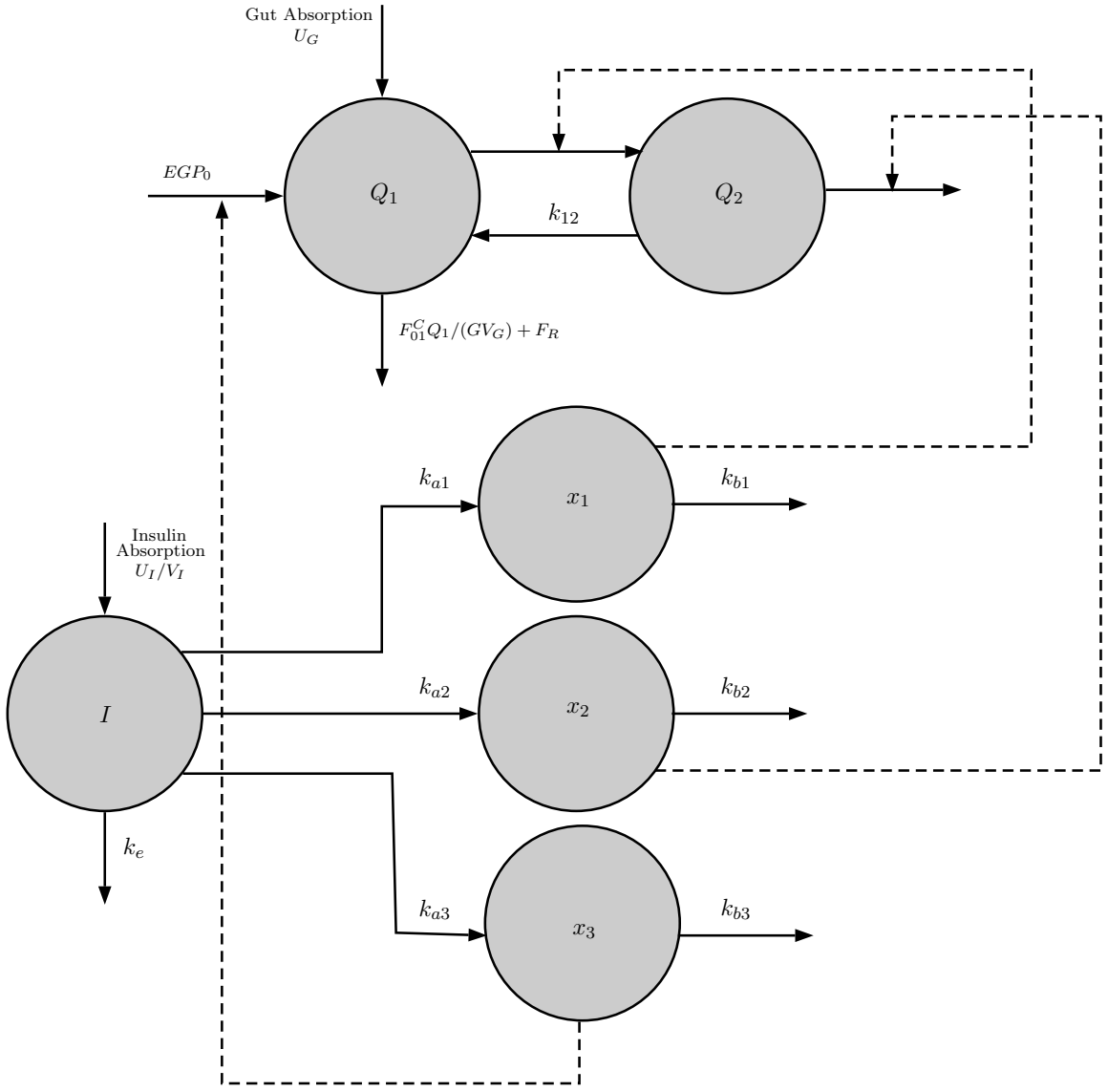

FIGURE 2.12: Block diagram of Cambridge's glucose-insulin system. Adapted from [8].

Glucose submodel (see Fig. 2.12):

$$\dot{Q}_1(t) = -\left[\frac{F_{01}^c}{V_G G(t)} + x_1(t)\right] Q_1(t) + k_{12} Q_2(t) - F_R + EGP(t) + U_G(t) \tag{2.71}$$

$$\dot{Q}_2(t) = x_1(t) Q_1(t) - [k_{12} + x_2(t)]\, Q_2(t) \tag{2.72}$$

$$y(t) = G(t) = \frac{Q_1(t)}{V_G} \tag{2.73}$$

$$EGP(t) = \begin{cases} EGP_0\,[1 - x_3(t)]\,, & EGP \geq 0 \\ 0 & EGP < 0 \end{cases} \tag{2.74}$$

$$F_{01}^c = \frac{F_{01}^s G}{G + 1} \tag{2.75}$$

$$F_R(t) = \begin{cases} R_{cl}\,(G - R_{thr})\,V_G, & G \geq R_{thr} \\ 0 & G < R_{thr} \end{cases} \tag{2.76}$$

with $F_{01}^{s} = \frac{F_{01}}{0.85}$.

Gut absorption submodel (see Fig. 2.13):

$$\dot{G}_1(t) = -\frac{G_1(t)}{t_{max}} + Bio \cdot D(t) \tag{2.77}$$

$$\dot{G}_2(t) = \frac{G_1(t)}{t_{max}} - \frac{G_2(t)}{t_{max}} \tag{2.78}$$

$$U_G = \frac{G_2(t)}{t_{max}} \tag{2.79}$$

$$t_{max} = \begin{cases} t_{max\_ceil}, & U_G > U_{G\_ceil} \\ t_{max} & U_G \leq U_{G\_ceil} \end{cases} \tag{2.80}$$

with $t_{max\_ceil} = \frac{G_2}{U_{G\_ceil}}$.

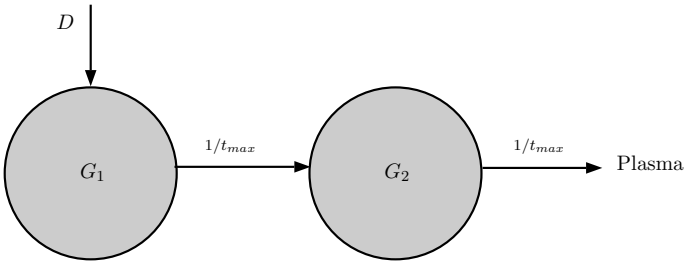

FIGURE 2.13: Block diagram of Cambridge's absorption model. Adapted from [8].

Interstitial glucose submodel (see Fig. 2.14):

$$\dot{C}(t) = k_{a\_int}(G - C)(t). \tag{2.81}$$

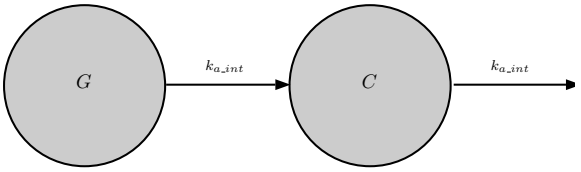

FIGURE 2.14: Block diagram of Cambridge's interstitial glucose model. Adapted from [8].

Subcutaneous insulin absorption/kinetics submodel (see Fig. 2.15):

$$\dot{S}_1(t) = u(t) - k_a S_1(t) \tag{2.82}$$

$$\dot{S}_2(t) = k_a S_1(t) - k_a S_2(t) \tag{2.83}$$

$$\dot{I}(t) = \frac{k_a S_2(t)}{V_1} - k_e I(t). \tag{2.84}$$

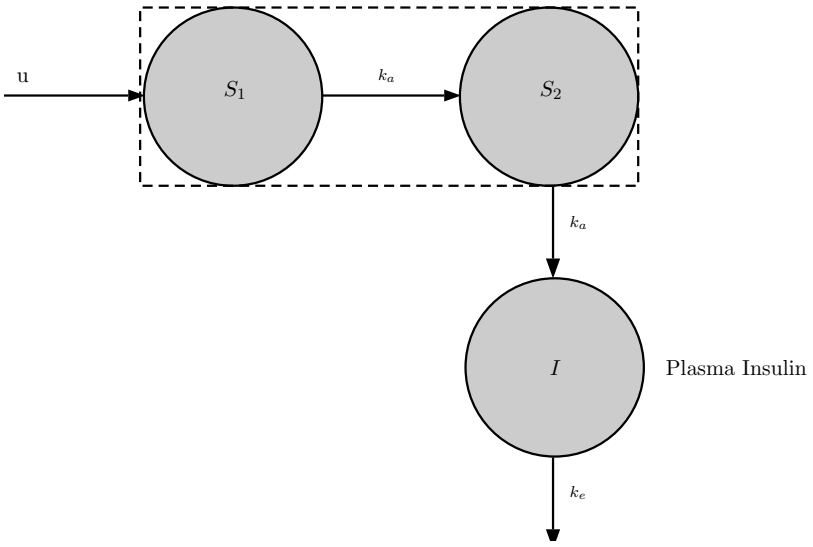

FIGURE 2.15: Block diagram of Cambridge's subcutaneous insulin model. Adapted from [8].

A detailed description of variables and parameters is given in Table 2.7.

There was a change in notation between [8] and [104], where parameters $k_{a1,2,3}$ and $k_{b1,2,3}$ have been reversed. In [105], however, there is an error in Fig. 1, where $k_{a1,2,3}$ and $k_{b1,2,3}$ should be swapped around. On the other hand, if one calculates $k_{a1,2,3}$ with the information presented in Table 1 of [104], the values obtained differ from the ones listed in Table 1 of [105]. In accordance with Dr. Wilinska's opinion about this issue, there might be an error in Table 1 of [104], where $k_{a1,2,3}$ should replace $k_{b1,2,3}$. In addition, equations (2.68), (2.69) and (2.70) are inconsistent in [8]. The activation rate constants $k_{a1,2,3}$ which multiply the states $x_i(t)$ should be replaced with the corresponding deactivation rate constants $k_{b1,2,3}$. Finally, also in that work, Eqn. (2.74) appears with a plus sign instead of a minus sign when compared to the same equation in the simulator description document.

In contrast to the other simulators, this one includes a submodel of physical exercise by a single parameter from a log-normal distribution, representing a drop in plasma concentration. The simulator environment has a virtual population of 18 subjects with T1DM, and considers the subcutaneous glucose measurement and insulin pump delivery errors. These virtual subjects were validated with clinical studies in [8]. These were carried out with an identical closed-loop control algorithm (MPC), and similar results were obtained. The educational version of this simulator has only 6 virtual subjects. A subset of the individual parameters has been estimated from experimental data collected in subjects with T1DM, and others have been drawn from informed probability distributions. An important issue

Variable/Parameter	**Unit**
Q_1 and Q_2: Masses of glucose in accessible and non-accessible compartment.	[mmol]
k_{12}: Transfer rate constant from the non-accessible to the accessible compartment.	[min^{-1}]
V_G: Distribution volume of glucose in the accessible compartment.	[L]
U_G: Gut absorption rate.	[mmol/min]
F_{01}^C: Total non-insulin dependent glucose flux.	[mmol/min]
F_R: Renal glucose clearance.	[mmol/L/min]
G: Measured glucose concentration.	[mmol/L]
EGP_0: Endogenous glucose production extrapolated to the zero insulin concentration.	[mmol/min]
I: Plasma insulin concentration.	[mU/l]
x_1, x_2 and x_3: Remote effect of insulin on glucose distribution, disposal and EGP, respectively.	x_1, x_2, [min^{-1}]; x_3, dimensionless
k_{a1}, k_{a2} and k_{a3}: Activation rate constants.	k_{a1}, k_{a2}, [min^{-2} per mU/l]; k_{a3}, [min^{-1} per mU/l]
k_{b1}, k_{b2} and k_{b3}: Deactivation rate constants.	[min^{-1}]
U_I: Insulin mass in plasma.	[mU]
k_e: Elimination rate constant for plasma insulin.	[min^{-1}]
R_{thr}: Glucose threshold.	[mmol/l]
V_I: Volume of distribution of plasma insulin.	[l]
R_{cl}: Renal clearance constant.	[min^{-1}]
S_1 and S_2: Insulin masses in the accessible and non-accessible compartments.	[mU]
U_{G_ceil}: Maximum glucose flux from the gut.	[mmol/kg/min]
u: Administration of rapid-acting insulin.	[mU/min]
k_a: Insulin absorption rate constant.	[min^{-1}]
G_1 and G_2: Glucose masses in the accessible and non-accessible compartments.	[mmol]
t_{max}: Time to maximum appearance rate of glucose in the accessible compartment.	[min]
$D(t)$: Amount of carbohydrates ingested.	[mmol/min]
Bio: Carbohydrate bioavability of the meal.	dimensionless
C: Glucose concentration in the subcutaneous tissue.	[mmol/l]
k_{a_int}: Transfer rate constant.	[min^{-1}]

TABLE 2.7: Variables and parameters used in Cambridge's model.

concerns the concept of synthetic subject. It represents the inter-subject variability when a unique set of parameters is assigned to each individual, and the intra-subject variability when certain parameters are considered to be time-varying.

2.5 Model/Simulator Comparisons

Here, some pros and cons from the different models/simulators are presented in terms of their uncontrolled (open-loop) behaviour and are summarised in Table 2.8.

Sorensen's model was one of the first complete compartmental dynamics which presented the notion of an average patient that could be tuned parametrically. It allows an immediate transformation from a normal to a controlled T1DM patient by eliminating the Γ_{PIR}

factor associated with the insulin released from the pancreas. Nevertheless, it has several drawbacks. It contemplates only intravenous insulin, eliminating the significant delay in the injection of this hormone, which is of great importance from a subcutaneous control standpoint. Although in [2] the model capacity for predicting diabetic metabolic abnormalities is proved, it is also acknowledged that an individualised parameter adjustment is desirable. An attempt to compensate for the lack of inter-subject variability is made in [87], through the variation of some physiological parameters. Nevertheless, these parameter variations were synthesised through the T1DM model, in the absence of data from real T1DM patients.

The GIM model is also compartmental, and represents an average patient that may be tuned parametrically [4]. Still, in contrast with Sorensen's model, this one solves the inter-subject variability problem through a large cohort of *in silico* subjects [74]. It includes a glucose absorption model which has several advantages with respect to the one presented in [95] (see [3]). It also adds models of CGM and subcutaneous insulin delivery, which allow more realistic simulations. Furthermore, this system has been accepted by the FDA as a substitute to animal trials in the pre-clinical testing of closed-loop control strategies. The validity of the UVA/Padova simulation environment is presented in [80], where the design of the control algorithm employed for the clinical trials was entirely developed using this simulator. The drawback with respect to Sorensen's model is that in [74], the glucagon has not been considered. However, this has been overcome with the incorporation of the glucagon kinetics, secretion and action models in [7].

From Cambridge's model, the following may be concluded. It is a simulation environment designed specifically to support the development of closed-loop insulin delivery systems in T1DM, whereas in [6] an average T2DM is also obtained. The software allows for a comprehensive assessment of an individual, as well as the population *in silico* study results. The validity of population-based predictions generated by this simulation environment was demonstrated by comparison with a clinical study in young subjects with T1DM in an overnight evaluation (see [8]). Two advantages with respect to the UVA/Padova model are: the intra-subject variability is induced by adopting time-varying parameters, and a physical exercise model is included. The drawback is that the glucagon has not been considered. Finally, the hormonal effects of epinephrine, growth hormone and cortisol have been neglected in all these models.

Model/Simulator	Pros	Cons
Sorensen	✓Immediate transformation of a normal to a controlled T1DM patient. ✓Considers glucagon dynamics.	✓Insulin injection is intravenous. ✓Inter and intra-subject variability are not taken into account.
UVA/Padova	✓Includes inter-subject variability. ✓Has a large cohort of virtual subjects. ✓An average T2DM patient has also been obtained through this model. ✓Has a reliable glucose absorption model. ✓Adds models of CGM and CSII pumps (specific brands). ✓It is accepted by the FDA.	✓Intra-subject variability is not included (under investigation). ✓Glucagon secretion depends on plasma insulin instead of the insulin level in the alpha cells.
Cambridge	✓Has a cohort of *in silico* patients validated with a clinical study. ✓Includes intra-subject variability, and a physical exercise model. ✓Adds general models of CGM and CSII pumps.	✓Glucagon dynamics are not considered. ✓Its glucose absorption model is oversimplified.

TABLE 2.8: Pros and cons of the three models/simulators.

2.6 Conclusion

Comparisons are always difficult and no single answer is possible. Besides the differences between the simulation environments pointed out in Section 2.5, attention should be paid to all of the following issues:

- Model uncertainty (dynamics, intra- and inter-patient).
- Nonlinear phenomena.
- Time delays, actuator saturation, measurement noise.
- Real-time implementation.

These items need to be achieved, and in that sense, the inter- and intra-patient variability cannot be represented adequately in all of these models, except for Cambridge's model. On the other hand, the FDA acceptance, which skips animal testing, is only possible for

the complete UVA/Padova simulator. Sorensen's model has as a unique advantage over Cambridge's model: the inclusion of glucagon, which could be relevant in future control approaches. Finally, although both the UVA/Padova simulator, as well as Cambridge's simulator, are implemented in Matlab® (The Mathworks, Natick, MA), the last one is slower from a computational point of view, due to the fact that many text files are generated in the process.

Chapter 3

Robust Control For Blood Glucose Regulation

3.1 Motivation

The problem of automatically controlling the blood glucose level in patients with T1DM has been approached in different ways using different models (see [71] for a survey). Solutions go from PID control [77,106] to heuristic fuzzy-logic procedures or parametric-programming [107]. One of the main challenges associated with this problem is that T1DM models present significant sources of uncertainty which are worth considering. In that sense, Robust Control Theory has been applied in [86,87,96], centred on the uncertainty issue. Also, a LPV model has been derived in [98] based on Sorensen's model, and controlled by an $\mathcal{H}_\infty$ Linear Time Invariant (LTI) controller in [97, 99]. In addition, due to the nature of the dynamics in all models, MPC [8,108–110], nonlinear control design methods [105], LPV and Unfalsified Control (UC) [84,94] have also been implemented.

This chapter is devoted to the application of the three T1DM models presented in Chapter 2 to the synthesis of $\mathcal{H}_\infty$ controllers. To this end, firstly, a continuous-time design for Sorensen's model is introduced in order to carry on with the work presented in [84]. Then, focus is put on discrete $\mathcal{H}_\infty$ methods to test the main characteristics of all the aforementioned models. Hence, three sources of uncertainty (nonlinearities, inter- and intra-patient variations) are considered. The first is interpreted as model variations among different linearisation points, while the second, among different subjects. The intra-patient variability

considers the time-varying behaviour within a certain subject. All the four items mentioned in Section 2.6 will be included in the closed-loop simulation tests.

3.2 Continuous-Time $\mathcal{H}_\infty$ Control Applied To Sorensen's Model

3.2.1 Controller Design

As shown in Section 2.2, this model has two inputs: Γ_{meal} (meal disturbance) and Γ_{IVI} (insulin infusion). In order to consider subcutaneous glucose measurements, G_P^T is defined as the output signal. The linearisation is performed by gridding Γ_{IVI} from 0 to 35 mU/min, assuming no disturbance ($\Gamma_{meal} = 0$ mg/min), which moves the steady state value of G_P^T from 183 to 46 mg/dl, respectively. The Bode plots of this grid are represented in Fig. 3.1.

The *normoglycaemic* condition, which defines the nominal model, is associated with a concentration of $G_P^T \simeq 87$ mg/dl, produced when the insulin infusion is 22 mU/min. The similarities between the different plots denote their low level of nonlinearity. It allows representing the nominal system as an LTI model, which can be reduced from 19 to 6 states with no major impact (see Fig. 3.2). The modelling error is covered by additive uncertainty $(G - G_r)$. The difference between all previous curves and the reduced order nominal model is represented in Fig. 3.3. There, the uncertainty weight $W_\Delta(s)$ covers all additive errors at all frequencies. Note that this model order reduction is based on a balanced and truncated

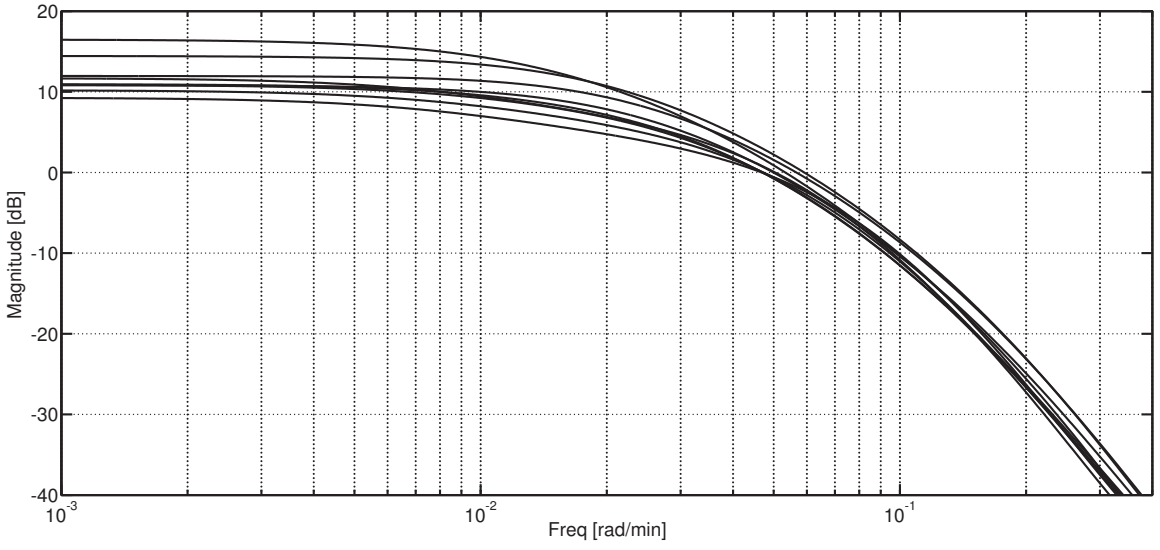

FIGURE 3.1: Bode plots of Sorensen's model at different linearisation points.

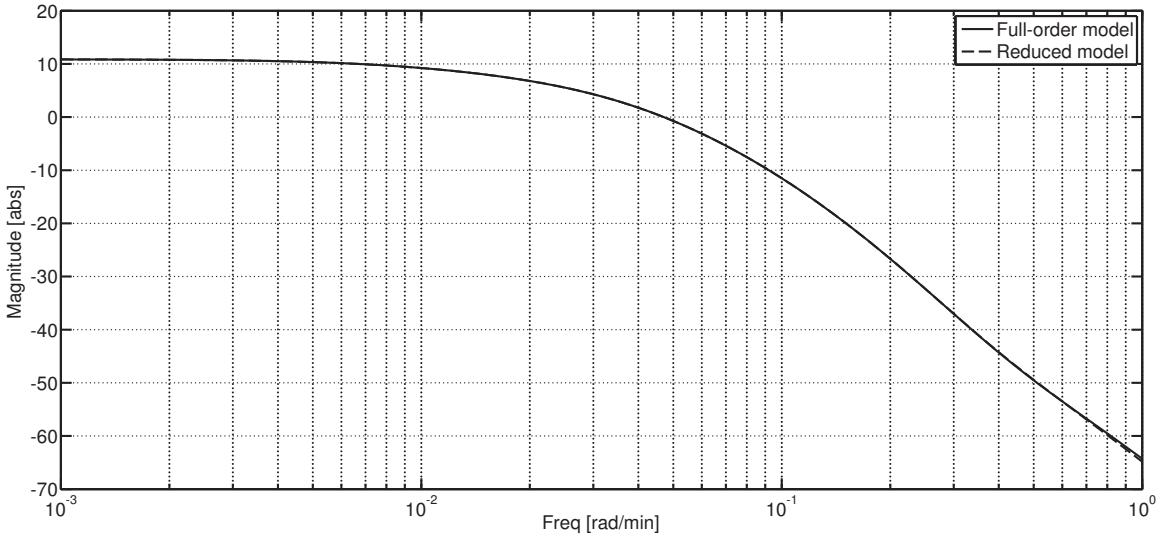

FIGURE 3.2: Bode diagrams of the nominal model (continuous line) and the reduced-order model (dashed line).

state-space realisation of the original LTI model, whose precision is measured in terms of its Hankel singular values.

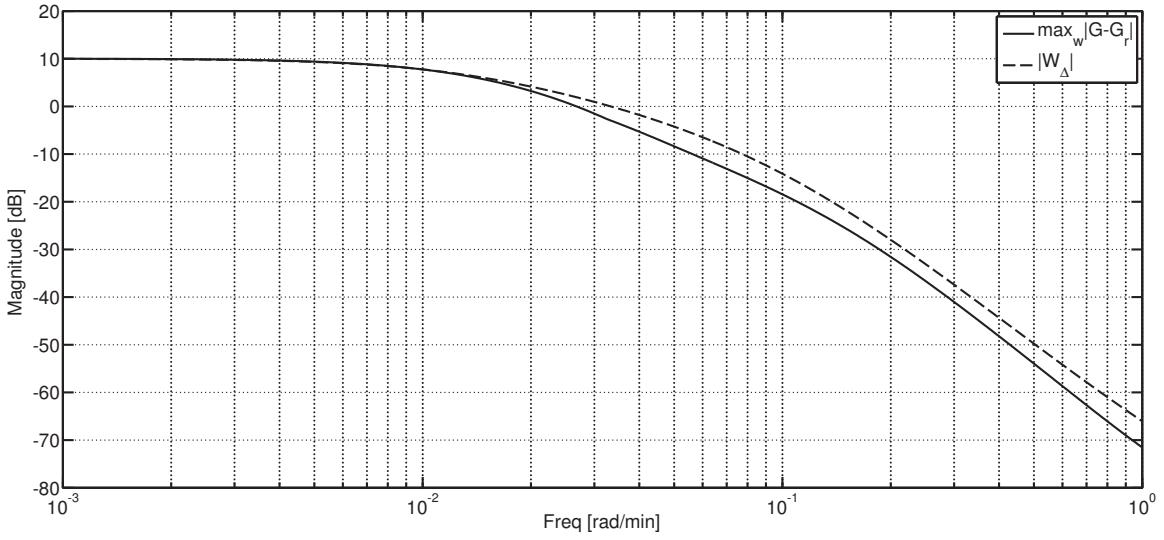

FIGURE 3.3: Additive uncertainty (continuous line) and uncertainty weight (dashed line).

A brief explanation of the analysis and design methodology follows (see [111, 112]). The set

$$\mathcal{G} \triangleq \{G = G_r + \Delta W_\Delta, \quad \|\Delta\| < 1\} \tag{3.1}$$

known as the additive uncertainty model set, represents the physical phenomena. This

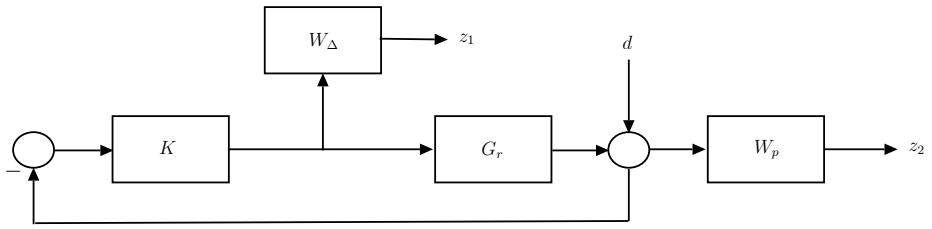

FIGURE 3.4: Standard feedback loop.

dynamical description, instead of a single model, may include nonlinearities, high order unknown phenomena, and time delays. Here, $G_r(s)$ is the reduced-order nominal model, and $W_\Delta(s)$ represents the variation of model uncertainty with frequency. Nominal performance (NP) is defined as the weighted tracking error of the nominal model $G_r(s)$ measured in terms of its signal energy, for all perturbations d in a set measured accordingly (see Fig. 3.4):

$$\|z_2\|_2 < \gamma \text{ for all } \|d\|_2 < 1. \tag{3.2}$$

Robust stability (RS) is the (internal) stability[1] of all possible closed-loops which combine a single controller $K(s)$ with all elements of set $\mathcal{G}$. Finally, Robust performance (RP) is defined as the validity of condition (3.2) for all elements of set $\mathcal{G}$. Standard robust control results guarantee that these conditions are equivalent to:

$$NP \iff \frac{1}{\gamma}\|W_p(s)S(s)\|_\infty < 1 \tag{3.3}$$

$$RS \iff \frac{1}{\gamma}\|W_\Delta(s)K(s)S(s)\|_\infty < 1 \tag{3.4}$$

$$RP \iff \frac{1}{\gamma}\mu_\Delta\{T_{zd}(\jmath w)\} < 1 \quad \forall\omega \tag{3.5}$$

where $S(s) = (I + GK)^{-1}$ is the sensitivity function, $\mu_\Delta(\cdot)$ is the structured singular value, $T_{zd}(s)$ the transfer matrix between d and $z = [z_1; z_2]$ in Fig. 3.4, and γ is a scalable variable. A sufficient condition to guarantee RP is the so called mixed-sensitivity condition, which can be used for controller design:

$$\min\left\{\gamma \text{ such that } \left\|\begin{bmatrix} W_p(s)S(s) \\ W_\Delta(s)K(s)S(s) \end{bmatrix}\right\|_\infty < \gamma\right\}. \tag{3.6}$$

[1]Internal stability of a closed-loop interconnection is equivalent to the input/output (I/O) stability of all possible I/O transfer functions in the loop.

The performance weight $W_p(s)$ is selected in order to have a small steady state tracking error to follow the reference, almost like an integrator. The reference is based on the response of an average normal patient to a 100 g glucose disturbance at $t = 0$. This response can be represented as the impulse response of a second order system [86]:

$$P_{ref}(s) = \frac{Kw_n^2}{s^2 + 2w_n\xi s + w_n^2} \tag{3.7}$$

with $K = 3900$, $w_n = 0.02$ and $\xi = 0.7$.

The design is performed via the $\mathcal{H}_\infty$ optimal control method using Linear Matrix Inequality (LMI) optimisation and considering the following performance and uncertainty weights, respectively:

$$W_p(s) = \frac{0.1667s + 0.05}{s + 0.0025} \tag{3.8}$$

$$W_\Delta(s) = 10^{-4} \times \frac{0.1976s^3 + 1.779s^2 + 4.743s + 3.953}{s^3 + 0.2125s^2 + 0.0125s + 0.000125}. \tag{3.9}$$

The controller designed has order 10, and is reduced to order 8 also based on a balanced truncated method. The optimal performance/robustness value is $\gamma = 0.9038$. Robust stability and performance and nominal performance necessary and sufficient conditions are represented in Fig. 3.5, based on equations (3.3)–(3.5).

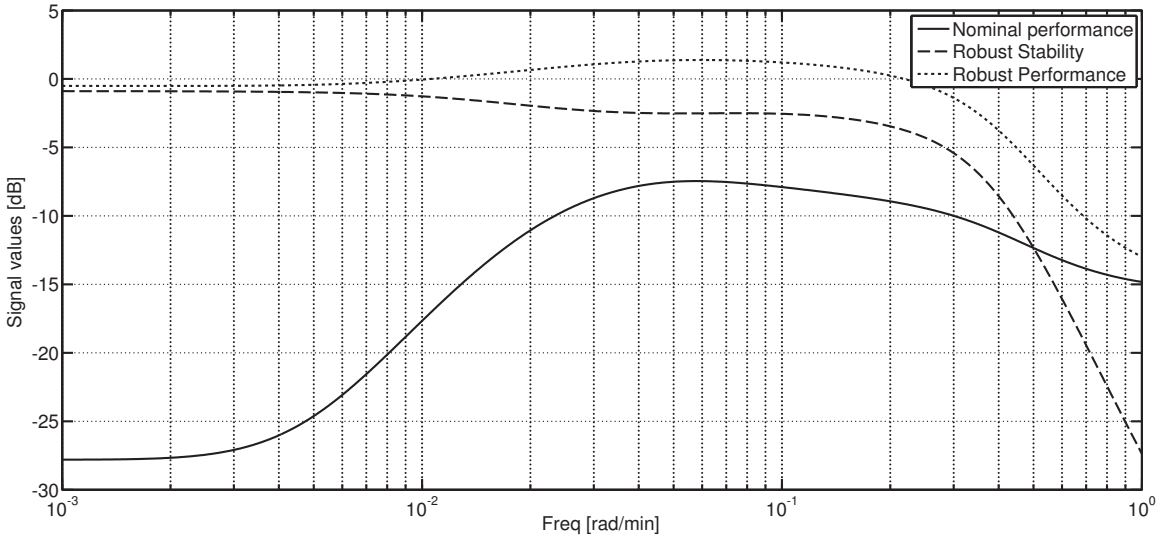

FIGURE 3.5: Robust stability (dashed line) and nominal (continuous line) and robust performance (dotted line) conditions.

Concerning the practical limitation of the insulin pumps of 100 mU/min, W_Δ can also be considered as a weight to bound the control signal. As illustrated in the following section, no further adjustments were necessary in order to limit the insulin injection to the previous bound.

3.2.2 Results

For the simulations, a meal disturbance which contains 100 g carbohydrate is considered, and the Lehmann and Deutsch's model presented in Section 2.2 is used to describe the rate of gastric emptying Γ_{meal} (see Fig. 2.5). Since there is no simulator for Sorensen's model, one was developed in Matlab®. In addition, noise was included as random errors in the measurement of the glucose concentration, with a band limited value of 5 mg/dl. The time response of the closed-loop system with measurement noise, injected insulin levels bounded by 100 mU/min, the meal disturbance of 100 g of glucose, and the delay in glucose measurements (the insulin injection is intravenous here), can be seen in Fig. 3.6.

The control action shows that there was no saturation of the pump, which tends to a steady state value of 22 mU/min. This is due to the fact that the reference steady state is approximately 87 mg/dl. A fact that was also considered when simulating was that the reference is related to the blood concentration while the output is the interstitial glucose concentration. Therefore, a 5 min delay was added to the reference in order to assimilate this behaviour. This value was taken from the computed delay in these two values in Sorensen's model.

To close, it can be noted that the output remains in a safe region. The glucose peak is considerably lower than 180 mg/dl and even lower, under similar analysis conditions, to the results obtained in [84, 86]. In fact, the difference between the reference and the actual output is below 13 mg/dl.

3.3 Discrete-Time $\mathcal{H}_\infty$ Control Applied To T1DM Models

Here, discrete-time $\mathcal{H}_\infty$ controllers are synthesised to test the main characteristics of all the T1DM models presented in Section 2. The objective is to compare them in practical scenarios which include: model uncertainty, time variance, nonlinearities, glucose measurement noise,

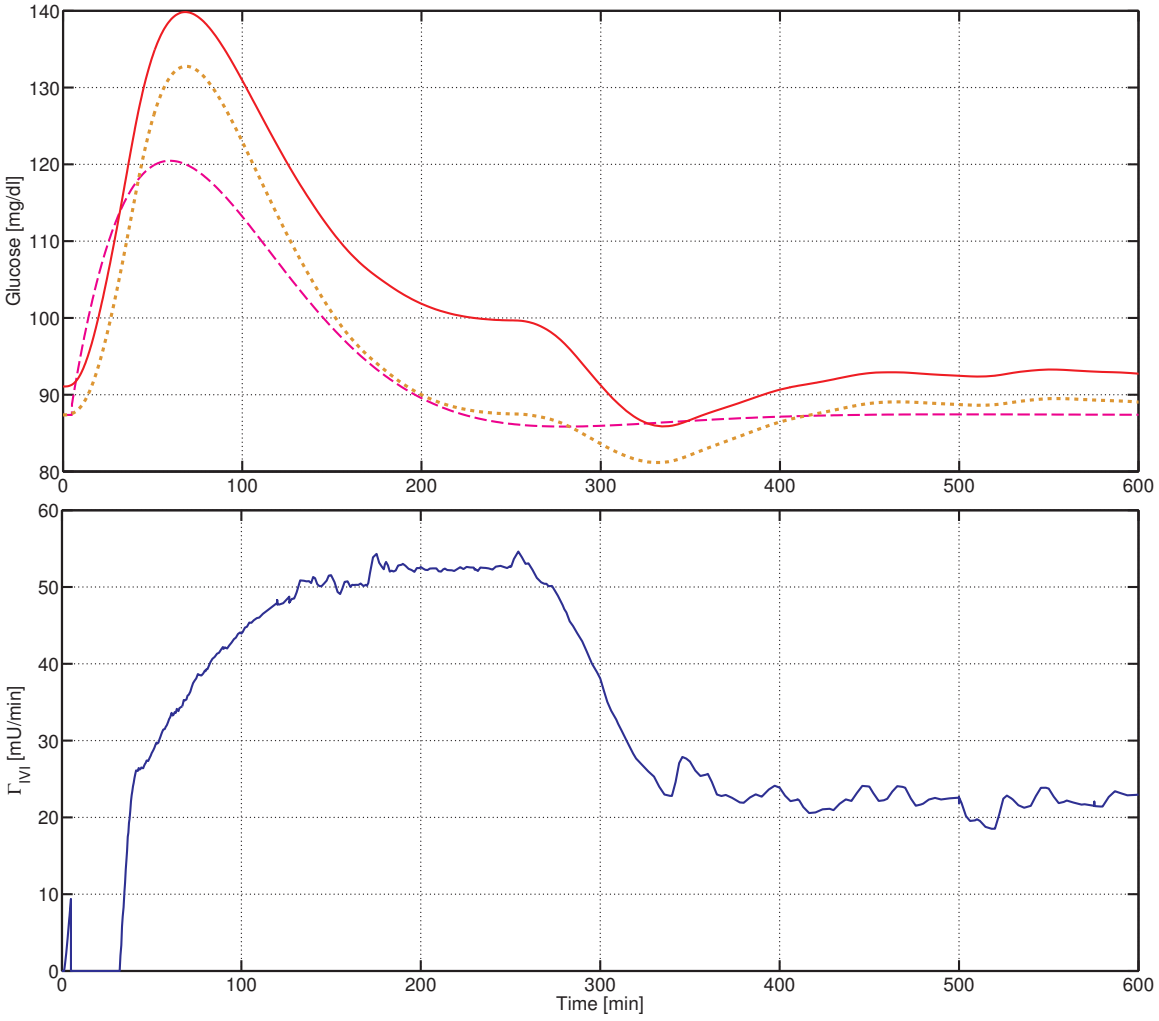

FIGURE 3.6: Closed-loop response for Sorensen's averange patient. Above: $G_P^C(t)$ (continuous line), $G_P^T(t)$ (dotted line), and the reference signal (dashed line). Below: Insulin infusion rate.

delays between subcutaneous and plasma levels, pump saturation, and real-time controller implementation. Because the glucose concentration is measured in mg/dl in Sorensen's model and the UVA/Padova simulator, and in mmol/l[2] in the Cambridge model, in this chapter, the glucose concentration will be expressed in mmol/l for comparison purposes.

3.3.1 Sorensen's Model

The nonlinear model is linearised at nine different interstitial glucose concentrations which range from 2.56 to 10.17 mmol/ℓ. As mentioned previously, the low level of nonlinearity

[2] 1 mmol/l = 18 mg/dl.

allows the representation of the system as a nominal LTI model plus uncertainty. Furthermore, the nominal model can be reduced from 19 to 6 states with no major impact. A discrete $\mathcal{H}_\infty$ controller is designed based on a mixed-sensitivity performance objective defined as:

$$\min \left\{ \gamma \text{ such that } \left\| \begin{bmatrix} W_p(z)S(z) \\ W_\Delta(z)K(z)S(z) \end{bmatrix} \right\|_\infty < \gamma \right\} \tag{3.10}$$

where $S(z) = (I + GK)^{-1}$ is the sensitivity function, $W_p(z)$ and $W_\Delta(z)$ are the performance and additive uncertainty weights, respectively, and $K(z)$ is the controller. Note that this is the discrete-time version of the performance objective presented in Eqn. 3.6.

The design is performed via the $\mathcal{H}_\infty$ optimal control method using the *loop-shifting formulae* of [113], considering the following weights:

$$W_p(z) = \frac{0.015z + 0.015}{z - 0.999990} \tag{3.11}$$

$$W_\Delta(z) = \frac{0.0002494z^3 + 0.0001069z^2 + 8.882 \times 10^{-16}z - 2.22 \times 10^{-16}}{z^3 - 2.797z^2 + 2.606z - 0.8084}. \tag{3.12}$$

The controller, which provides stability and performance at all different working points, operates with a sampling time of 1 min and has order 10 with a $\gamma = 0.9683$. In this simulation, the reference signal is generated as in Section 3.2, starting from an initial concentration value of 4.85 mmol/ℓ. The results of two glucose intakes of 100 g each without insulin infusion (open-loop) and with the controller in place (closed-loop) are depicted in Fig. 3.7.

3.3.2 UVA/Padova's Simulator

The database of the GIM and the distribution version of the UVA/Padova (v2.10) simulators were used to obtain a discrete $\mathcal{H}_\infty$ robust controller which could handle three different patients with T1DM. One of the patients was the average one proposed in [4]. These three models were linearised around the glucose level of 5.1 mmol/ℓ. The same design technique used in Sorensen's model was used here, but considering the following weights:

$$W_p(z) = \frac{0.001075z + 0.001075}{z - 0.999970} \tag{3.13}$$

$$W_\Delta(z) = \frac{0.000127z^2 + 0.000244z + 0.0001172}{z^2 - 1.993z + 0.993}. \tag{3.14}$$

Also, the same sampling time and measurement noise as in Sorensen's model were used[3],

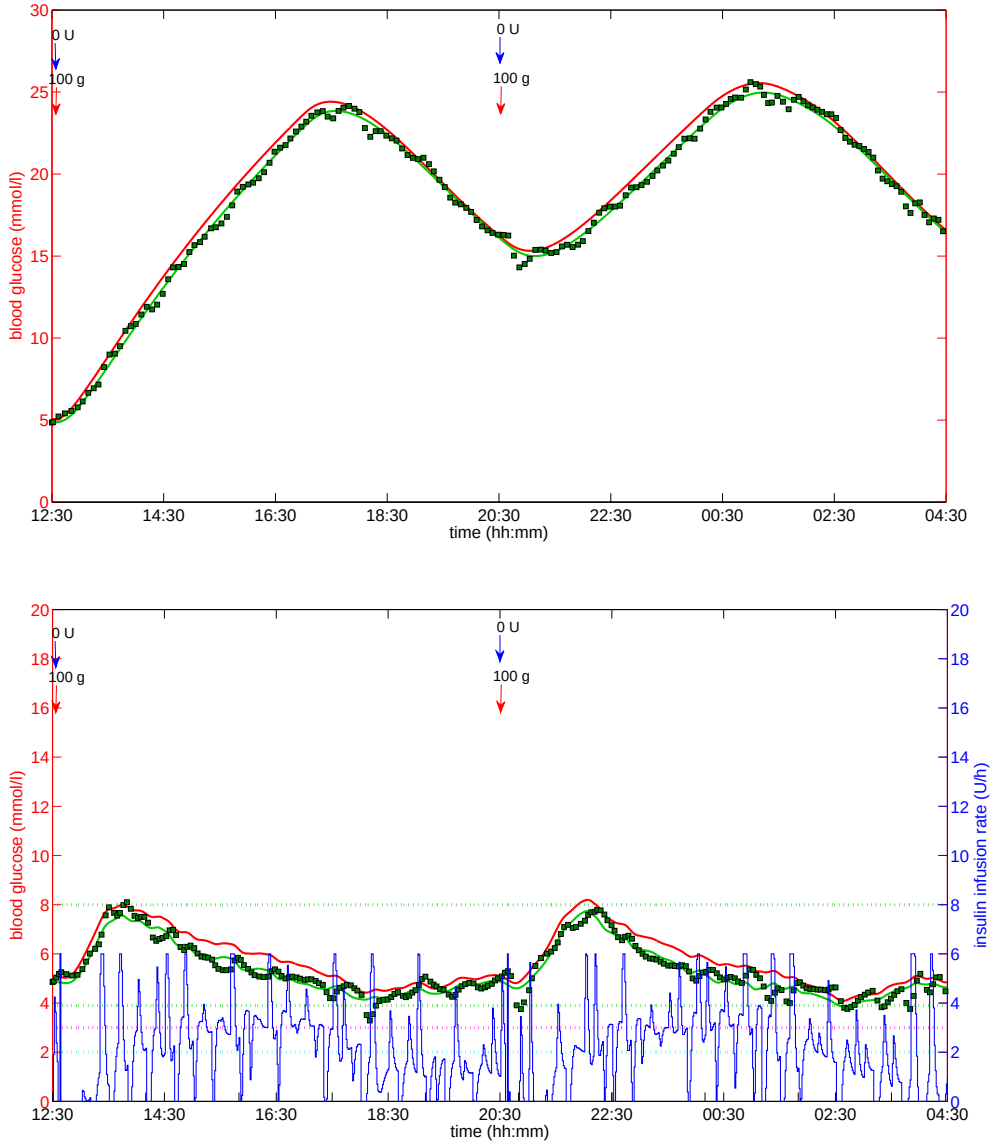

FIGURE 3.7: Above: Uncontrolled simulation in Sorensen's model. Below: Closed-loop simulation of Sorensen's model with the discrete $\mathcal{H}_\infty$ controller. The continuous (red) line is the plasma glucose concentration, the (green) squares are glucose measurements, the (blue) continuous line is the insulin injection rate, the dash (green) lines are the desired glucose range (3.9 to 8 mmol/ℓ), the dashed (magenta) line indicates the hypoglycaemia level (3 mmol/ℓ), and the light blue line the severe hypoglycaemia level (2 mmol/ℓ).

and an insulin pump saturation of 30 U/h (OmniPod) was included. The designed controller has order 16 and is reduced to order 6 with a $\gamma = 2.5359$.

In Figs. 3.8, 3.9, and 3.10, the open- and closed-loop responses with two glucose perturbations of 100 g each for all three patients are depicted. In the controlled simulations, the

[3]The author wanted to compare the controlled simulations with similar measurement error characteristics.

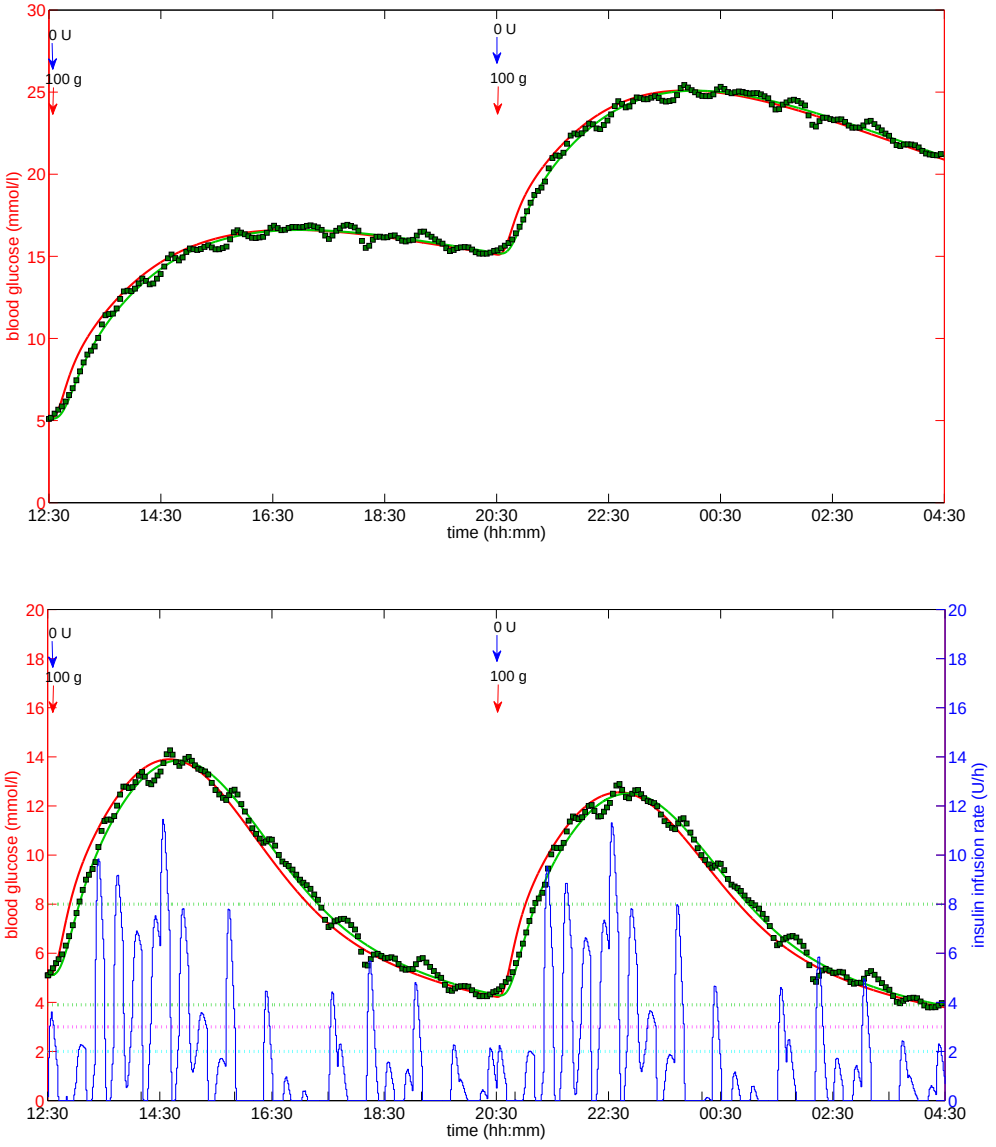

FIGURE 3.8: Average adult of the UVA/Padova simulator. Above: Uncontrolled simulation. Below: Closed-loop simulation with the discrete $\mathcal{H}_\infty$ controller. The line indications are the same as the ones in Fig. 3.7.

evolution of the average normal patient was used as a reference, according to the parameters presented in [6].

3.3.3 Cambridge's Simulator

As mentioned in Section 2, the advantage of this simulator is the intra-patient variability representation by considering time-varying parameters. Hence, the strategy here is a linearisation of the nonlinear dynamics at different sampling times but with a constant interstitial

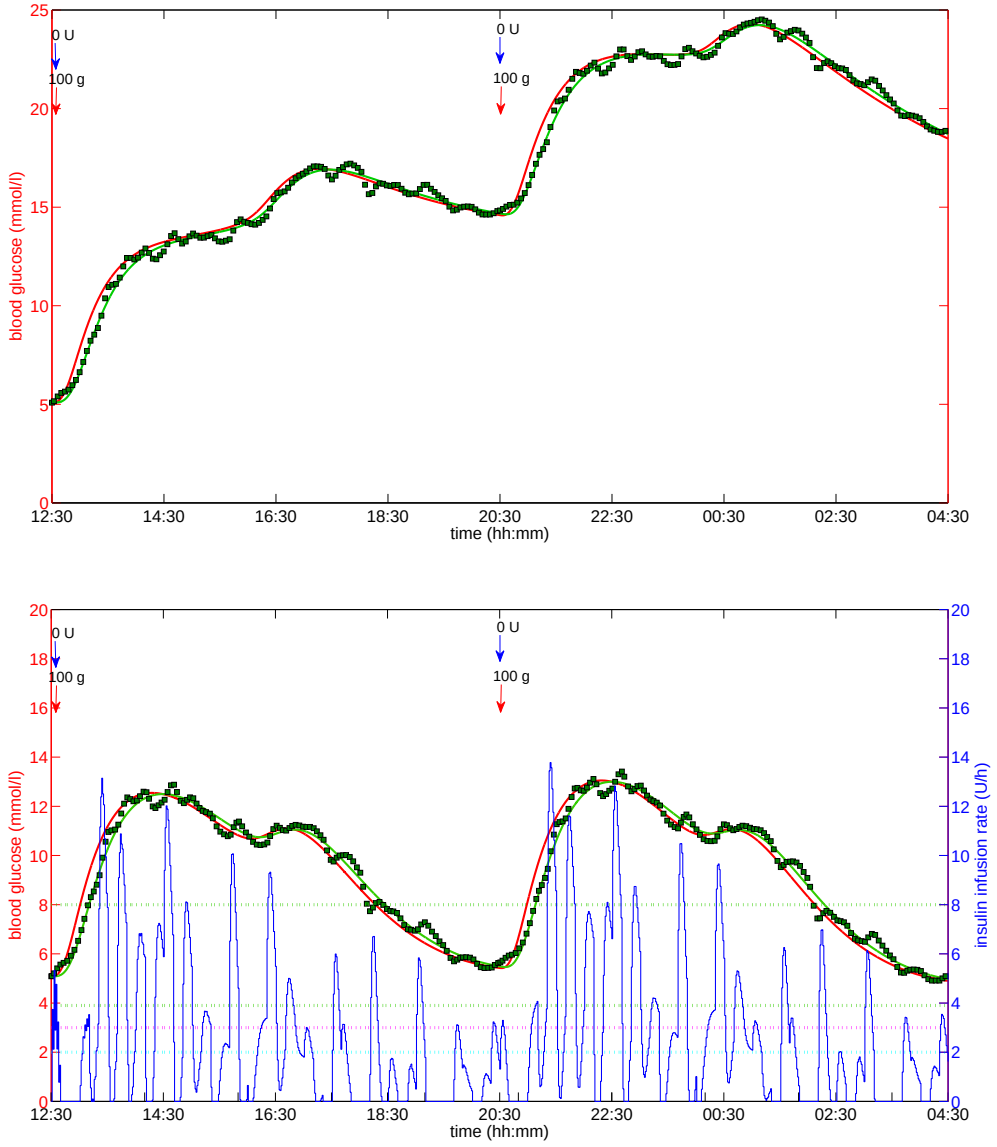

FIGURE 3.9: Adult #5 of the UVA/Padova simulator. Above: Uncontrolled simulation. Below: Closed-loop simulation with the discrete $\mathcal{H}_\infty$ controller. The line indications are the same as the ones in Fig. 3.7.

glucose concentration. The first virtual subject (there are six in the Simulator Educational Version) at $\{0, 60, 120\}$ minutes and a concentration of 5.10 mmol/ℓ were considered. The parameter variation in this simulator is periodic, hence parameters at 0 and 180 min are repeated.

Based on these 3 models, and after repeating the procedure followed in the previous designs, a discrete $\mathcal{H}_\infty$ controller is obtained which guarantees stability and performance. In this case, the design is achieved using LMI optimisation [114] and considers the following

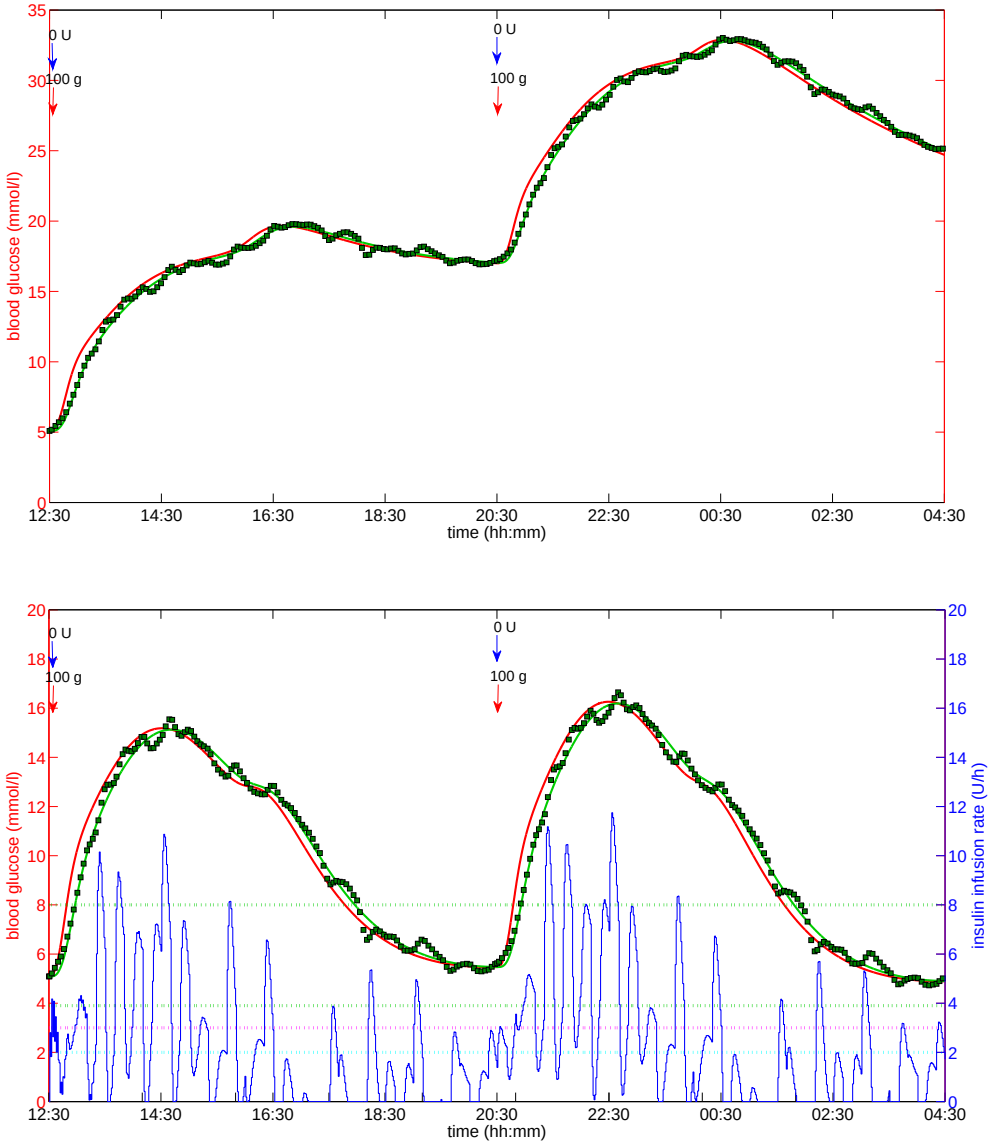

FIGURE 3.10: Adult #10 of the UVA/Padova simulator. Above: Uncontrolled simulation. Below: Closed-loop simulation with the discrete $\mathcal{H}_\infty$ controller. The line indications are the same as the ones in Fig. 3.7.

weights:

$$W_p(z) = \frac{0.00475z + 0.00475}{z - 0.999990} \tag{3.15}$$

$$W_\Delta(z) = \frac{3.177 \times 10^{-6} z^2 + 6.354 \times 10^{-6} z + 3.177 \times 10^{-6}}{z^2 - 1.994z + 0.9935}. \tag{3.16}$$

A controller of order 11 is obtained and is reduced to order 9 with a $\gamma = 1$. As a consequence, it allows, after an ingestion, the average plasma glucose level to return to a

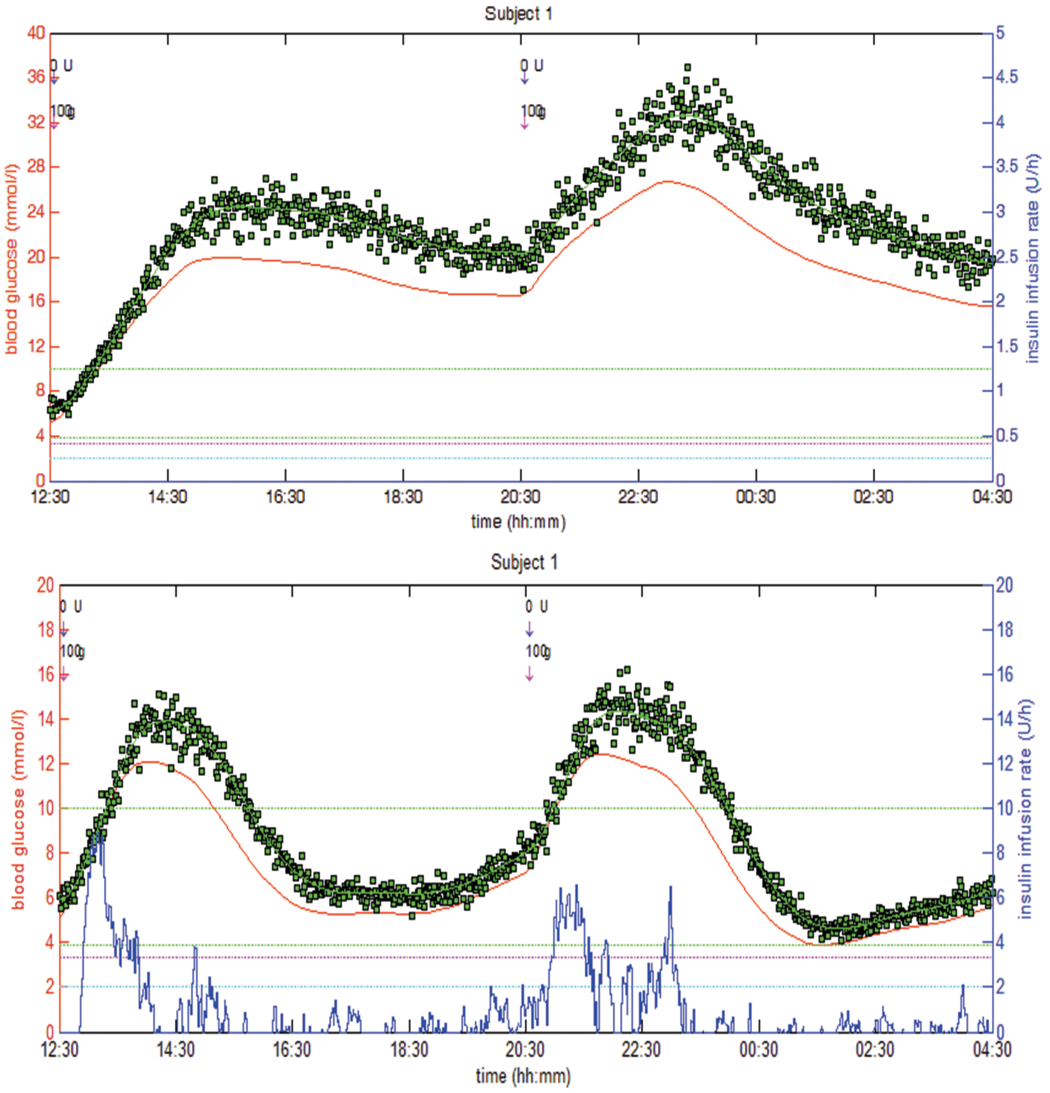

FIGURE 3.11: Subject #1 of Cambridge's simulator. Above: Uncontrolled simulation. Below: Closed-loop simulation with the discrete $\mathcal{H}_\infty$ controller. The line indications are the same as the ones in Fig. 3.7.

constant and safe value. In Fig. 3.11, the simulated uncontrolled and controlled responses for Subject #1 after two glucose intakes of 100 g each are represented. The controlled (closed-loop) response for the same patient with the MPC controller proposed in the simulator is depicted in Fig. 3.12.

All simulations are based on the following conditions:

- No bolus is applied previous to food ingestion.
- The sampling time and controller application interval is 1 min.
- Glucose measurements and insulin injection are both subcutaneous.

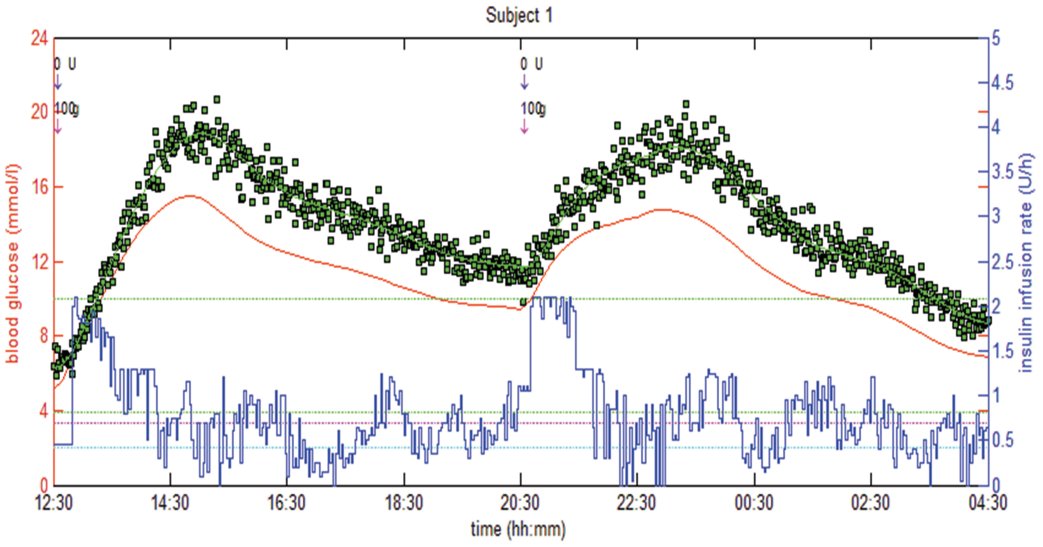

FIGURE 3.12: Simulation of Cambridge's model with their proposed MPC. The line indications are the same as the ones in Fig. 3.7.

- The Coefficient of Variation (CV) of the error in the continuous insulin injection for the calibration and for the glucose measurement errors are all 5%.

The closed-loop simulations show that the MPC signal is not enough to guarantee a good performance by itself. For this reason, a pre-meal insulin bolus is used in these cases. The aim of this research is to obtain a control signal without any correction bolus, hence the $\mathcal{H}_\infty$ controller seems to be better than MPC in this case.

3.4 Conclusion

In this chapter, the design and simulation of closed-loop controlled patients have been instrumental as an application of the previous model/simulator analysis presented in Chapter 2. As for (robust) control issues, here the uncertainty has been represented by nonlinearities, inter- and intra-patient variations, the latter as a time-varying behaviour. For these three sources of uncertainty and with different discrete $\mathcal{H}_\infty$ robust controllers applied to three different simulations, a satisfactory answer has been achieved. Nevertheless, the most accurate control seems to be achieved by Sorensen's model. This is because the interstitial-plasma delay in the control signal and the inter- and intra-subject variability are not included. Therefore, and as Figs. 3.8–3.10, and 3.11 indicate, more realistic scenarios induce a more

difficult problem, and hence less performance. Also, it tends to be harder when a single controller is used to control a group of T1DM patients. In a real situation, all three sources of uncertainty mentioned above should be considered simultaneously. In that case, most probably a robust LTI controller such as the one designed here would not be enough. Therefore, an exploration of different approaches will be presented in the following chapters.

Chapter 4

A Time-Varying Approach Based On The $\mathcal{H}_\infty$ Control Design

4.1 Motivation

In any artificial pancreas scheme based on subcutaneous insulin delivery and/or glucose measurement, there is great difficulty in dealing with the long actuation/sensing delays, and also the large inter- and intra-patient variability. Due to the fact that the system is highly uncertain and time-varying, it is clear that some tuning to patient-specific characteristics is necessary to achieve high closed-loop performance [115].

One way to tune or adapt to a particular patient would be to perform an in-depth *a priori* identification procedure [116], although the complexity of such a procedure, and the time required to perform it, are likely to render such individualisation infeasible in practice. Fortunately, recent results seem to be very promising as for model identification from CGM data (see [117]). Nevertheless, a general model structure could be adapted to a particular patient by using certain *a priori* clinical information that is easily obtainable, e.g., the patient's Total Daily Insulin (TDI) amount. Here, only adult patients are considered to present the first results of this algorithm, because a lack of efficacy in adults could lead to dismissal of possible therapies that could benefit children, the highest-risk population [23]. In this chapter a control model is synthesised by performing system identification on the ten adult *in-silico* subjects of the UVA/Padova simulator. A third order model was chosen, and the model gain is personalised by means of the subjects' TDI. That personalised model,

whose parameters lack physiological meaning because so-called black-box procedures were used to identify the model, is employed to synthesise an $\mathcal{H}_\infty$ controller by solving a mixed-sensitivity problem. The $\mathcal{H}_\infty$ control, which to my knowledge has never before been tested on the complete adult cohort of the UVA/Padova metabolic simulator, represents an alternative approach to other well known control algorithms. This technique provides a good balance between insulin dosing and glucose tracking, by a practical, low order controller.

In order to achieve safe hypoglycaemia control, an IFL has been added to adequately regulate an estimate of the patient's Insulin on Board (IOB). In addition, a SM is used to perform better control based on a prediction, over a 20 minute horizon, of future glucose levels. Auxiliary modules that modify insulin dosing when safety alarms are detected have been applied in several papers, demonstrating their importance in achieving safe blood glucose control [118–122].

4.2 Model Identification & Patient Tuning

As shown in Chapter 2, several models that describe the glucose-insulin dynamics have been developed [2, 6, 8]. However, the model parameters typically have physiological significance and cannot easily be estimated in real patients. In addition, for control synthesis a simple, low-order model is frequently more desirable than a complex, sophisticated model [123]. Therefore, a low-order control-relevant model is identified using a black-box approach, and subsequently adjusted based solely on *a priori* patient data, as in [124]. The procedure is described next.

For each *in-silico* adult of the distribution version of the T1DM simulator, a linear model of the transfer characteristics from the insulin delivery (pmol/min/kg) to the deviation from a particular glucose concentration (mg/dl) is identified. Three different interstitial glucose concentrations[1] are considered here: 90, 120 and 150 mg/dl to capture the frequency response at different operating points. Hence, three linear models are obtained for each patient.

The identification process for a particular glucose concentration is as follows. First, the basal insulin (I_b) that produces the particular glucose concentration at steady state is obtained. Then, I_b is added to a sinusoidal insulin sweep. Over 12 h, and with a sampling

[1]The simulator has access to that particular variable without the CGM measurement noise.

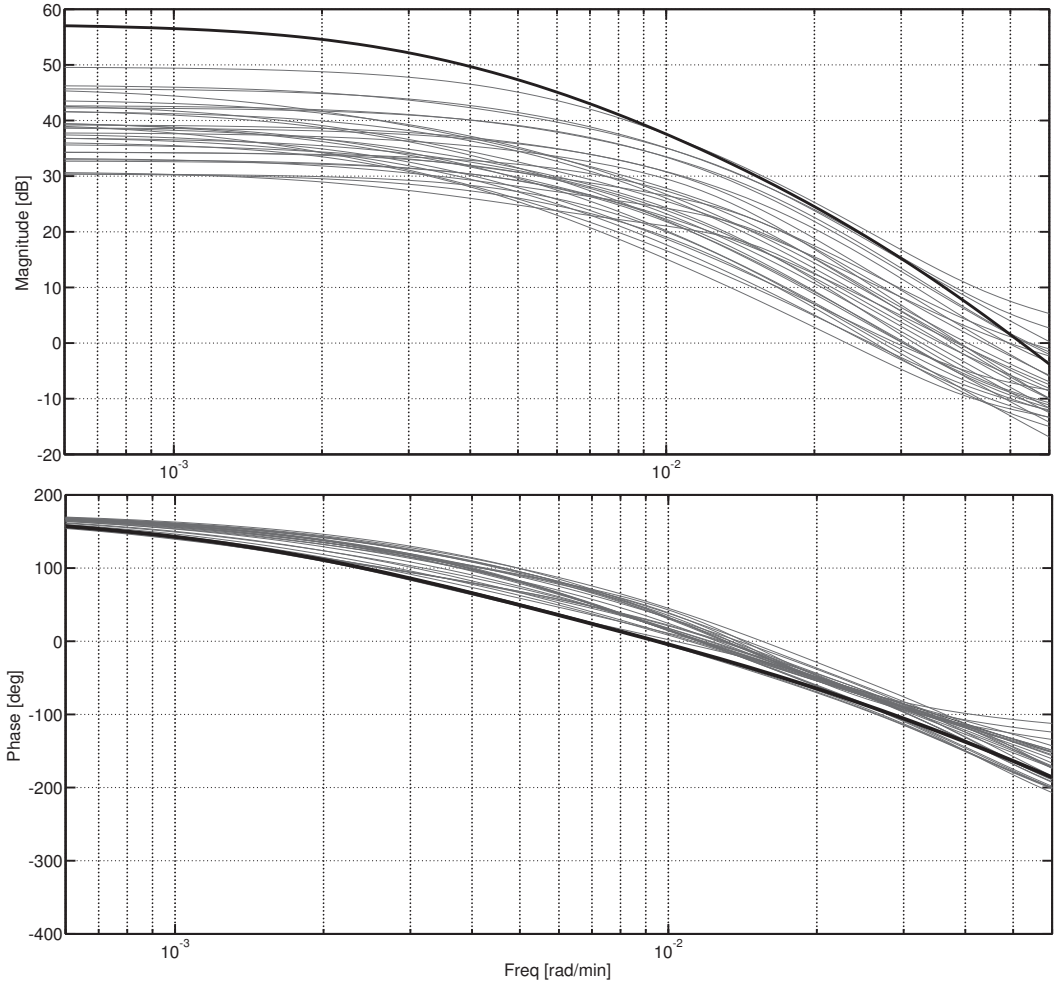

FIGURE 4.1: Bode diagram of all 10 virtual adult patients at three different glucose levels (thin lines) and $G_0(z)$.

time of $T_s = 10$ min, this signal is infused through a CSII pump, and the glucose deviation is captured.

Third-order models were obtained in all 30 cases using subspace identification algorithms [125], [126]. Considering these models, the following discrete-time transfer function is defined:

$$G_0(z) = -\frac{c_0 z^{-3}}{(1 - z^{-1}p_1)(1 - z^{-1}p_2)(1 - z^{-1}p_3)} \tag{4.1}$$

where $c_0 = 0.132$ and the poles are: $p_1 = 0.965$, $p_2 = 0.95$ and $p_3 = 0.93$. Figure 4.1 depicts the Bode diagrams of $G_0(z)$ and all identified models. The gain of $G_0(z)$ is intentionally overestimated, and its phase is purposefully chosen lower than the phase of all identified models, in order to obtain robust controllers as in [124]. From previous experience, a

controller based on this *nominal* model could be too conservative and consequently may lead to poor performance. In order to limit this conservatism, an individualised transfer function $G_{0,j}(z)$ is defined:

$$G_{0,j}(z) = -\frac{cr_j z^{-3}}{(1-z^{-1}p_1)(1-z^{-1}p_2)(1-z^{-1}p_3)}. \tag{4.2}$$

Here, as in [124], $r_{\mathrm{j}} = 1800/\mathrm{TDI}_j$ is based on the *1800 rule* (see [127]) and represents the gain, which adapts to the patient's TDI, where the TDI of the patient with index j is denoted by TDI_j, and

$$c = \frac{60}{100}\,(1-p_3)(1-p_2)(1-p_1)T_s \tag{4.3}$$

is a constant that scales units. Therefore, cr_j is adapted to each patient instead of using the constant value c_0.

4.3 Controller Design

The glucose controller consists of 3 parts:

1. an $\mathcal{H}_\infty$ controller;
2. a SM;
3. an IFL.

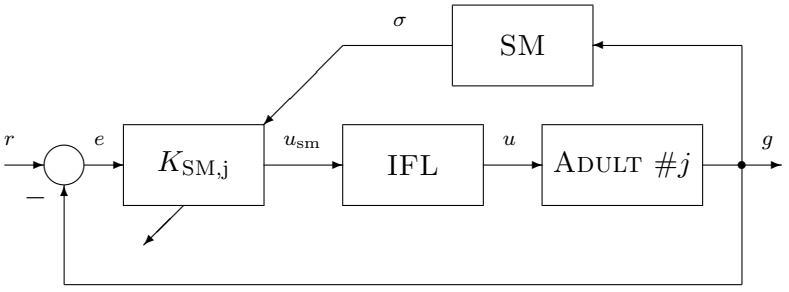

FIGURE 4.2: Block diagram of the closed-loop.

A schematic of the closed-loop system, considering one adult from the simulator database, is depicted in Fig. 4.2, in which $K_{\mathrm{SM},j}$ is the $\mathcal{H}_\infty$ controller modified by the SM, g is the

measured glucose concentration, u_{sm} is the control signal proposed by $K_{\text{SM},j}$, u is the insulin input that is finally commanded to the CSII pump, r and e are, respectively, the reference and error signals, and σ is a switching signal, which is defined in Section 4.3.2.

4.3.1 $\mathcal{H}_\infty$ Controller

$\mathcal{H}_\infty$ has proven to be a practical controller synthesis approach when using LTI plant models. The low order robust controller characterised by $\mathcal{H}_\infty$ naturally performs an effective tradeoff between the strength of control action and the tracking error. This compromise is known as the *mixed-sensitivity* problem and the optimal solution in terms of the lowest gain between the input disturbance and the output errors is achieved by this optimal control procedure.

Consider Adult $\#j$ from the simulator database and let $G_{0,j}(z)$ be its nominal model. A discrete $\mathcal{H}_\infty$ controller K_j is synthesised solving a mixed-sensitivity problem with a performance objective as the one defined in Eqn. 3.10:

$$\min \left\{ \gamma \text{ such that } \left\| \begin{bmatrix} W_{\text{p}}(z) S_{0,j}(z) \\ W_{\Delta,j}(z) K_j(z) S_{0,j}(z) \end{bmatrix} \right\|_\infty < \gamma \right\}. \tag{4.4}$$

Here, $S_{0,j}(z) = (1 + G_{0,j}(z)K_j(z))^{-1}$ is the sensitivity function, $W_{\text{p}}(z)$ and $W_{\Delta,j}(z)$ are the performance and control weights, respectively, and the sample-period is 10 min.

To reduce the risk of hypoglycaemia, $W_{\Delta,j}(z)$ resembles a derivative in order to penalise fast changes in the insulin delivery. Regarding $W_{\text{p}}(z)$, it is chosen to be close to an integrator, i.e., large at low frequencies, to induce fast tracking of the safe blood glucose levels.

In all cases, $W_{\text{p}}(z)$ and $W_{\Delta,j}(z)$ are as follows:

$$W_{\text{p}}(z) = \frac{0.01434z - 0.01365}{z - 0.9993} \tag{4.5}$$

$$W_{\Delta,j}(z) = \text{IS}_j \times \frac{0.001992(z-1)}{z - 0.992} \tag{4.6}$$

where IS_j is the individualised gain based on the subject's sensitivity to insulin, which is related to the following *a priori* clinical information:

- the average TDI regimen, in units of insulin;

- the Correction Factor (CF), which is the maximum drop in mg/dl per unit of insulin;
- the Carbohydrate Ratio (CR), which is used to compute the meal bolus as a function of the meal size.

IS values greater than unity are desired for patients with high insulin sensitivity, in order to increase the weighting on the control signal, and thereby reduce the amount of insulin infused. In general:

$$\downarrow \text{TDI and} \uparrow \{\text{CF, CR}\} \Rightarrow \uparrow \text{insulin sensitivity} \Rightarrow \text{IS} > 1$$

and vice versa. It means that low TDI and high CF and CR are likely related to patients with high insulin sensitivity and therefore, IS should be defined greater than unity, and vice versa. In order to quantify the effect of CR and CF, we define $C_{\text{av}} = \alpha\text{CR} + \beta\text{CF}$, with $\alpha \geq 0$, $\beta \geq 0$, and $\alpha + \beta = 1$. Units of α and β are [U/g] and [UdL/mg], respectively. Here, the solution is obtained choosing $\alpha = 0.5$ U/g, and $\beta = 0.5$ UdL/mg. However, if one coefficient (CR or CF) needs to be emphasised because it is more important or accurate than the other, then α and β can be selected with different weightings.

The TDI and the C_{av} of an adult from the simulator database, should be selected as the reference values: TDI_r, C_avr and $\text{IS}_\text{r} = 1$. Due to the fact that both the patient's model and also its design weight $W_{\Delta,j}(z)$ both depend on its *a priori* TDI_j, any adult from the database can be selected as the reference. Without loss of generality, patient #9 has been considered as a starting point. Finally, for Adult #j the IS_j is calculated as follows:

$$\text{IS}_j = \frac{\text{TDI}_\text{r}}{\text{TDI}_j}\frac{\text{C}_{\text{av}j}}{\text{C}_\text{avr}}. \tag{4.7}$$

Therefore, if Adult #j is likely to be more sensitive to insulin than Adult #9, IS_j will be greater than unity, otherwise it will be less than unity.

4.3.2 Safety Mechanism

In order to reduce the risk of hypoglycaemia and hyperglycaemia, a SM is included to modify the $\mathcal{H}_\infty$ controller output (u_K). As shown in Fig. 4.3, the SM is composed of a Decision Algorithm (DA) and 2 prediction strategies:

- Linear Extrapolation (E) to predict future glucose levels considering the last 3 glucose measurements;
- Kalman Filtering (F) to predict the levels, rates of change, and acceleration, of future glucose concentrations.

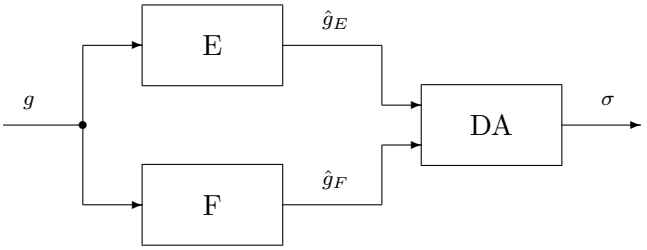

FIGURE 4.3: Block diagram of the SM including the decision (DA) and prediction (E and F) algorithms.

Any one prediction strategy has disadvantages compared to others, and a safety module based on only one single strategy would suffer from these weaknesses as a consequence. In this work the use of parallel prediction strategies E and F, in conjunction with a DA, allows us to exploit the strengths of the individual algorithms, to better predict dangerous future glucose scenarios and thereby to create a more robust system [128].

Both E and F have a sample-period of 10 min and a forecasting horizon of 20 min. In [128] a similar approach is presented, but considering a greater number of prediction algorithms and a different DA. Here, the SM process can be described as follows.

- At every sampling time k, the glucose is measured (g) and the prediction algorithms estimate the future glucose level ($\hat{g}$). According to the following 4 regions:
  - Region λ_1: $\hat{g} < 90$ mg/dl
  - Region λ_2: $90 \leq \hat{g} \leq 110$ mg/dl
  - Region λ_3: $110 < \hat{g} \leq 220$ mg/dl
  - Region λ_4: $\hat{g} > 220$ mg/dl

  the DA defines the variables

$$n_{i,p,k} = \begin{cases} 1 & \text{if } \hat{g}_{p,k} \ \epsilon \text{ Region } \lambda_i \\ 0 & \text{otherwise} \end{cases}$$

$\forall\, i \,\epsilon\, \{1, ..., 4\}$ and $p \,\epsilon\, \{E, F\}$. The variable $\hat{g}_{p,k}$ represents the estimated glucose value at step $k + 2$ (twenty minutes later) by the prediction algorithm p as predicted at actual step k.

- Finally, the switching signal σ is defined in the following Matlab-like code.

---

if $n_{1,F} \geq 1$ && $n_{1,E} \geq 1$ || $g < 90$ mg/dl
  $\sigma = 1$;
elseif $n_2 \geq n_3$ && $n_2 > 0$
  $\sigma = 2$;
elseif $n_3 \geq n_4$ && $n_3 > 0$
  $\sigma = 3$;
else
  $\sigma = 4$;
end
$u_{\text{sm}} = \rho_\sigma u_K$;

---

where $n_i = \sum_{p,m} n_{i,p,m}$, $n_{i,p} = \sum_m n_{i,p,m}$, $\rho_1 = 0$, $\rho_2 = 0.5$, $\rho_3 = 1$, $\rho_4 = 1.25$ and $m = \{k-2, k-1, k\}$.

Therefore, if low glucose values are predicted, the insulin delivery is either suspended or attenuated. On the other hand, if high glucose values are predicted, the insulin delivery proposed by the $\mathcal{H}_\infty$ controller is increased.

4.3.3 Insulin Feedback Loop

The main risks of insulin therapy are an overdose of insulin and a high level of IOB in the body. An estimate of IOB is made and employed to prevent insulin stacking due to frequent insulin boluses. Therefore, an IFL as shown in Fig. 4.4 is included at the $K_{\text{SM},j}$ output to inhibit the insulin infusion when the plasma insulin concentration is estimated to be excessive [121, 122]. The SIM block is the Subcutaneous Insulin Model presented in Section 2.3 and employs the mean population values for all its parameters. The model is discretised with a sample-period of 10 min and it is used to estimate the plasma insulin relative to the basal conditions. The parameter μ is $\frac{\zeta(I_{pe}-I_{pb})}{I_{pb}}$, where I_{pe} and I_{pb} are the estimated current and basal plasma insulin levels, respectively, and ζ is a tuning gain, fixed to 7.5

for all subjects according to the magnitude of the signals involved and the desired closed-loop performance. Its selection depends on the compromise between having a slow (high ζ) or a more aggressive and fast (low ζ) response, after verifying the closed-loop stability. Consequently, if the estimated insulin concentration is higher than its nominal value the control signal is reduced by an amount proportional to that difference.

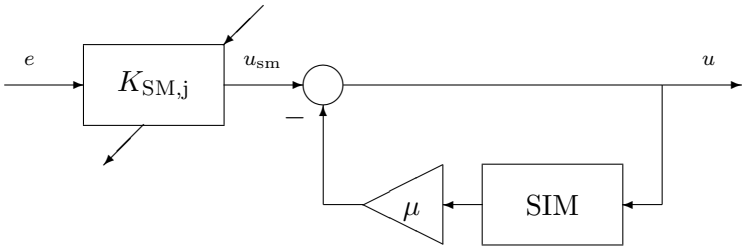

FIGURE 4.4: Block diagram of $K_{\mathrm{SM,j}}$ and the IFL.

4.4 Results

The complete UVA/Padova T1DM simulator, which is accepted by the FDA in lieu of animal trials in the development of an artificial pancreas [74], is used to test the closed-loop performance.

Simulations are performed for all 101 *in silico* adults (one is an average patient), considering unannounced meals, a CSII pump, CGM as sensor, and two different protocols, which are presented in Table 4.1. Protocol #1 includes three meals per day, while protocol #2 is used to evaluate the safety of the algorithm when long fasting periods appear. In addition, in both protocols the simulation starts in the fasting state of each subject, and the basal insulin is infused during the first 4 hours. Then, the glucose controller takes over the insulin delivery considering a constant setpoint. A postprandial period (PP) is defined as the 5 hour time interval following the start of a meal, and night (N) is defined as the period from 00:00 to 7:00 AM.

	Breakfast 1		**Lunch 1**		**Dinner 1**		**Breakfast 2**		**Lunch 2**		**Dinner 2**		**Breakfast 3**		**Lunch 3**		**Dinner 3**	
	Time	**gCHO**	**Time**	**gCHO**	**Time**	**gCHO**	**Time**	**gCHO**	**Time**	**gCHO**	**Time**	**gCHO**	**Time**	**gCHO**	**Time**	**gCHO**	**Time**	**gCHO**
#1	7 AM	50	2 PM	60	8 PM	50	6 AM	50	1 PM	70	7 PM	50	7 AM	50	1 PM	65	9 PM	55
#2	7 AM	50	-	-	8 PM	60	-	-	12 PM	55	9 PM	50	7 AM	50	2 PM	55	8 PM	50

TABLE 4.1: Protocol #1 and #2. Here gCHO stands for grams of carbohydrates.

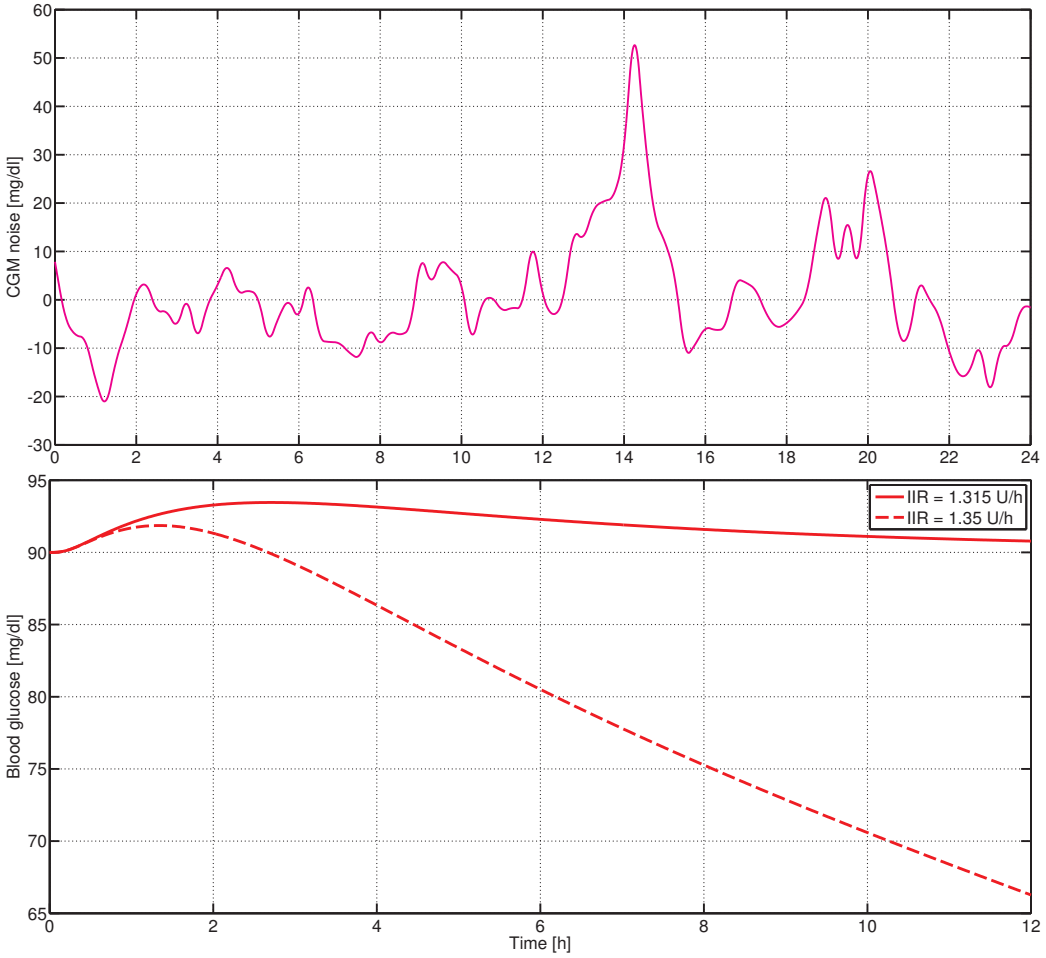

FIGURE 4.5: Simulation of CGM noise (above) and subject's sensitivity to insulin (below).

There are various issues that the glucose controller has to manage. Simulation examples of the high measurement noise and subject's sensitivity to insulin are depicted in Fig. 4.5. In order to represent the latter, Adult #7 of the T1DM simulator is considered. As shown in the aforementioned figure, when the insulin infusion rate is 1.315 U/h, the blood glucose level tends to 90 mg/dl. On the other hand, when the insulin infusion rate is 1.35 U/h, the blood glucose level decreases below 70 mg/dl. Note that, the difference between the two infusion rates is 0.035 U/h, while an insulet Omnipod has a 0.05 U/h increment. This means that small errors in the infusion rate may lead to hypoglycaemic events.

The glucose responses to protocol #1 are depicted in Fig. 4.6, employing differing colors to differentiate between risky and safe situations. Note that the glucose graph is mainly green and the insulin graph blue, which means that glucose levels are mostly near the safe values, and that the insulin injection is generally low.

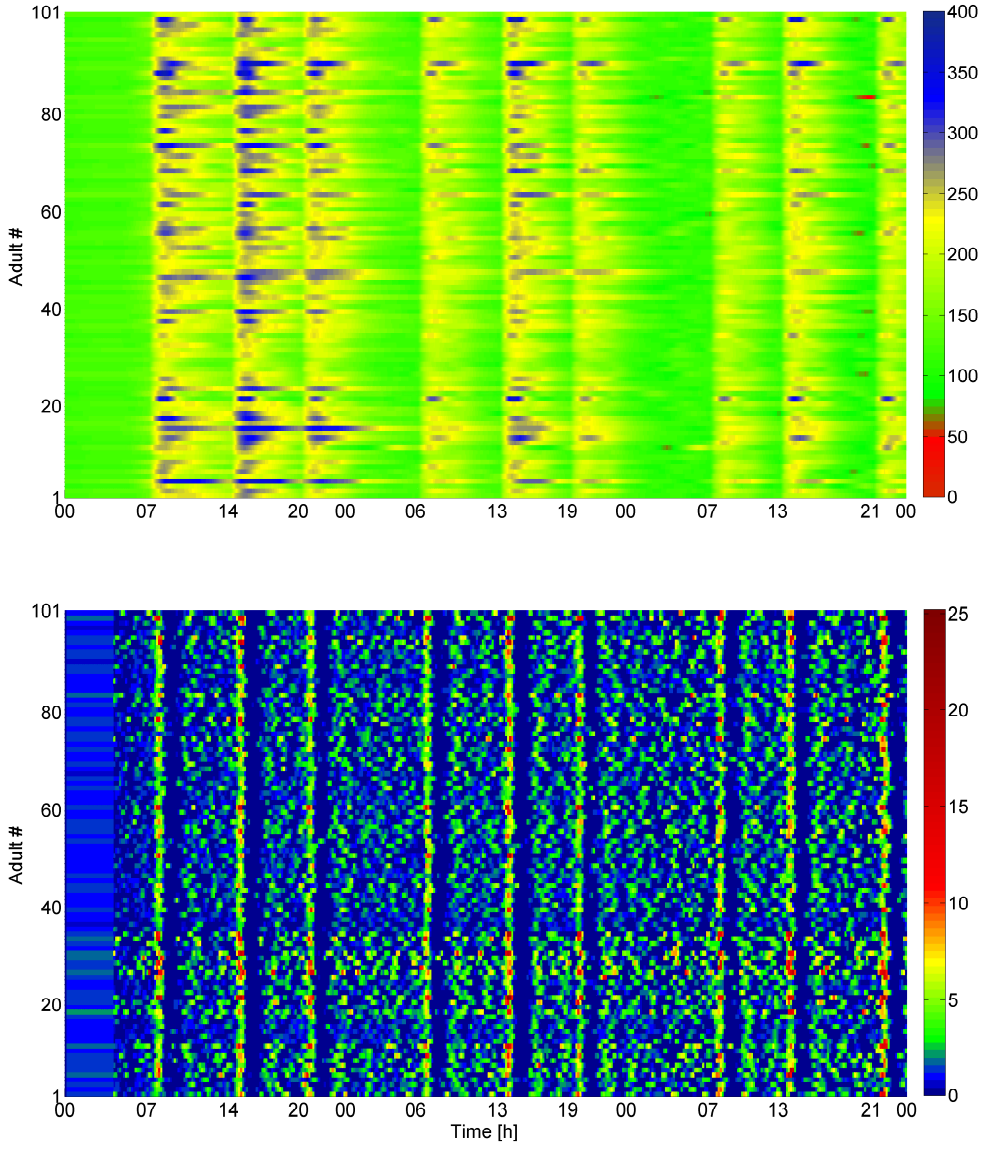

FIGURE 4.6: Closed-loop responses for the 101 *in silico* adults to protocol #1. Above: Blood glucose [mg/dl]. Below: Insulin [U/h].

The average time responses to both protocols are depicted in Fig. 4.7. As shown in that figure, large insulin spikes appear after meals. Then, the insulin infused is reduced and thereafter, a constant amount of insulin is administered on average.

The CVGA and the average results for both protocols are presented in Fig. 4.8 and Table 4.2, respectively. In Table 4.2 the overall (O), PP and N time intervals are analysed separately. Because of the high measurement noise[2], a reduced closed-loop bandwidth has

[2]In [74] it is anticipated that the real sensor errors would tend to be smaller during controlled inpatient clinical trials.

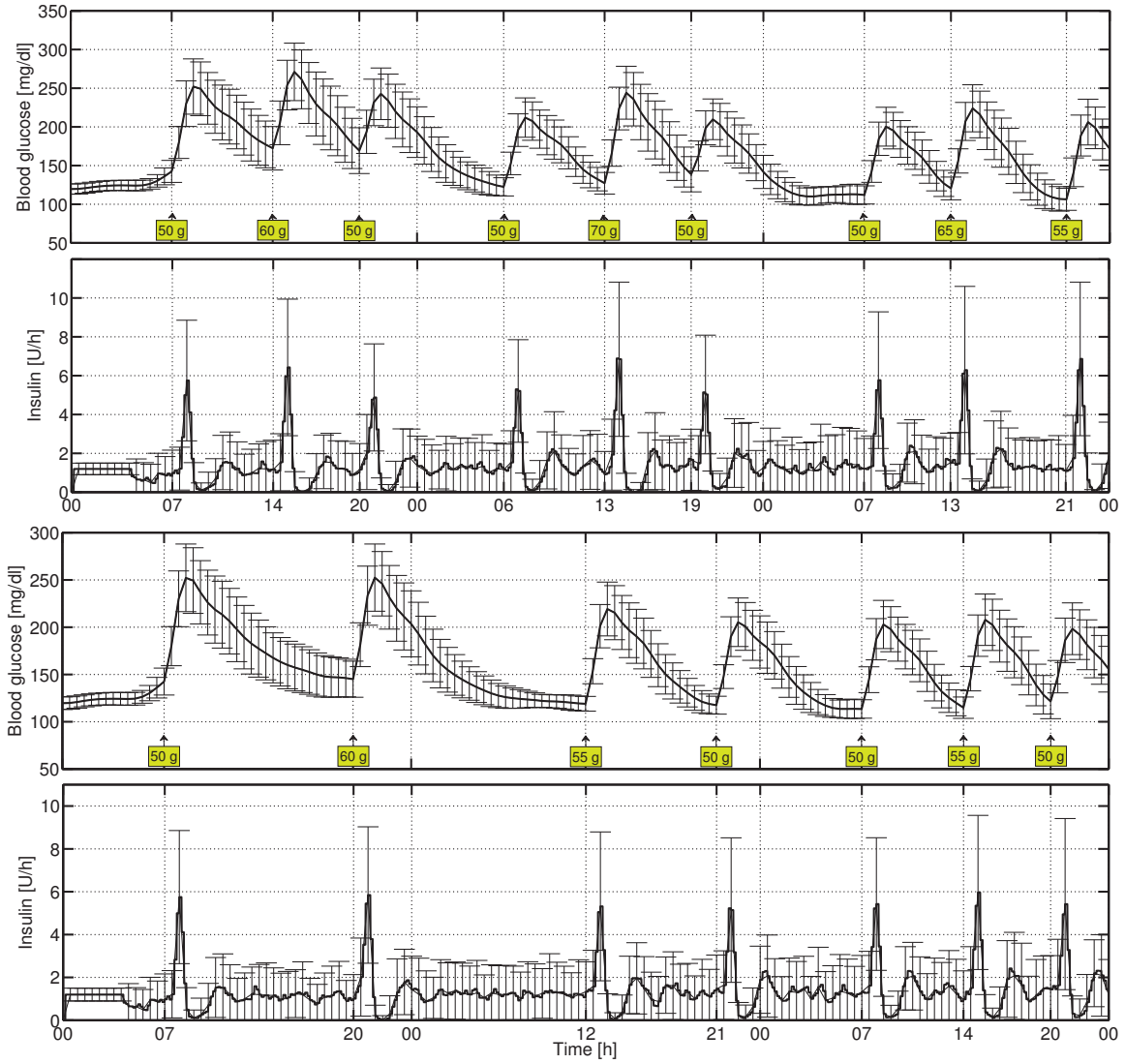

FIGURE 4.7: Average closed-loop responses for the 101 *in silico* adults to protocol #1 (above) and to protocol #2 (below). The mean ±1 STD values are represented by vertical bars, every 30 minutes.

been proposed. Therefore, higher blood glucose peaks appear during the first day of trial due to the lack of insulin. Consequently, and furthermore because each day of the protocol has similarly sized meals, both the CVGA plot, as well as the average results, related to protocol #1 are computed based on the results of the third day. The average time response to that day is depicted in Fig. 4.9. On the other hand, the CVGA plot and the average results related to protocol #2 are obtained considering the data from the second day, to include its long fasting period.

As shown in Table 4.2, for both protocols the proposed controller achieves meal glucose

Protocol		#1	#2
Mean BG [mg/dl]	**O**	148	154
	PP	176	177
	N	116	135
Max BG [mg/dl]	**O**	226	220
	PP	229	224
	N	142	183
Min BG [mg/dl]	**O**	96	108
	PP	108	114
	N	100	107
% time in [70 180] mg/dl	**O**	75.9	75.5
	PP	54.2	54.4
	N	99.5	91.4
% time > 300 mg/dl	**O**	0.1	0.0
	PP	0.3	0.1
	N	0.0	0.0
% time > 180 mg/dl	**O**	24.0	24.5
	PP	45.8	45.6
	N	0.4	8.6
% time < 70 mg/dl	**O**	0.1	0.0
	PP	0.0	0.0
	N	0.0	0.0
LBGI		0.1	0.0
HBGI		4.3	4.6
TDI [U]		30.8	29.3

TABLE 4.2: Average results for the 101 adults to protocol #1 and #2.

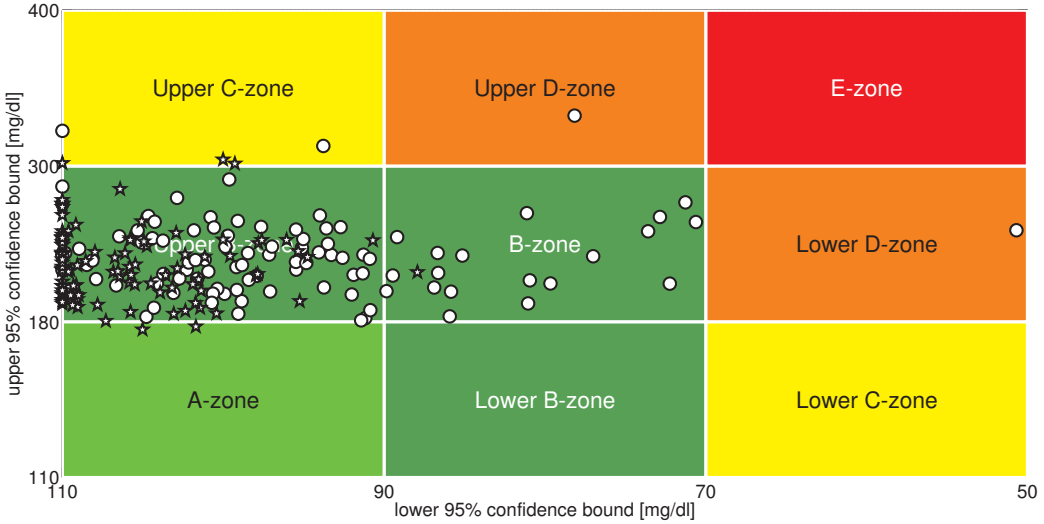

FIGURE 4.8: CVGA of all the 101 closed-loop responses to protocol #1 (circles) and protocol #2 (stars).

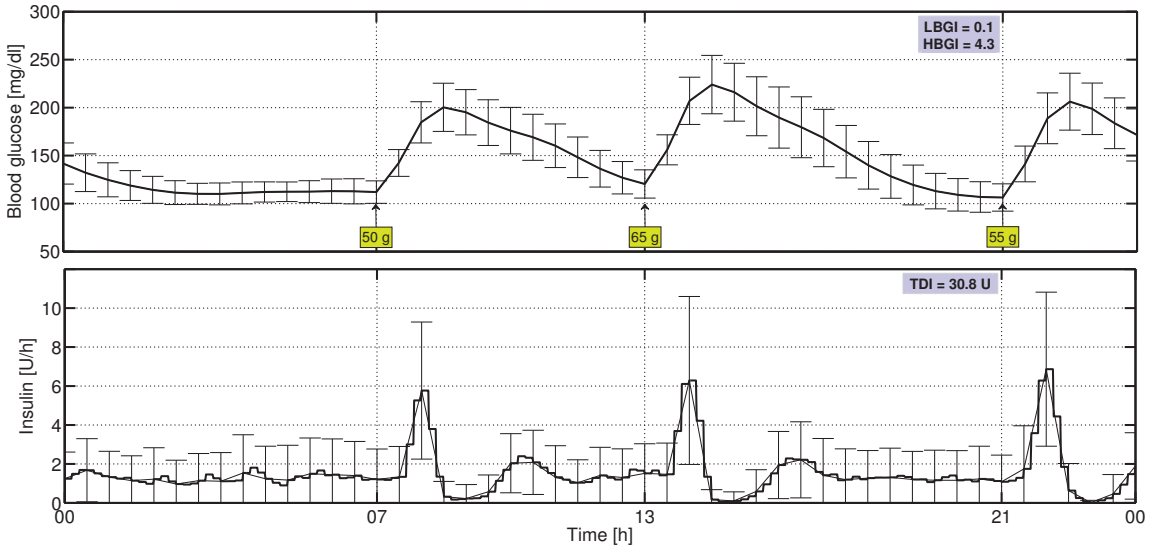

FIGURE 4.9: Average closed-loop response for the 101 *in silico* adults to the third day of protocol #1. The mean ±1 STD values are represented by vertical bars, every 30 minutes.

values that are less than, or equal to, 154 mg/dl, which is in accordance with recommendations made by the ADA [9]. Therefore, due to the fact that hypoglycaemia occurs only for one subject, we conclude that safe hyperglycaemic control has been achieved.

Although meals are unannounced and there is not any particular adjustment for any patient, besides the automatic one at the controller design stage, a minimal High BG Index (HBGI < 5.0) and a minimal Low BG Index (LBGI < 1.1) were achieved in both protocols.

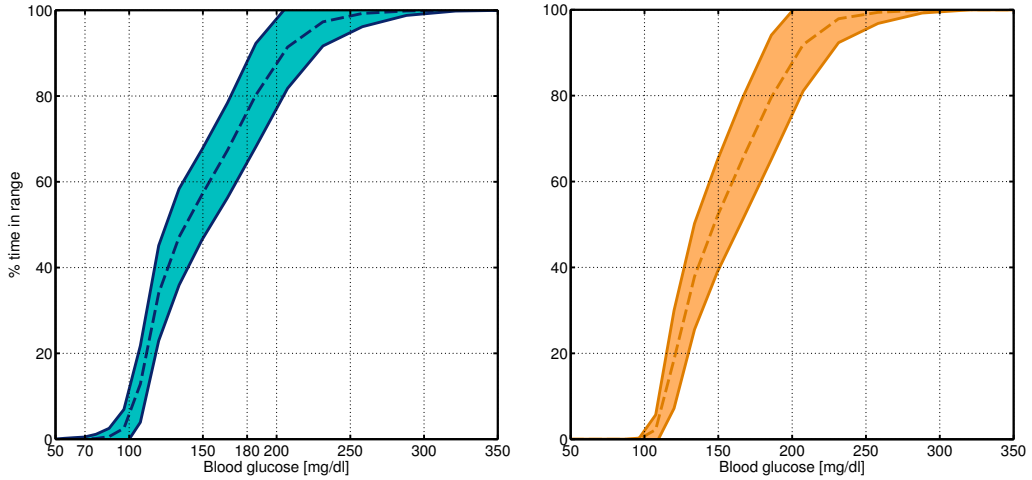

FIGURE 4.10: Average cumulative time in range to protocol #1 (left) and #2 (right). The mean ±1 STD values are represented by the filled areas.

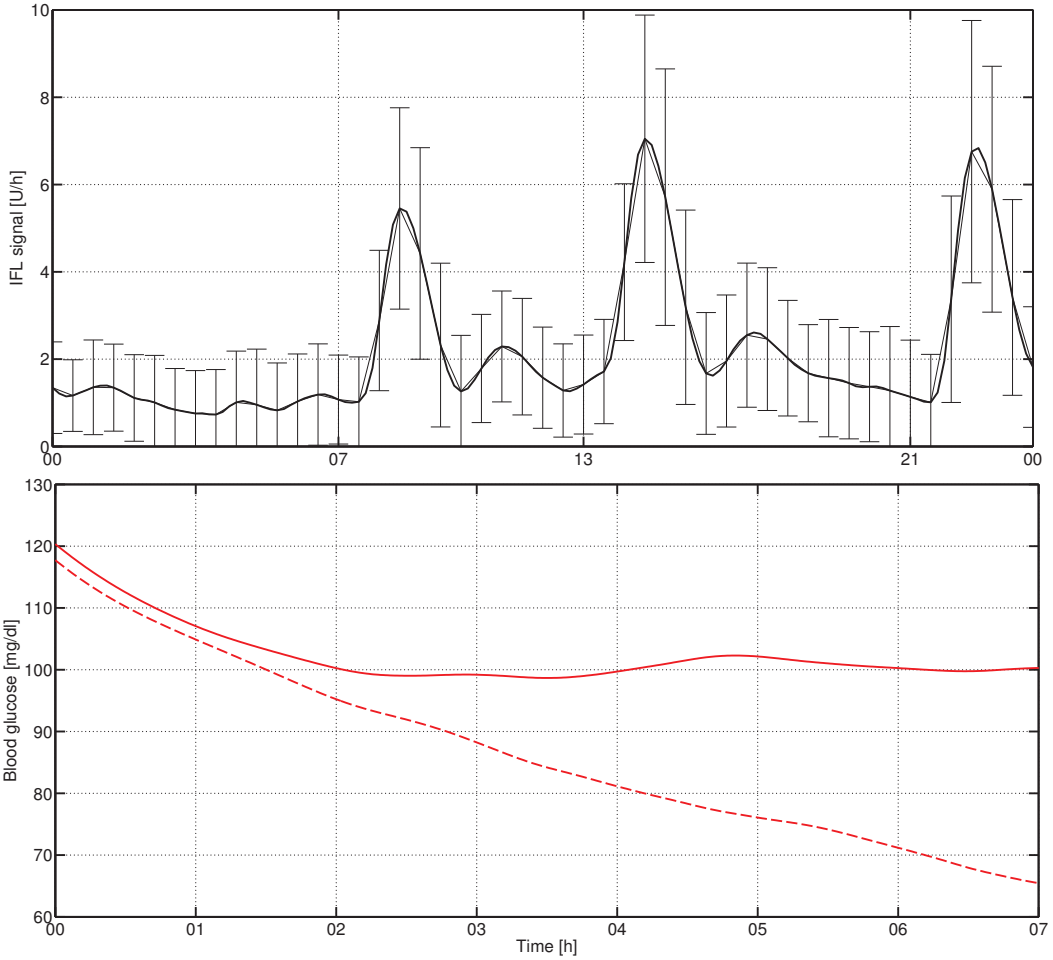

FIGURE 4.11: Above: Average IFL signal for the 101 *in silico* adults to the third day of protocol #1. The mean ± 1 STD bar is plotted every 30 minutes. Below: The mean minus one STD value of the 101 closed-loop night response to protocol #1 with (continuous line) and without (dashed line) the SM.

In order to reflect how the IFL helps to avoid postprandial hypoglycaemia, the IFL signal obtained considering the last day of protocol #1 is depicted in Fig. 4.11. As was mentioned above, a large insulin spike appears after a meal. Consequently, as u_{ifl} starts to increase the insulin infused $u = u_{\text{sm}} - u_{\text{ifl}}$ starts to be reduced. This process avoids insulin overdosing, and therefore mitigates postprandial hypoglycaemia. The usefulness of the SM is also reflected in Fig. 4.11. For protocol #1, the mean minus one STD value obtained every 30 minutes for all 101 adults, both with and without the SM, are compared. As illustrated, the SM assists the algorithm in preventing low glucose outcomes. For how long each value of σ is selected is represented in Fig. 4.12. According to this figure, the algorithm settles on $\sigma = 3$, the unscaled $\mathcal{H}_\infty$ controller, more than 70% of the time in both protocols. The last situation is also reflected in Table 4.2 and Fig. 4.10 in which the percentages of time in the range

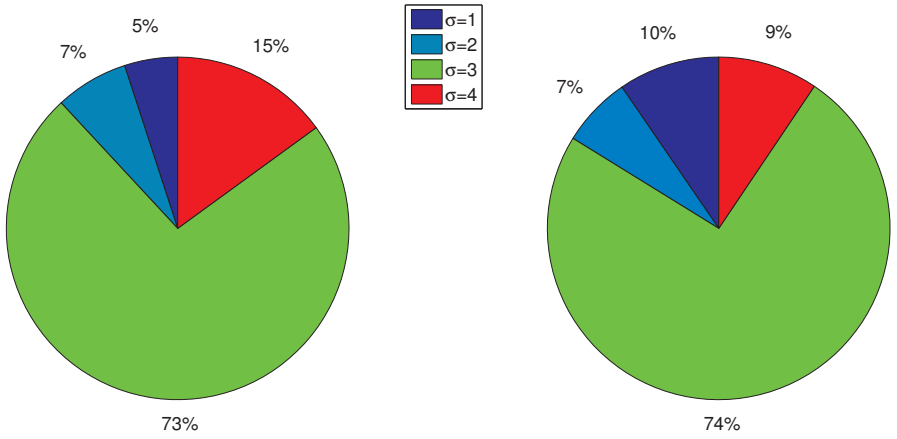

FIGURE 4.12: Percentage of time each value of σ is selected. Left: protocol #1. Right: protocol #2.

[70, 180] mg/dl are presented. This is a desirable situation, because the selection of this control implies that the glucose values tend to remain in a safe region. Hence, according to the results obtained, it could be concluded that a safe hyper- and hypoglycaemia blood glucose control has been achieved. Because the UVA/Padova metabolic simulator does not include intra-patient variations, that scenario could not be tested. However, the PA has proved robust to large inter-patient variations. In addition, parameter IS_j could also be modified to a controller that is either more, or less, aggressive, depending on whether the subject's sensitivity to insulin changed drastically over time. Finally, results for the standard open-loop basal-bolus treatment, with boluses delivered at the time of meal ingestion, are

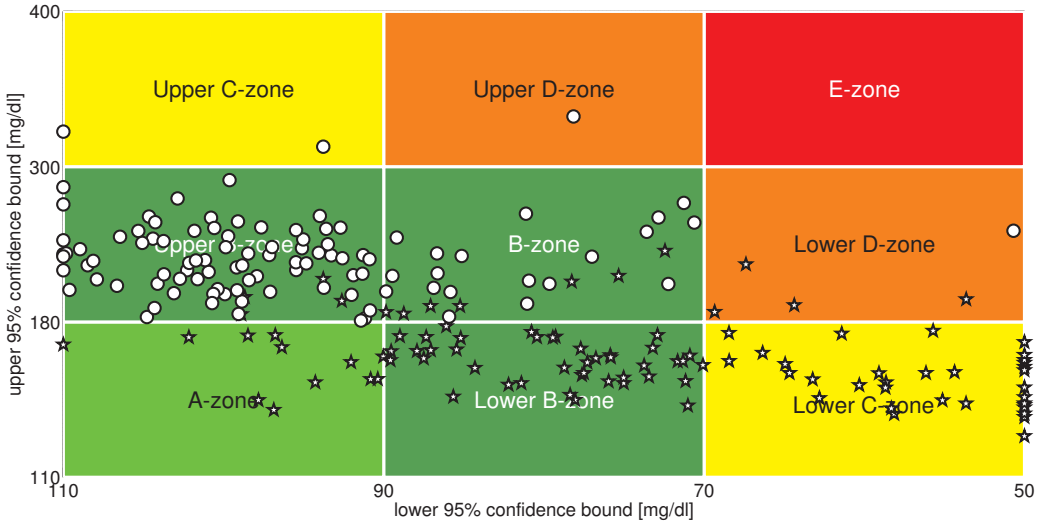

FIGURE 4.13: CVGA of all the 101 closed-loop responses to protocol #1. (Circles) PA. (Stars) OBT overestimating the bolus sizes by 30%.

Control Strategy		PA	70% of OB	OBT	130% of OB
	O	148	144	127	110
Mean BG [mg/dl]	**PP**	176	165	143	125
	N	116	119	109	99
	O	226	199	175	162
Max BG [mg/dl]	**PP**	229	202	178	164
	N	142	129	117	115
	O	96	115	99	73
Min BG [mg/dl]	**PP**	108	119	105	80
	N	100	115	101	76
	O	75.9	86.5	95.9	92.2
% time in [70 180] mg/dl	**PP**	54.2	73.6	91.8	94.6
	N	99.5	100	100	91.2
	O	0.1	0.0	0.0	0.0
% time > 300 mg/dl	**PP**	0.3	0.0	0.0	0.0
	N	0.0	0.0	0.0	0.0
	O	24.0	13.5	4.1	1.9
% time > 180 mg/dl	**PP**	45.8	26.5	8.2	3.7
	N	0.4	0.0	0.0	0.0
	O	0.1	0.0	0.0	5.9
% time < 70 mg/dl	**PP**	0.0	0.0	0.0	1.7
	N	0.0	0.0	0.0	8.8

TABLE 4.3: Comparison between the average results for the 101 adults to protocol #1 obtained with the PA, with an OBT, with a 30% underestimated OBT, and with a 30% overestimated OBT.

presented in Table 4.3 for comparison. As expected, because the PA considers unannounced meals, better performance is obtained with an OBT. However, in practice the meal is sometimes wrongly estimated, and as a result the bolus size is not appropriate. In order to illustrate the risk of that situation, the CVGA obtained with the PA and with a 30% overestimated OBT is presented in Fig. 4.13.

4.5 Conclusion

A controller structure is designed focused on hyper– and hypoglycaemia protection. The system identification is based on the 10 subject cohort, in order to mimic a reduced spectrum of information present for controller design, and to design a controller that is suitably safe. The robust $\mathcal{H}_\infty$ controller is synthesised via a mixed-sensitivity problem with weights focused on maintaining the glucose level near to the reference value while being cautious with the insulin injection. The IFL is intended as a postprandial hypoglycaemia risk reduction based

on the IOB estimation. Finally, the SM considers an estimation of future glucose levels in order to maintain the patient's glucose concentration in a safe region. The method is practical because it only uses *a priori* patient information that is easily obtainable, and works for both different patients and unannounced meals. For validation purposes, the full cohort of the 101 subject simulator was employed to rigorously test the proposed control strategy, showing good performance and minimal hyper– and hypoglycaemia risks.

Chapter 5

Switched LPV Glucose Control in Type 1 Diabetes

5.1 Motivation

In the previous chapter, a robust $\mathcal{H}_\infty$ controller with a so-called SM and IFL was developed to reduce the risks of hyper- and hypoglycemia in T1DM [129]. A time-varying controller that reproduces this $\mathcal{H}_\infty$ control structure, but in an LPV framework, was presented in [130] and achieved similar results. Here, I continue to pursue the LPV controller framework. The contribution of this chapter is to consider a *switched* LPV controller that switches between a selection of multiple LPV controllers that have been designed for slightly different tasks. Specifically, the possibility of switching between only two LPV controllers is investigated, where one controller is dedicated to dealing with large and persistent hyperglycemic excursions, e.g., as occur after a meal, and the second controller is responsible for glucose control at all other times. The proposed strategy results in a controller that is conservative most of the time but switches into an "aggressive" mode when the need arises. In this chapter the "need" is based purely on CGM feedback, with no need of meal announcement, via an estimator that detects persistent high glucose values. This is akin to the proposal of [131]. However, the notion of switched LPV control can be expanded to other cases, e.g., for the controller to be triggered into a "meal" mode by means of an auxiliary meal-detection algorithm [132,133], or by user notification. In this work simulation scenarios with only unannounced meals are investigated, as this is, in some sense, the most difficult case

with respect to correcting hyperglycemia and preventing controller-induced hypoglycemia. Simulations are performed using the FDA accepted UVA/Padova metabolic simulator [134].

This chapter focuses on switching to improve the controller's response with respect to hyperglycemia. However, the proposed switching strategy is inherently flexible, and extensible to a variety of other scenarios also, e.g., in order to deal strategically with exercise. Analogously as with meal-related hyperglycemia, the proposed switching framework would allow to design to handle hypoglycemia that typically follows exercise, by strategically including modes, e.g., where exercise is inferred from CGM trends, or through an auxiliary exercise detection mechanism, or by user input. However, the exercise component is not explicitly investigated in this chapter, because the FDA accepted UVA/Padova simulator currently has no means of simulating a person's exercise response.

The outcome produces comparable or improved results with respect to previous works, and a very flexible procedure that opens the possibility of taking into account, at the design stage, unannounced meals and/or patients' physical exercise.

5.2 Main Results

Two LPV controllers are designed for each *in silico* Adult $\#j$ of the complete UVA/Padova simulator: $\mathcal{K}_{i,j}$ with $i \in \{1, 2\}$. Controller $\mathcal{K}_{1,j}$ is designed to control most of the time, while $\mathcal{K}_{2,j}$ is applied only when high and rising glucose values are estimated, e.g., after a meal. Because this strategy can estimate decreasing glucose values as well, perturbations like physical exercise may be detected and managed by another controller that was purposefully designed for such situations.

5.2.1 Patient design model

The model structure presented in Section 4 is considered here to design both $\mathcal{K}_{1,j}$ and $\mathcal{K}_{2,j}$. The main advantage of such a model structure is that it can be personalized based solely on *a priori* clinical information that can easily be obtained with high accuracy. Therefore, for each *in silico* Adult $\#j$, the following individualized discrete-time transfer function $G_{i,j}(z)$

from the insulin delivery input to the glucose concentration output is defined:

$$G_{i,j}(z) = -\frac{F_i c r_j z^{-3}}{(1 - z^{-1}p_1)(1 - z^{-1}p_2)(1 - z^{-1}p_3)}, \tag{5.1}$$

where F_i is a design factor (unitless) defined in (5.2) and (5.3), $r_j = 1800/\text{TDI}_j$, which is based on the *1800 rule* [127], adapts the model's gain to the TDI of Adult $\#j$ (TDI_j), $p_1 = 0.965$, $p_2 = 0.95$ and $p_3 = 0.93$ are the poles, and c is a constant that scales units and sets the correct gain. The factor F_i is defined as follows:

$$F_1 = \begin{cases} F_1^\star & \text{if } F_1^\star < 2 \\ 2 & \text{otherwise} \end{cases} \tag{5.2}$$

$$F_2 = \begin{cases} 0.7F_1 & \text{if } F_1 < 1 \\ F_1 & \text{if } F_1 > 2 \\ (0.3F_1 + 0.4)\, F_1 & \text{otherwise} \end{cases} \tag{5.3}$$

where:

$$F_1^\star = \begin{cases} \overline{\text{M}}/\text{M}_j & \text{if } \text{M}_j < \overline{\text{M}} \text{ and } \text{CR}_j < \overline{\text{CR}} \\ \text{CR}_j/\overline{\text{CR}} & \text{if } \text{M}_j > \overline{\text{M}} \text{ and } \text{CR}_j > \overline{\text{CR}} \\ \overline{\text{M}} \cdot \text{CR}_j / \left(\text{M}_j \cdot \overline{\text{CR}}\right) & \text{if } \text{M}_j < \overline{\text{M}} \text{ and } \text{CR}_j > \overline{\text{CR}} \\ 1 & \text{otherwise} \end{cases} \tag{5.4}$$

with M_j and CR_j the body weight and the carbohydrate ratio, respectively, of Adult $\#j$, and with $\overline{\text{M}}$ and $\overline{\text{CR}}$, the mean population values based on the 10 virtual adult patients of the distribution version of the UVA/Padova simulator. This more cautious decision has been made in order not to over-design with respect to the complete simulator. Instead, the TDI is readily and accurately obtainable from subjects, hence in that case, the value is based on the complete cohort of adults.

The factor F_1 is defined to make a finer adjustment to the model's gain, including the effect of both M and CR. Thus, patients with low M and high CR are associated with an F_1 value greater than unity, and therefore, with a more conservative model. On the other

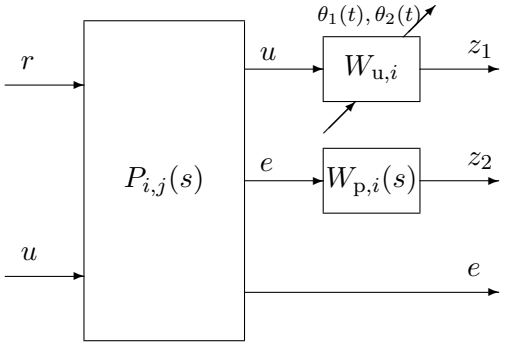

FIGURE 5.1: Augmented model for controller design.

hand, F_2 is intentionally smaller than F_1 in order to obtain a more aggressive control law when high and rising glucose levels are detected. However, according to the definition of F_2, the more sensitive to insulin the patient, the more conservative the model, and, therefore, the less aggressive the control law. For example, if $F_1 > 2$, the model's gain is not reduced to design $\mathcal{K}_{2,j}$.

5.2.2 Controller Design

Here, the Matlab Robust Control Toolbox$^{\mathrm{TM}}$ was used to compute the controllers. Because that toolbox provides a solution only to the continuous-time LPV control synthesis problem, the discrete-time plant model $G_{i,j}(z)$ is converted to the continuous-time plant model $G_{i,j}(s)$ at the design stage. However, the desired control system operates in discrete-time, therefore the derived continuous-time control law is converted to a discrete-time control law later, prior to implementation.

The augmented continuous-time model for controller design is depicted in Fig. 5.1, where:

$$P_{i,j}(s) = \begin{bmatrix} 0 & 1 \\ 1 & -G_{i,j}(s) \\ 1 & -G_{i,j}(s) \end{bmatrix}, \tag{5.5}$$

r and e are, respectively, the reference and error signals, u is the control action, and $W_{\mathrm{u},i}$ and $W_{\mathrm{p},i}(s)$ are the design weights. As shown in Fig. 5.1, two parameters have been included in each augmented model in order to adapt the controller during the closed-loop implementation. The time-varying parameters are $\theta_1(t) = \frac{110 \text{ mg/dl}}{g(t)}$ and $\theta_2(t) = \frac{i_{pe}(t)}{i_{pb}}$. The

first parameter is real-time measurable and depends on the glucose level $g(t)$ measured by the CGM. The second parameter depends on $[i_{pe}(t), i_{pb}]$, which are the estimated current and basal plasma insulin levels, respectively. The estimation is performed through the subcutaneous insulin model proposed in [4], considering its mean population values. In the case of $i_{pe}(t)$, the input to the model is the current injected insulin, and in the case of i_{pb}, the basal insulin dosage. Note that i_{pb} can be obtained off-line, before the simulation.

In order to design both LPV controllers, the performance and actuator weights, which are closely related to the ones presented in Chapter 4, are defined as follows:

$$W_{\mathrm{p},i}(s) = \alpha \frac{sT_1 + 1}{sT_2 + A_i}, \tag{5.6}$$

$$\begin{aligned} W_{\mathrm{u},i} =: & \left[\begin{array}{cc|c} \begin{bmatrix} 0 & 1 \\ -\frac{1}{R_2^2} & -\frac{2}{R_2} \end{bmatrix} & & \begin{bmatrix} 0 \\ 1 \end{bmatrix} \\ \hline \frac{[\theta_1(t)+\theta_2(t)]R_{1,i}}{2R_2^2} \begin{bmatrix} 0 & 1 \end{bmatrix} & & 0 \end{array}\right] \\ =: & \left[\begin{array}{c|c} A_{\mathrm{u},i} & B_{\mathrm{u},i} \\ \hline C_{\mathrm{u},i}(t) & 0 \end{array}\right] \end{aligned} \tag{5.7}$$

with $T_1 = 200$, $T_2 = 10^5/7$, $A_i = \{8, 7\}$, $\alpha = 3$, $R_{1,i} = \{1/4, 1/8\}$ and $R_2 = 10^4/18$. Here $C_{\mathrm{u},i}(t)$ is linear in the time-varying parameters, therefore, as they increase, $W_{u,i}$ forces a less aggressive control. According to these parameters, both design weights related to $\mathcal{K}_{2,j}$ are defined slightly less conservatively than those related to $\mathcal{K}_{1,j}$. The weight $W_{\mathrm{p},i}(s)$ is chosen to be a low-pass filter to induce fast tracking of the safe blood glucose levels. On the other hand, note that in the case of time invariant $\theta_1(t) = \theta_1(0) = \theta_{10}$ and $\theta_2(t) = \theta_2(0) = \theta_{20}$ $\forall t \in [0, \infty)$, then:

$$W_{\mathrm{u},i}(s) = (\theta_{10} + \theta_{20}) \frac{sR_{1,i}}{2\left(R_2 s + 1\right)^2} \tag{5.8}$$

is LTI and resembles a derivative at low frequencies. Therefore, it helps to penalize fast changes in the insulin delivery. In addition, the model is strictly proper, in order to have the closed-loop system affine in the time-varying parameters.

The parameter $\theta(t) = [\theta_1(t),\, \theta_2(t)]^T$ is constrained to lie within the rectangular sets $\mathcal{P}_1 = [0.2, 5] \times [0, 8]$ and $\mathcal{P}_2 = [0.2, 1] \times [0, 8]$ for $\mathcal{K}_{1,j}$ and $\mathcal{K}_{2,j}$, respectively, according to the expected values of $g(t)$ and $i_{pe}(t)$. Therefore, both sets $\mathcal{P}_1$ and $\mathcal{P}_2$, which are depicted in

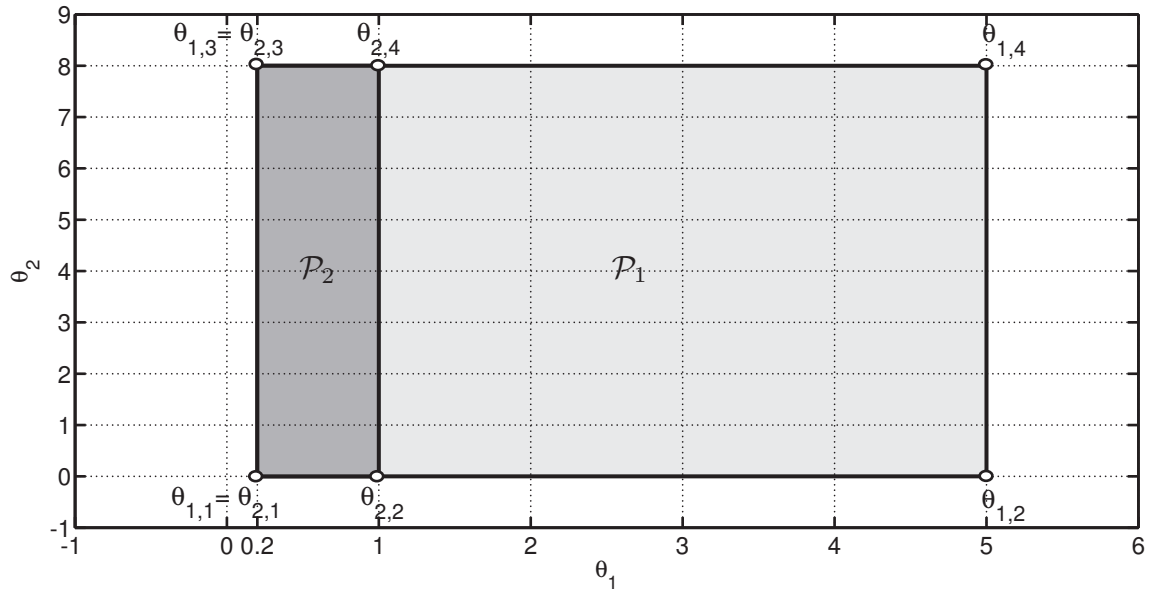

FIGURE 5.2: Glucose-insulin regions $\mathcal{P}_1$ and $\mathcal{P}_2$.

Fig. 5.2, have $v = 4$ vertices. An increase in $\theta_1(t)$ due to a low glucose level and/or in $\theta_2(t)$ due to a high level of IOB will reduce fast and aggressive increases in insulin injection.

Because the augmented open-loop model matrices (see Fig. 5.1 and Eqns. (5.6) and (5.7)) depend affinely on the parameter $\theta(t) = [\theta_1(t),\ \theta_2(t)]^T$, and that the parameter regions are convex polytopes with a finite number of vertices (see Fig. 5.2), the optimization problem related to the LPV controller synthesis can be stated in terms of a finite number of Linear Matrix Inequalities (LMIs). Specifically, for each LPV controller, the problem is solved in terms of $2v + 1$ LMIs, i.e., a common Single Quadratic Lyapunov Function (SQLF) for each set of $v = 4$ vertices. Note that the vertex controllers can be synthesized off-line.

During the implementation phase, the two LPV controllers for $i = 1, 2$ can be computed as follows:

$$\mathcal{K}_{i,j}[\theta(t)] = \sum_{\ell=1}^{v} \eta_\ell(t)\mathcal{K}_{i,j}(\theta_{i,\ell}) \tag{5.9}$$

with

$$\theta(t) = \sum_{\ell=1}^{v} \eta_\ell(t)\theta_{i,\ell} \ \text{ and } \ \sum_{\ell=1}^{v} \eta_\ell(t) = 1, \tag{5.10}$$

where $\eta_\ell(t) \geq 0 \, \forall t \in [0, \infty)$ are the polytopic coordinates of the measured parameter $\theta(t)$, and $\theta_{i,\ell}$ are the vertices of $\mathcal{P}_i$.

One of the problems of the LPV control is known as the "fast poles" problem. By "freezing" any point in the parameter variation set, the resulting LTI model usually presents a small number of poles with a small (i.e., large negative) real part [135, 136]. Fast poles lead to problems from the practical point of view, e.g., integration and/or implementation becomes difficult with these fast dynamics. The approach utilized to deal with these difficulties is LPV pole placement [136]. Through LMI constraints, the objective of the LPV pole placement is to keep the poles of each LTI closed-loop system, resulting from holding the parameter fixed at each point of the parameter variation set, in a prescribed region of the complex plane. Therefore, in order to solve numerical issues in the implementation and/or simulation, for each LPV controller, the (continuous-time) closed-loop poles are constrained to the region $\mathcal{D} = \left\{q \in \mathbb{C} : -\frac{2\pi}{100} < \mathrm{Re}(q) < 0\right\}$, i.e., at least ten times slower than the controller sampling time $T_s = 10$ min.

Before implementation, each polytopic LPV controller is converted to a representation which is affine in the time-varying parameters. Finally, a trapezoidal LPV state-space discretization is applied at the implementation stage (see pp. 143-169, [137]).

5.2.3 Stability and Performance Analysis

Note that the design was performed by computing a SQLF for *each* controller. In order to guarantee closed-loop stability and performance under arbitrary switching amongst controllers, a *common* SQLF is sought for *both* LPV controllers [138].

The block diagram of the closed-loop is depicted in Fig 5.3, where:

$$L_j = \begin{bmatrix} 0 & W_{\mathrm{u},i} \\ W_{\mathrm{p},i} & -W_{\mathrm{p},i} G_{1,j} \\ 1 & -G_{1,j} \end{bmatrix}. \tag{5.11}$$

Only $G_{1,j}(s)$ is considered in the analysis, because it represents the "real" transfer-function ($G_{2,j}(s)$ is a fictitious system) and therefore, describes the patient's glucose-insulin dynamics more accurately.

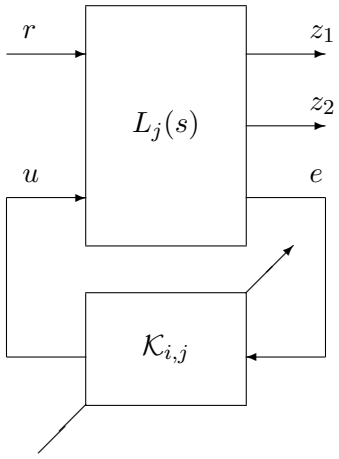

FIGURE 5.3: Feedback interconnection of plant and controller.

To proceed, the following arguments will be used:

- The dependence of the state space matrices of both LPV controllers on the parameter $\theta(t)$ is affine.
- From Eqn. (5.7), only the output matrix $C_{\mathrm{u},i}$ of $W_{\mathrm{u},i}$ is a function of $\theta(t)$.

Therefore, considering that:

$$W_{\mathrm{u},i} \equiv \left[\begin{array}{c|c} A_{\mathrm{u},i} & B_{\mathrm{u},i} \\ \hline C_{\mathrm{u},i}(\theta(t)) & 0 \end{array}\right] \tag{5.12}$$

$$W_{\mathrm{p},i} \equiv \left[\begin{array}{c|c} A_{\mathrm{p},i} & B_{\mathrm{p},i} \\ \hline C_{\mathrm{p},i} & D_{\mathrm{p},i} \end{array}\right] \tag{5.13}$$

and

$$G_{1,j} \equiv \left[\begin{array}{c|c} A_{\mathrm{g},j} & B_{\mathrm{g},j} \\ \hline C_{\mathrm{g},j} & 0 \end{array}\right] \tag{5.14}$$

then

$$L_j \equiv \left[\begin{array}{c|cc} A_{\mathrm{l},j} & B_{\mathrm{l},j,1} & B_{\mathrm{l},j,2} \\ \hline C_{\mathrm{l},j,1}(\theta(t)) & D_{\mathrm{l},j,11} & D_{\mathrm{l},j,12} \\ C_{\mathrm{l},j,2} & D_{\mathrm{l},j,21} & D_{\mathrm{l},j,22} \end{array}\right] \tag{5.15}$$

where

$$A_{\mathrm{l},j} = \begin{bmatrix} A_{\mathrm{g},j} & 0 & 0 \\ 0 & A_{\mathrm{u},i} & 0 \\ -B_{\mathrm{p},i}C_{\mathrm{g},j} & 0 & A_{\mathrm{p},i} \end{bmatrix} \tag{5.16}$$

$$B_{\mathrm{l},j} = \begin{bmatrix} B_{\mathrm{l},j,1} & B_{\mathrm{l},j,2} \end{bmatrix} = \begin{bmatrix} 0 & B_{\mathrm{g},j} \\ 0 & B_{\mathrm{u},i} \\ B_{\mathrm{p},i} & 0 \end{bmatrix} \tag{5.17}$$

$$C_{\mathrm{l},j}(\theta(t)) = \begin{bmatrix} C_{\mathrm{l},j,1}(\theta(t)) \\ C_{\mathrm{l},j,2} \end{bmatrix} = \begin{bmatrix} 0 & C_{\mathrm{u},i}(\theta(t)) & 0 \\ -D_{\mathrm{p},i}C_{\mathrm{g},j} & 0 & C_{\mathrm{p},i} \\ -C_{\mathrm{g},j} & 0 & 0 \end{bmatrix} \tag{5.18}$$

and

$$D_{\mathrm{l},j} = \begin{bmatrix} D_{\mathrm{l},j,11} & D_{\mathrm{l},j,12} \\ D_{\mathrm{l},j,21} & D_{\mathrm{l},j,22} \end{bmatrix} = \begin{bmatrix} 0 & 0 \\ D_{\mathrm{p},i} & 0 \\ 1 & 0 \end{bmatrix}. \tag{5.19}$$

Hence, the closed-loop system matrices of the feedback interconnection between $L_j(s)$ and the controllers $\mathcal{K}_{i,j}$ as indicated in Fig. 5.3 are given by:

$$A_{i,j} = \begin{bmatrix} A_{\mathrm{l},j} + B_{\mathrm{l},j,2}D_{K,i,j}(\theta(t))C_{\mathrm{l},j,2} & B_{\mathrm{l},j,2}C_{K,i,j}(\theta(t)) \\ B_{K,i,j}(\theta(t))C_{\mathrm{l},j,2} & A_{K,i,j}(\theta(t)) \end{bmatrix} \tag{5.20}$$

$$B_{i,j} = \begin{bmatrix} B_{\mathrm{l},j,1} + C_{\mathrm{l},j,2}D_{K,i,j}(\theta(t))D_{\mathrm{l},j,21} \\ B_{K,i,j}(\theta(t))D_{\mathrm{l},j,21} \end{bmatrix} \tag{5.21}$$

$$C_{i,j} = \begin{bmatrix} C_{\mathrm{l},j,1}(\theta(t)) + D_{\mathrm{l},j,12}D_{K,i,j}(\theta(t))C_{\mathrm{l},j,2} & D_{\mathrm{l},j,12}C_{K,i,j}(\theta(t)) \end{bmatrix} \tag{5.22}$$

and

$$D_{i,j} = \begin{bmatrix} D_{\mathrm{l},j,11} + D_{\mathrm{l},j,12}D_{K,i,j}(\theta(t))D_{\mathrm{l},j,21} \end{bmatrix}. \tag{5.23}$$

As a consequence, after tedious but straightforward algebra, the linear fractional interconnection between $L_j(s)$ and the controllers $\mathcal{K}_{i,j}$ as depicted in Fig. 5.3 produce closed-loop state space matrices that are also affine in the parameter $\theta(t)$. Therefore, each affine LPV

system can be completely defined by the vertex systems [139], i.e., the images of the v vertices that make up each parameter set $\mathcal{P}_i$, with $i = 1, 2$. In this way, the problem consists in seeking, for each Adult $\#j$, a symmetric and positive-definite matrix $X_j \in \mathbb{R}^{n\times n}$, with n the number of closed-loop states, that satisfies the following $2v + 1$ LMIs:

$$\begin{bmatrix} A_{i,j,\ell}^T X_j + X_j A_{i,j,\ell} & X_j B_{i,j,\ell} & C_{i,j,\ell}^T \\ B_{i,j,\ell}^T X_j & -\gamma_j I & D_{i,j,\ell}^T \\ C_{i,j,\ell} & D_{i,j,\ell} & -\gamma_j I \end{bmatrix} < 0 \tag{5.24}$$

$$X_j > 0 \tag{5.25}$$

for $\ell = 1, ..., v$ and $i = 1, 2$. Here $(A, B, C, D)_{i,j,\ell}$ is the tuple of the model's closed-loop matrices that result from the feedback interconnection of $L_j(s)$ and $\mathcal{K}_{i,j}$ evaluated at vertex $\theta_{i,\ell}$.

By solving one such set of $2v + 1$ LMIs for each patient, the existence of such matrices proved switching stability and performance in all cases. Due to the fact that a more restrictive condition is sought with respect to the design stage, the performance index γ is 30% higher on average for all patients. In any case, this is only a necessary condition, because the final test is performed on the complete adult cohort of the UVA/Padova metabolic simulator in Section 5.3.

5.2.4 Switching Signal

As mentioned above, $\mathcal{K}_{2,j}$ is applied only when high and rising glucose values are detected, e.g., after a meal. The block diagram associated with the generation of the switching signal that commands which LPV controller is selected is depicted in Fig. 5.4. The glucose measured by the CGM is filtered by a Noise-Spike Filter (NSF), setting to 3 mg/dl/min the maximum allowable glucose Rate of Change (ROC) [140]. Then, $g_{\mathrm{f}}(t)$ is filtered by a fourth-order Savitzky-Golay Filter (SGF) [141] to estimate the glucose ROC denoted by $\hat{\dot{g}}(t)$. If $g_{\mathrm{f}}(t)$ is higher than 110 mg/dl, and if the last three estimated glucose ROC values are higher than 1.2 mg/dl/min or the last two are higher than 1.4 mg/dl/min, the signal $h_{\mathrm{d}}(t)$, which is zero by default, is set to unity by the Hyperglycemia Detector (HD) block. When the latter condition is no longer met, $h_{\mathrm{d}}(t)$ is reset to zero. Because of the high measurement noise, some unrealistic hyperglycemic conditions may be detected, and in order to reduce the number of such false positive detections within a short period of time, it is considered

that $h_{\mathrm{d}}(t)$ can be set to unity only if the time period from the last falling edge to the new detection is longer than 30 min.

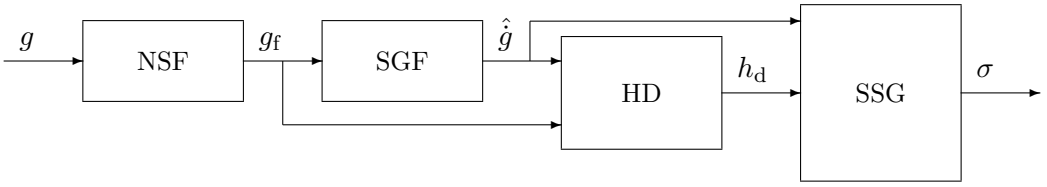

FIGURE 5.4: Block diagram of the switching signal algorithm. NSF: Noise-spike Filter; SGF: Savitzky-Golay Filter; HD: Hyperglycemia Detector, and SSG: Switching Signal Generator.

The evolution of the index i that indicates which controller $\mathcal{K}_{i,j}$ is applied, is described by a continuous-time function $\sigma(t) \in \{1, 2\}$. The variables $g_{\mathrm{f}}(t)$, $\hat{\dot{g}}(t)$, and $h_{\mathrm{d}}(t)$ are inputs to the Switching Signal Generator (SSG) block to define $\sigma(t)$ as follows. The sampling time after $h_{\mathrm{d}}(t)$ is set to unity, $\sigma(t)$ is set to two when $\hat{\dot{g}}(t) \geq 1$ mg/dl/min. Thus, if $\sigma(t) = 2$, $\mathcal{K}_{2,j}$ is selected until $\hat{\dot{g}}(t) < 1$ mg/dl/min, consequently guaranteeing that $\theta(t) \in \mathcal{P}_2$ while $\sigma(t) = 2$.

5.3 Results

All *in silico* adults of the complete UVA/Padova metabolic simulator are considered for simulations, using CGM as the sensor, a generic CSII pump, and with unannounced meals.

The two protocols (see Table 4.1), and the same simulation and analysis conditions used in Chapter 4 are employed for controller performance comparison. Note that protocol #1 has a fairly high meal content, whereas protocol #2 has fasting periods. Thus:

- The fasting state of each subject is assumed at the start of the simulation.
- Open-loop control that infuses the basal insulin is applied during the first 4 hours. After that, the switched LPV controller takes over the insulin delivery until the end of the simulation, with a constant setpoint of 110 mg/dl.
- A postprandial period (PP) and night (N) are defined as the 5 hour time interval following the start of a meal, and the period from midnight to 7:00 AM, respectively. In Chapter 4, both the CVGA plot [142], as well as the average results, are computed

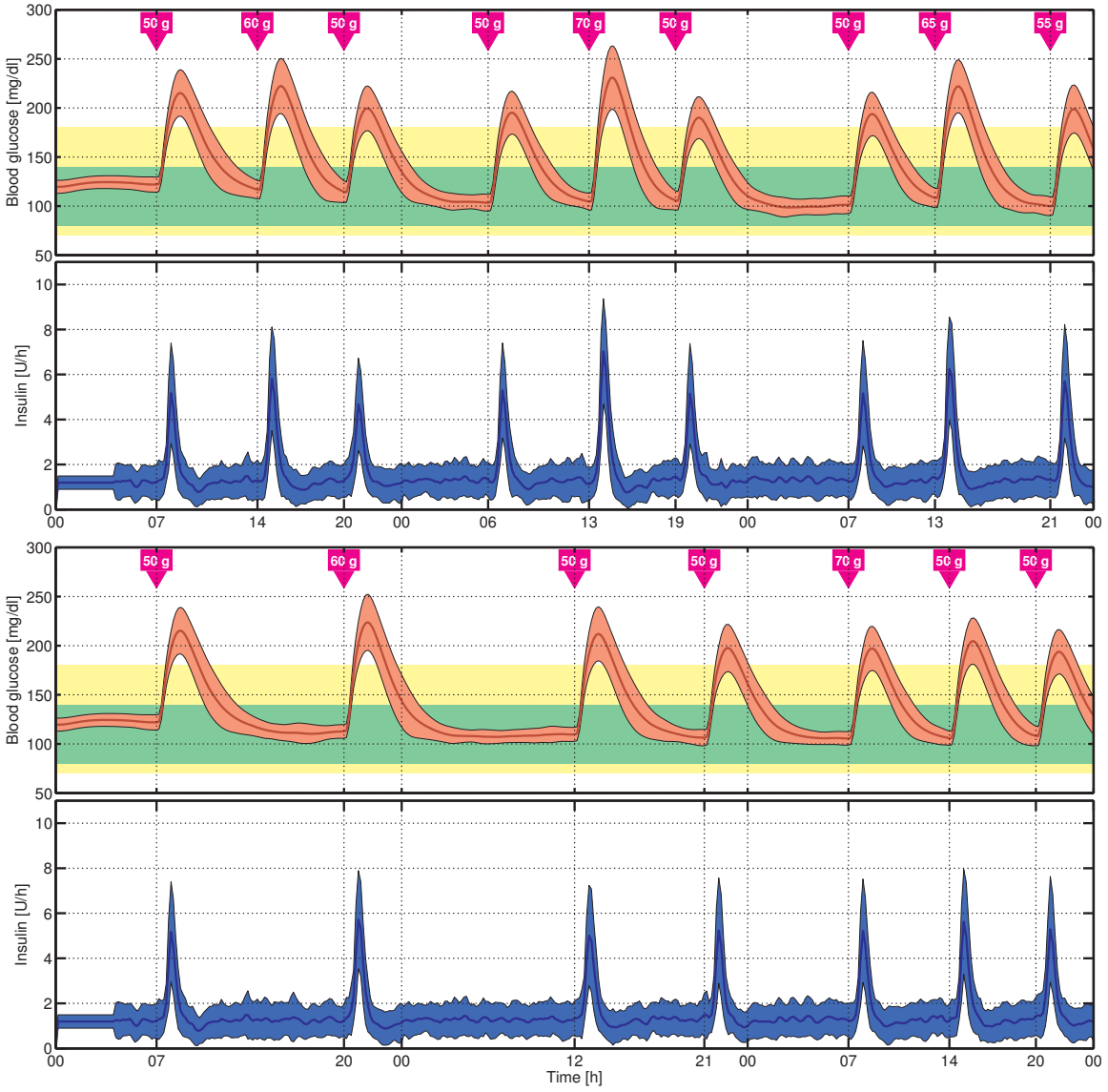

FIGURE 5.5: Average closed-loop responses for all the *in silico* adults (complete UVA/-Padova simulator) to protocol #1 (above) and to protocol #2 (below). The thick lines are the mean values, and the boundaries of the filled areas are the mean ±1 STD values. The filled yellow and green regions represent the 70-180 mg/dl and 80-140 mg/dl ranges, respectively.

based on the results of the third day for protocol #1, and based on the data from the second day for protocol #2. Therefore, to facilitate a direct comparison with the control strategy proposed in Chapter 4, here, the same analysis strategy to interpret the results is adopted.

During the implementation phase, the control action $u(t)$ added to the basal insulin $i_b = I_{b,j}$ is delivered by the CSII pump. In order to avoid dangerous scenarios, when $\sigma(t) = 1$, $g_{\mathrm{f}}(t) <$

130 mg/dl and $\hat{\dot{g}}(t) < -0.3$ mg/dl/min, the basal insulin is reduced 25%, i.e., $i_b = 0.75 I_{b,j}$. Based on the small gain theorem [143], the latter does not affect the closed-loop stability.

The average time responses to both protocols are depicted in Fig. 5.5. In order to show how the switching system works, an individual closed-loop response to protocol #1 is presented in Fig. 5.6. As shown in that figure, when $\mathcal{K}_{2,j}$ is selected ($\sigma(t) = 2$), insulin delivery

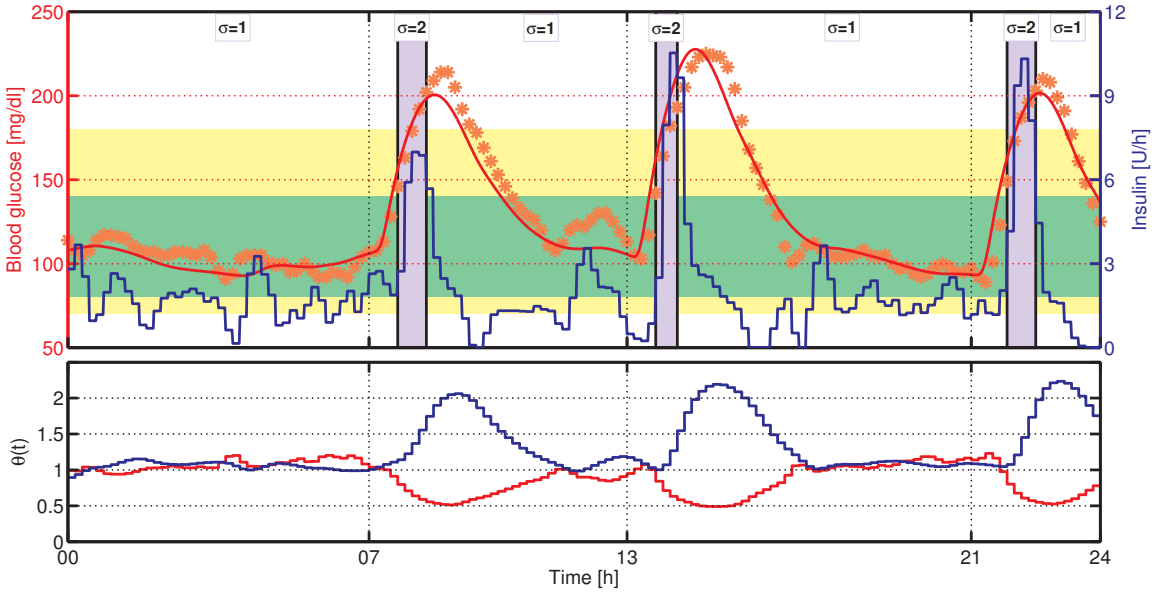

FIGURE 5.6: Switching LPV system functioning. Above: The blue line is the insulin infusion rate (right axis), the red line is the blood glucose (left axis), and the points are the CGM measurements. Below: Variation of $\theta_1(t)$ (red line) and $\theta_2(t)$ (blue line).

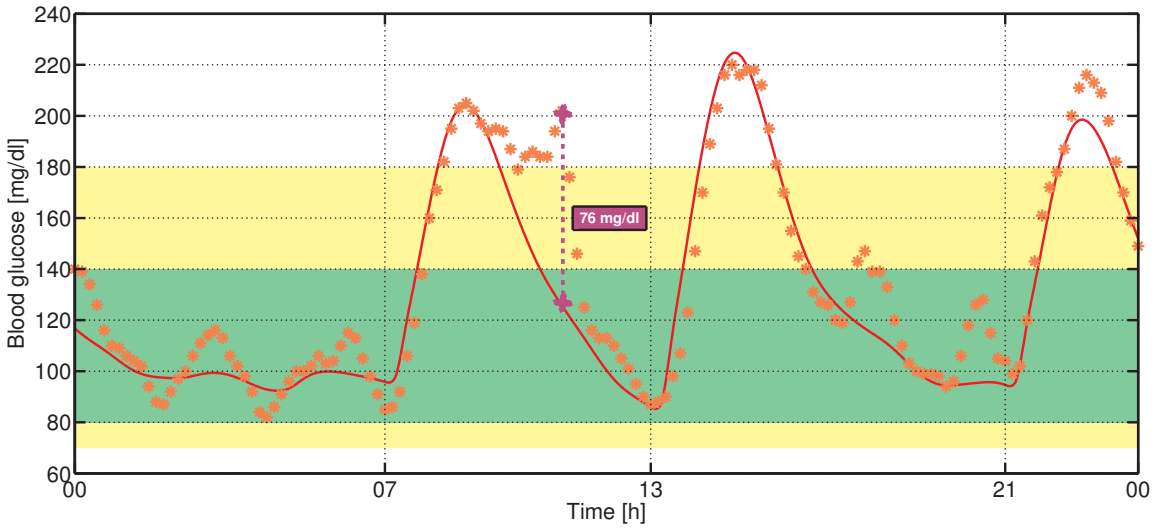

FIGURE 5.7: Closed-loop response for Adult #8, showing noisy CGM signal. The continuous line is the blood glucose concentration, and the noisy points are the glucose measurements via simulated CGM.

experiences spikes, reducing postprandial glucose levels. The delay between meal ingestion and controller switching is mainly related to the long sensing delays.

It is well-known that high measurement noise appears when CGM is used as the sensor. Despite the noisy CGM signal as depicted in Fig. 5.7, the controller manages to maintain the blood glucose at a safe level.

The CVGA plots and the average results related to both protocols are presented in Fig. 5.8 and Table 5.1, respectively. Results for the $\mathcal{H}_\infty$ approach presented in Chapter 4 are

Control Strategy		Protocol #1		Protocol #2	
		Switched-LPV	$\mathcal{H}_\infty$	**Switched-LPV**	$\mathcal{H}_\infty$
Mean BG [mg/dl]	**O**	134	148	134	154
	PP	162	176	159	177
	N	101	116	114	135
Max BG [mg/dl]	**O**	220	226	207	220
	PP	223	229	213	224
	N	113	142	153	183
Min BG [mg/dl]	**O**	90	96	96	108
	PP	98	108	103	114
	N	92	100	98	107
% time in [70 180] mg/dl	**O**	83.3	75.9	86.7	75.5
	PP	67.5	54.2	71.2	54.4
	N	99.4	99.5	99.3	91.4
% time > 300 mg/dl	**O**	0.0	0.1	0.0	0.0
	PP	0.1	0.3	0.0	0.1
	N	0.0	0.0	0.0	0.0
% time > 180 mg/dl	**O**	16.5	24.0	13.3	24.5
	PP	32.5	45.8	28.8	45.6
	N	0.0	0.4	0.7	8.6
% time < 70 mg/dl	**O**	0.2	0.1	0.0	0.0
	PP	0.0	0.0	0.0	0.0
	N	0.6	0.0	0.1	0.0
% CVGA zone inclusion	**A**	0	0	6.9	2.0
	B	93.1	96.0	91.1	95.0
	C	0.0	2.0	0.0	3.0
	D	6.9	2.0	2.0	0.0
	E	0.0	0.0	0.0	0.0
LBGI		0.3	0.1	0.1	0.0
HBGI		3.0	4.3	2.6	4.6
TDI [U]		34.5	30.8	32.2	29.3

TABLE 5.1: Comparison between the average results for all the adults (complete UVA/-Padova simulator) to protocol #1 and #2 obtained with the switched-LPV control, and with the $\mathcal{H}_\infty$ strategy proposed in the previous chapter. The overall (O), and the PP and N time intervals defined previously are analysed separately.

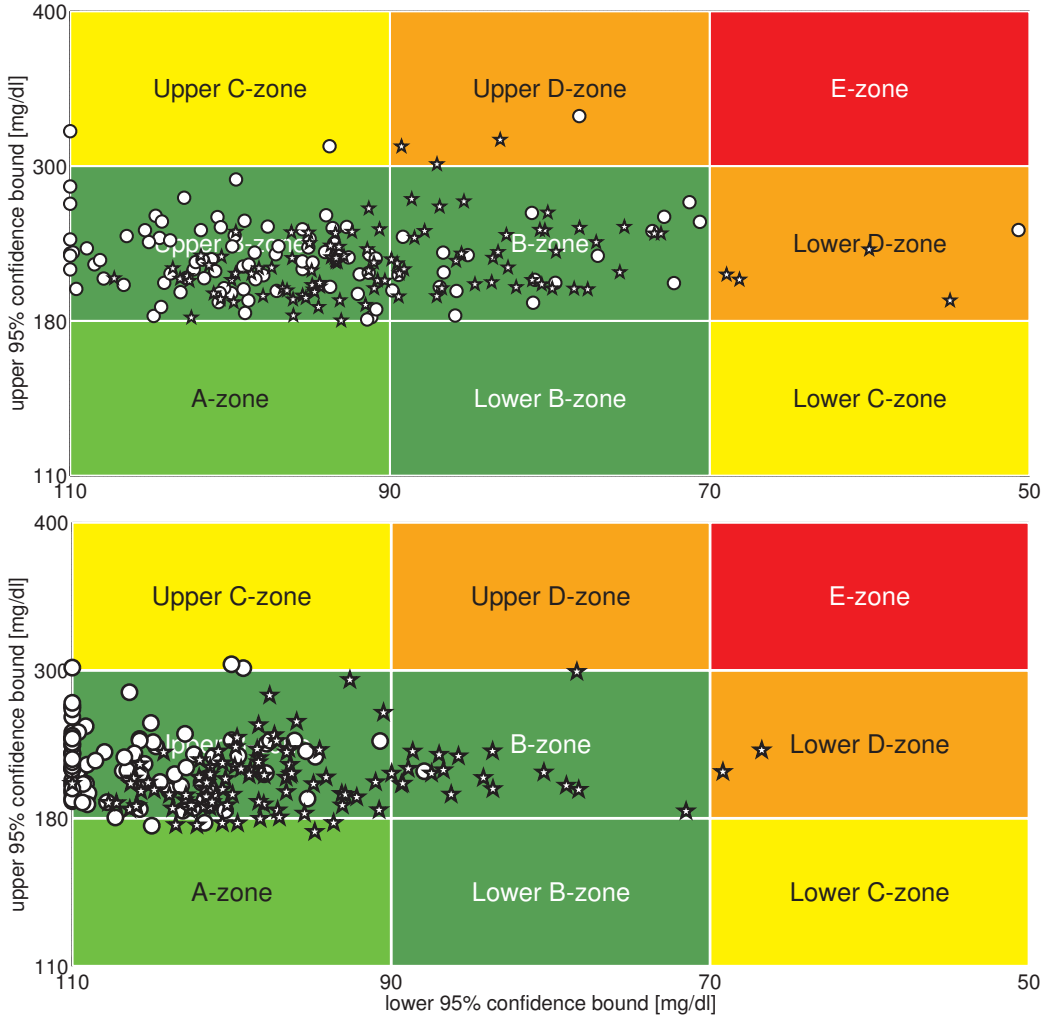

FIGURE 5.8: CVGA plots of the closed-loop responses of all *in silico* subjects (complete UVA/Padova simulator) for the proposed switched-LPV control (stars) and the previous $\mathcal{H}_\infty$ approach (circles) with respect to protocol #1 (above) and protocol #2 (below). The CVGA categories represent different levels of glucose control, as follows: accurate (A-zone), benign deviation into hypo/hyperglycemia (lower/upper B-zones), benign control (B-zone), overcorrection of hypo/hyperglycemia (upper/lower C-zone), failure to manage hypo/hyperglycemia (lower/upper D-zone), and erroneous control (E-zone).

also included in Fig. 5.8 and Table 5.1 for comparison. Note that the risk of hyperglycemia is substantially reduced, obtaining a HBGI < 3 with this control strategy. For example, the mean blood glucose is about 15 mg/dl lower, and the percentage of time in the range [70, 180] mg/dl is approximately 25% higher with this approach than with the $\mathcal{H}_\infty$ one. As a result of this more aggressive tuning, the CVGA plots are shifted to the right but the risk of hypoglycemia is scarcely increased, achieving a minimal Low Blood Glucose Index (LBGI < 1.1). In addition, a more aggressive control action also increases the TDI but again, with no significant increase in the risk of hypoglycemia.

The variation of $\theta(t) = [\theta_1(t),\ \theta_2(t)]^T$ is depicted in Fig. 5.9. Note that there is an orange

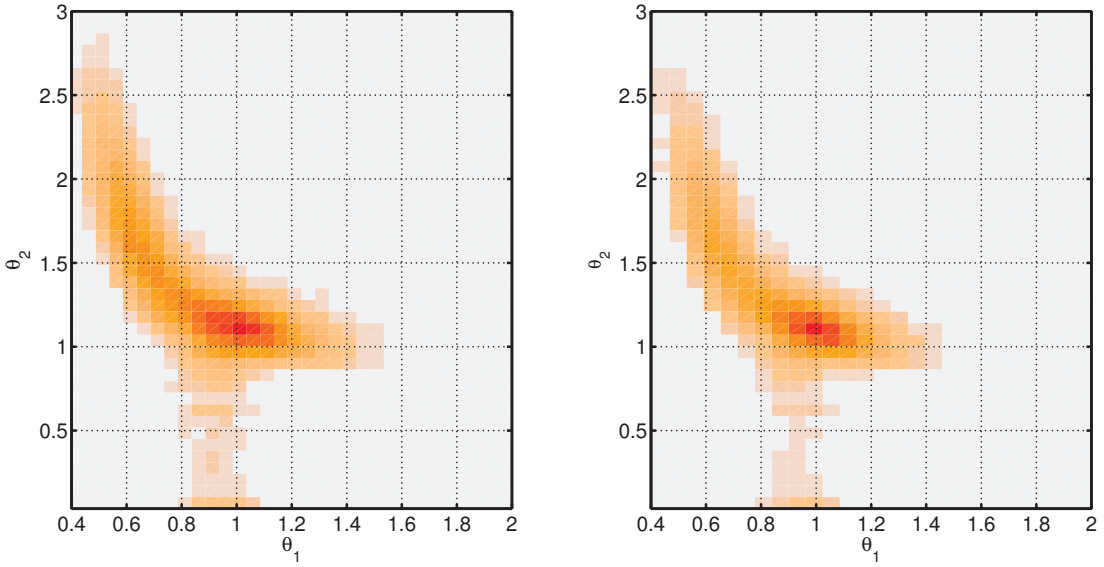

FIGURE 5.9: Variation of $\theta_1(t)$ and $\theta_2(t)$ parameters for all the *in silico* adults (complete UVA/Padova simulator) to protocol #1 (left) and to protocol #2 (right).

narrow stripe around $\theta_1(t) = 1$ and $0 \leq \theta_2(t) \leq 1$, because $\theta_2(0) = 0$, but this subsequently increases until the estimated plasma insulin converges to its steady-state value. As shown in Fig. 5.9, both parameters evolve within a safe region. This means that when the blood glucose level decreases ($\theta_1(t)$ increases), the plasma insulin level decreases ($\theta_2(t)$ decreases), avoiding an overdose of insulin. On the other hand, when the blood glucose level increases ($\theta_1(t)$ decreases), so does the plasma insulin level ($\theta_2(t)$ increases), reducing in this way the risk of hyperglycemia. Consequently, dangerous scenarios like low blood glucose values and high plasma insulin levels or *vice versa* do not occur with this switched LPV approach. Furthermore, the darkest area, which represents the region where both parameters spend the highest percentage of time, is $(\theta_1, \theta_2) \simeq (1, 1)$. This means that glucose values are usually around the setpoint (110 mg/dl) without high levels of IOB, despite perturbations like unannounced meals.

Although for the design stage both parameters are included in a rectangular region that is larger than the region where the actual time-varying parameters evolve, this conservative choice is necessary in order to have stability and performance guarantees when this is not the case, e.g. due to a large measurement error.

5.3.1 Additional *In Silico* Tests

In order to test the switched LPV controller in other scenarios, the following additional protocols have been considered.

5.3.1.1 Small-Meal Protocol Study

Breakfast 1		Lunch 1		Dinner 1		Breakfast 2		Lunch 2		Dinner 2	
Time	gCHO	Time	gCHO	Time	gCHO	Time	gCHO	Time	gCHO	Time	gCHO
7 AM	40 g	2 PM	30 g	8 PM	40 g	7 AM	35 g	1 PM	30 g	9 PM	40 g

TABLE 5.2: Protocol #3.

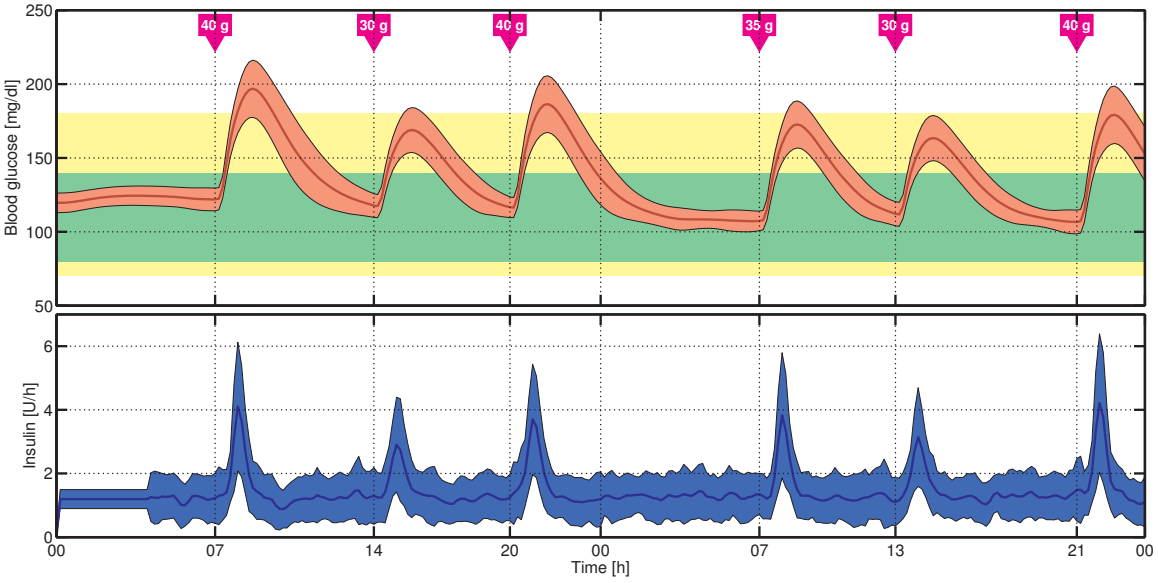

FIGURE 5.10: Average closed-loop responses for the 101 *in silico* adults to protocol #3. The thick lines are the mean values, and the boundaries of the filled areas are the mean ±1 STD values. The filled yellow and green regions represent the 70-180 mg/dl and 80-140 mg/dl ranges, respectively.

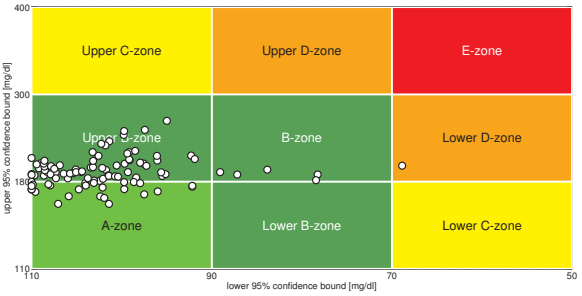

FIGURE 5.11: CVGA of all the 101 closed-loop responses to protocol #3.

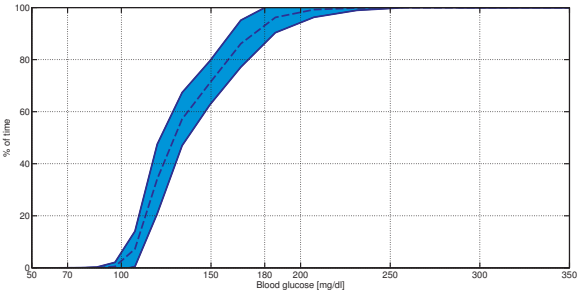

FIGURE 5.12: Average cumulative time in range to protocol #3. The mean ±1 STD values are represented by the filled area.

Mean BG	**Max BG**	**Min BG**	**% in** [70 180]	% > 180	% < 70	**LBGI**	**HBGI**	**TDI**
136	192	102	94.0	6.0	0.0	0.0	2.1	31.2

TABLE 5.3: Average results for the 101 adults to protocol #3.

5.3.1.2 Fasting Study

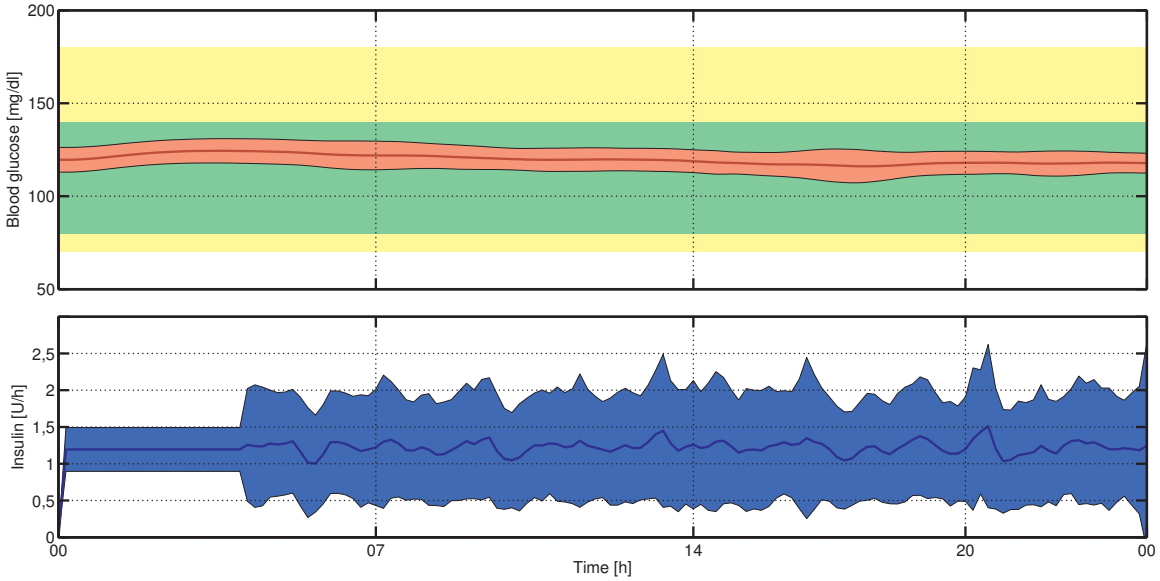

FIGURE 5.13: Average closed-loop responses for the 101 *in silico* adults to fasting study. The thick lines are the mean values, and the boundaries of the filled areas are the mean ±1 STD values. The filled yellow and green regions represent the 70-180 mg/dl and 80-140 mg/dl ranges, respectively.

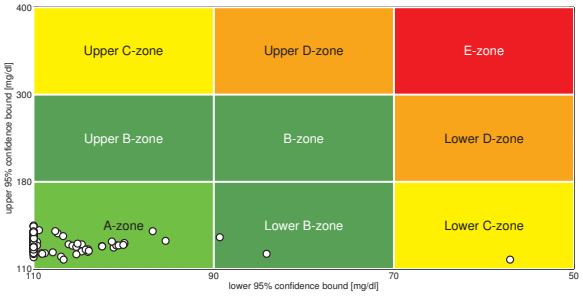

FIGURE 5.14: CVGA of all the 101 closed-loop responses to fasting study.

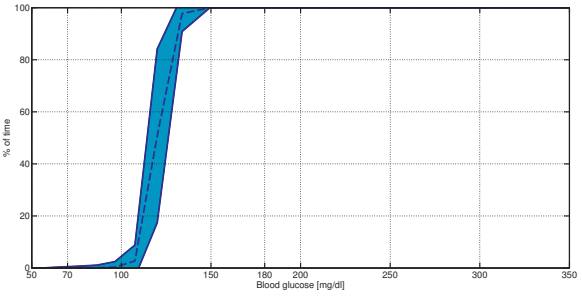

FIGURE 5.15: Average cumulative time in range to fasting study. The mean ±1 STD values are represented by the filled area.

Mean BG	**Max BG**	**Min BG**	% **in** [70 180]	% > 180	% < 70	**LBGI**	**HBGI**	**TDI** [U]
120	127	110	100.0	0.0	0.0	0.02	0.23	27.2

TABLE 5.4: Average results for the 101 adults to fasting study.

The closed-loop response for Adult #34 fell into the Lower C-zone, because a large glucose spike due to CGM noise is measured during the simulation as depicted in Fig. 5.16.

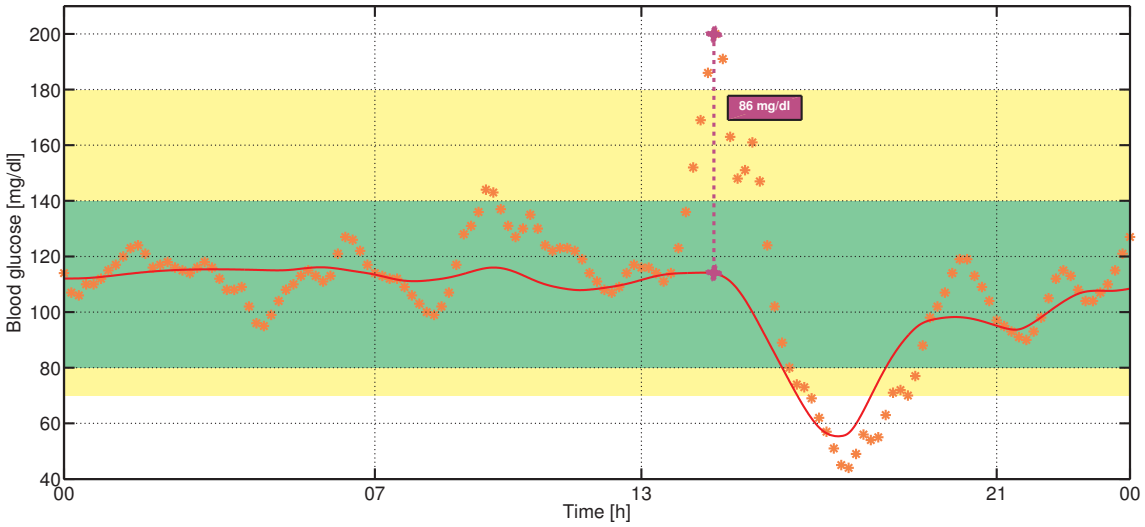

FIGURE 5.16: Closed-loop response for Adult #34. The continuous line is the blood glucose concentration, and the points are the glucose measurements.

5.4 Conclusions

A general switched-LPV controller was designed in order to minimize risks of hyper- and hypoglycemia. This control structure naturally accommodates the time-varying/nonlinear dynamics and intra-patient uncertainty. The controller is based on a model tuned with the patient *a priori* information in order to cover the inter-patient uncertainty. Finally, a hyperglycemia estimator is used to predict perturbations, e.g., risky postprandial periods. The outcome is an improvement on previous results. The key feature is the possibility of taking into account, at the design stage, important perturbations: unannounced meals and/or patient's physical exercise. Here, the first situation has been explored, due to the fact that the UVA/Padova simulator has no physical exercise model. Nevertheless, the same procedure could be applied to the latter situation by either estimating a negative ROC in glucose levels, or through a real-time measurement, e.g., increase in cardiac rhythm.

Chapter 6

Conclusion and Future Work

In this thesis, an overview of the state of the art of diabetes management has been presented in Chapter 1. New technologies applied to the development of minimally invasive subcutaneous insulin infusion and glucose measurement devices have made it possible for researchers to introduce the idea of an artificial pancreas. In this way, a CGM that measures glucose values in the interstitial fluid can be connected to a CSII pump through a control algorithm that decides how much insulin the patient needs.

Models that describe the insulin-glucose dynamics in T1DM patients are important in order to design different control algorithms. Therefore, an analysis of the three main models which are used in controller testing (Sorensen, UVA/Padova and Cambridge) has been presented in Chapter 2. There, some pros and cons from the aforementioned models, as well as several errors in the literature, have been pointed out. Besides the differences between the simulation environments, attention should be paid to all of the following issues:

- Model uncertainty (dynamics, intra- and inter-patient).
- Nonlinear phenomena.
- Time delays, actuator saturation, measurement noise.
- Real-time implementation.

These items need to be achieved, and therefore, an approach to $\mathcal{H}_\infty$ control for blood glucose regulation in T1DM has been presented in Chapter 3. However, as mentioned in that chapter, when all the previous items are considered simultaneously with unannounced

meals, robust controllers such as the ones designed there would not achieve high closed-loop performance. In that sense, a control scheme composed of an $\mathcal{H}_\infty$ robust controller, an IFL, and a SM has been introduced in Chapter 4. A general model structure that is adapted to a particular patient by using certain *a priori* clinical information that is easily obtainable is used to synthesise the $\mathcal{H}_\infty$ controller. In that way, the large inter-patient variability has been addressed, avoiding an in-depth *a priori* identification procedure that may be infeasible in practice. As for the IFL and the SM, they have been added to maintain the patient's glucose concentration in a safe region based on estimations of the IOB and future glucose levels, respectively.

An improvement of the latter approach has been presented in Chapter 5. In that chapter, a switched LPV glucose controller has been designed to take into account at the design stage important perturbations such as unannounced meals and/or patient's physical exercise. The time-varying model is used to replace the SM and the IFL. The LPV control has the advantage of proven stability and robustness guarantees based on Lyapunov theory and on-line tuning which takes care of inter-patient variability, and hypo– and hyperglycaemic situations. On the other hand, the inclusion of a real-time estimation, which takes into account perturbations without the need of announcements, enables the selection of a controller that can be specifically designed for that situation. Thus, an elegant and efficient way of minimising patient's risks has been obtained and later successfully tested on the complete *in silico* adult cohort of the UVA/Padova metabolic simulator.

A summary of how some issues associated with the blood glucose level control in T1DM patients can be addressed is given in Table 6.1.

Challenges (unannounced meals)	**Approaches**
Intra-patient variations, nonlinear/time-varying dynamics.	Nonlinear/time-varying controller.
Inter-patient uncertainty.	Patient tuning.
Subcutaneous-intravenous delays in CGM and insulin infusion.	Prediction.

TABLE 6.1: Problem challenges and possible approaches.

Regarding the future work, it can be summarised as follows.

- Test the algorithms on the *in silico* adolescents and children of the UVA/Padova simulator. Children are the highest-risk population, and therefore, a particular treatment might be necessary.
- Design and test bihormonal controllers. This is possible due to the fact that the glucagon counterregulatory response has been included in the UVA/Padova metabolic simulator. As for the use of other hormones, pramlintide may be a suitable option to reduce postprandial blood glucose excursions which are higher when unannounced meals are considered. This will anticipate the time when technology allows a stable deposit of these hormones.
- Cooperate in the development of protocols for clinical trials that should be later reviewed by an ethical committee.
- Start clinical tests to prove the feasibility of closed-loop blood glucose control using the algorithms presented in this work.

In order to achieve the latter two items, work in collaboration with Dr. León Litwak and physicians from the Hospital Italiano in Argentina, and with researchers from the Universidad Nacional de La Plata (UNLP) and from the UCSB has been initiated. As for the hardware needed to perform the clinical trials, contact has been established with Medtronic through the UCSB, and financial support may be obtained from Cellex and Nuria Foundations.

Bibliography

[1] International Diabetes Federation, "IDF Diabetes Atlas, 6th edn," Brussels, Belgium: International Diabetes Federation, 2013.

[2] J. Sorensen, "A Physiologic Model of Glucose Metabolism in Man and its Use to Design and Asses Improved Insulin Therapies for Diabetes," Ph.D. dissertation, Massachusetts Institute of Technology, Cambridge, MA, USA, 1985.

[3] C. Dalla Man and C. Cobelli, "A System Model of Oral Glucose Absorption: Validation on Gold Standard Data," *IEEE Transactions on Biomedical Engineering*, vol. 53, no. 12, pp. 2472–78, 2006.

[4] C. Dalla Man, D. Raimondo, R. Rizza, and C. Cobelli, "GIM, Simulation Software of Meal Glucose-Insulin Model," *Journal of Diabetes Science and Technology*, vol. 1, no. 3, pp. 323–30, 2007.

[5] C. Cobelli, C. Dalla Man, G. Sparacino, L. Magni, G. De Nicolao, and B. Kovatchev, "Diabetes: Models, Signals, and Control," *IEEE Reviews in Biomedical Engineering*, vol. 2, pp. 54–96, 2009.

[6] C. Dalla Man, R. Rizza, and C. Cobelli, "Meal Simulation Model of the Glucose-Insulin System," *IEEE Transactions on Biomedical Engineering*, vol. 54, no. 10, pp. 1740–49, 2007.

[7] C. Dalla Man, F. Micheletto, D. Lv, M. Breton, B. Kovatchev, and C. Cobelli, "The UVA/PADOVA Type 1 Diabetes Simulator: New Features," *Journal of Diabetes Science and Technology*, vol. 8, no. 1, pp. 26–34, 2014.

[8] M. Wilinska, L. Chassin, C. Acerini, J. Allen, D. Dunger, and R. Hovorka, "Simulation Environment to Evaluate Closed-Loop Insulin Delivery Systems in Type 1 Diabetes," *Journal of Diabetes Science and Technology*, vol. 4, no. 1, pp. 132–44, 2010.

[9] American Diabetes Association, "Standards of Medical Care in Diabetes - 2014," *Diabetes Care*, vol. 37 (Suppl. 1), pp. S14–S80, 2014.

[10] P. Pozzilli and U. Di Mario, "Autoimmune Diabetes Not Requiring Insulin at Diagnosis (Latent Autoimmune Diabetes of The Adult): Definition, Characterization, and Potential Prevention," *Diabetes Care*, vol. 24, no. 8, pp. 1460–7, 2001.

[11] S. Fajans, G. Bell, and K. Polonsky, "Molecular Mechanisms and Clinical Pathophysiology of Maturity-Onset Diabetes of the Young," *New England Journal of Medicine*, vol. 345, no. 13, pp. 971–80, 2001.

[12] S. Flanagan, E. Edghill, A. Gloyn, S. Ellard, and A. Hattersley, "Mutations in KCNJ11, Which Encodes Kir6.2, Are a Common Cause of Diabetes Diagnosed in the First 6 Months of Life, with the Phenotype Determined by Genotype," *Diabetologia*, vol. 49, no. 6, pp. 1190–7, 2006.

[13] American Diabetes Association, "Gestational Diabetes Mellitus," *Diabetes Care*, vol. 26 (Suppl. 1), pp. S103–S105, 2003.

[14] SEARCH for Diabetes in Youth Study, "The Burden of Diabetes Mellitus Among US Youth: Prevalence Estimates from the SEARCH for Diabetes in Youth Study," *Pediatrics*, vol. 118, no. 4, pp. 1510–8, 2006.

[15] ——, "Prevalence of Type 1 and Type 2 Diabetes Among Children and Adolescents From 2001 to 2009," *JAMA*, vol. 311, no. 17, pp. 1778–86, 2014.

[16] ——, "Projections of Type 1 and Type 2 Diabetes Burden in the U.S. Population Aged <20 Years Through 2050: Dynamic Modeling of Incidence, Mortality, and Population Growth," *Diabetes Care*, vol. 35, no. 12, pp. 2515–20, 2012.

[17] ——, "SEARCH for Diabetes in Youth: a Multicenter Study of the Prevalence, Incidence and Classification of Diabetes Mellitus in Youth," *Controlled Clinical Trials*, vol. 25, no. 5, pp. 458–71, 2004.

[18] DIAMOND Project Group, "Incidence and Trends of Childhood Type 1 Diabetes Worldwide 1990-1999," *Diabetic Medicine*, vol. 23, no. 8, pp. 857–66, 2006.

[19] C. Patterson, G. Dahlquist, E. Gyürüs, A. Green, and G. Soltész, the EURODIAB Study Group, "Incidence Trends for Childhood Type 1 Diabetes in Europe During

1989-2003 and Predicted New Cases 2005-20: a Multicentre Prospective Registration Study," *Lancet*, vol. 373, no. 9680, pp. 2027–33, 2009.

[20] American Diabetes Association, "Economic Costs of Diabetes in the U.S. in 2012," *Diabetes Care*, 2013.

[21] P. Zhang, X. Zhang, J. Brownb, D. Vistisenc, R. Sicree, J. Shawd, and G. Nichols, "Global Healthcare Expenditure on Diabetes for 2010 and 2030," *Diabetes Research and Clinical Practice*, vol. 87, pp. 293–301, 2010.

[22] B. Tao, M. Pietropaolo, M. Atkinson, D. Schatz, and D. Taylor, "Estimating the Cost of Type 1 Diabetes in the U.S.: A Propensity Score Matching Method," *PLoS ONE*, vol. 5, no. 7, pp. 1–11, 2010.

[23] A. Peters and L. Laffel, *Type 1 Diabetes Sourcebook*. American Diabetes Association, 2013.

[24] F. Kaufman, *Medical Management of Type 1 Diabetes*. American Diabetes Association, 2012.

[25] M. Fowler, "Microvascular and Macrovascular Complications of Diabetes," *Clinical Diabetes*, vol. 26, no. 2, pp. 77–82, 2008.

[26] S. Laing, J. Swerdlow, S. Slater, A. Burden, A. Morris, N. Waugh, W. Gatling, P. Bingley, and C. Patterson, "Mortality From Heart Disease in a Cohort of 23,000 Patients with Insulin-Treated Diabetes," *Diabetologia*, vol. 46, no. 6, pp. 760–5, 2003.

[27] D. Fong, L. Aiello, T. Gardner, G. King, G. Blankenship, J. Cavallerano, F. Ferris III, and R. Klein, "Retinopathy in Diabetes," *Diabetes Care*, vol. 27 (Suppl. 1), pp. S84–S87, 2004.

[28] D. Nathan, "The Diabetes Control and Complications Trial/Epidemiology of Diabetes Interventions and Complications Study at 30 Years: Overview," *Diabetes Care*, vol. 37, no. 1, pp. 9–16, 2014.

[29] The Diabetes Control and Complications Trial/Epidemiology of Diabetes Interventions and Complications (DCCT/EDIC) Study Research Group, "Intensive Diabetes Treatment and Cardiovascular Disease in Patients with Type 1 Diabetes," *New England Journal of Medicine*, vol. 353, no. 25, pp. 2643–53, 2005.

[30] S. Aronoff, K. Berkowitz, B. Shreiner, and L. Want, "Glucose Metabolism and Regulation: Beyond Insulin and Glucagon," *Diabetes Spectrum*, vol. 17, no. 3, pp. 183–90, 2004.

[31] C. Herrmann, R. Göke, G. Richter, H. Fehmann, R. Arnold, and B. Göke, "Glucagon-Like Peptide-1 and Glucose-Dependent Insulin-Releasing Polypeptide Plasma Levels in Response to Nutrients," *Digestion*, vol. 56, no. 2, pp. 117–26, 1995.

[32] P. MacDonald, J. Joseph, and P. Rorsman, "Glucose-Sensing Mechanisms in Pancreatic β-cells," *Philosophical Transactions of the Royal Society B: Biological Sciences*, vol. 360, no. 1464, pp. 2211–25, 2005.

[33] C. Newgard and J. McGarry, "Metabolic Coupling Factors in Pancreatic β-cell Signal Transduction," *Annual Review of Biochemistry*, vol. 64, pp. 689–719, 1995.

[34] I. Quesada, E. Tudurí, C. Ripoll, and A. Nadal, "Physiology of the Pancreatic α-cell and Glucagon Secretion: Role in Glucose Homeostasis and Diabetes," *Journal of Endocrinology*, vol. 199, no. 1, pp. 5–19, 2008.

[35] P. Haney, J. Slot, R. Piper, D. James, and M. Mueckler, "Intracellular Targeting of the Insulin-Regulatable Glucose Transporter (GLUT4) is Isoform Specific and Independent of Cell Type." *The Journal of Cell Biology*, vol. 114, no. 4, pp. 689–99, 1991.

[36] O. Schmitz, B. Brock, and J.Rungby, "Amylin Agonists: A Novel Approach in the Treatment of Diabetes," *Diabetes*, vol. 53, no. Suppl. 3, pp. S233–S238, 2004.

[37] M. Strowski, R. Parmar, A. Blake, and J. Schaeffer, "Somatostatin Inhibits Insulin and Glucagon Secretion via Two Receptors Subtypes: an in Vitro Study of Pancreatic Islets from Somatostatin Receptor 2 Knockout Mice," *Endocrinology*, vol. 141, no. 1, pp. 111–7, 2000.

[38] C. von Klein, "The Medical Features of the Papyrus Ebers," *JAMA*, vol. 45, pp. 1928–35, 1905.

[39] S. Clarke and J. Foster, "A History of Blood Glucose Meters and Their Role in Self-Monitoring of Diabetes Mellitus," *British Journal of Biomedical Science*, vol. 69, no. 2, pp. 83–93, 2012.

[40] A. Free and H. Free, "Self Testing, an Emerging Component of Clinical Chemistry," *Clinical Chemistry*, vol. 30, no. 6, pp. 829–38, 1984.

[41] R. Koenig, C. Peterson, R. Jones, C. Saudek, M. Lehrman, and A. Cerami, "Correlation of Glucose Regulation and Hemoglobin AIc in Diabetes Mellitus," *New England Journal of Medicine*, vol. 295, pp. 417–20, 1976.

[42] The Diabetes Control and Complications Trial Research Group, "Hypoglycemia in the Diabetes Control and Complications Trial," *Diabetes*, vol. 46, no. 2, pp. 271–86, 1997.

[43] S. Garg and I. Hirsch, "Self-monitoring of Blood Glucose – An Overview," *Diabetes Technology & Therapeutics*, vol. 15 (Suppl. 1), pp. S3–S12, 2013.

[44] D. Rodbard, T. Bailey, L. Jovanovič, H. Zisser, R. Kaplan, and S. Garg, "Improved Quality of Glycemic Control and Reduced Glycemic Variability with Use of Continuous Glucose Monitoring," *Diabetes Technology & Therapeutics*, vol. 11, no. 11, pp. 717–23, 2009.

[45] C. De Block, B. Manuel-y-Keenoy, and L. Van Gaal, "A Review of Current Evidence with Continuous Glucose Monitoring in Patients with Diabetes," *Journal of Diabetes Science and Technology*, vol. 2, no. 4, pp. 718–27, 2008.

[46] J. Selam, "Evolution of Diabetes Insulin Delivery Devices," *Journal of Diabetes Science and Technology*, vol. 4, no. 3, pp. 505–13, 2010.

[47] J. Pickup, H. Keen, J. Parsons, and K. Alberti, "Continuous Subcutaneous Insulin Infusion: An Approach to Achieving Normoglycaemia," *British Medical Journal*, vol. 1, no. 6107, pp. 204–7, 1978.

[48] Diabetes Control and Complications Trial Research Group, "The Effect of Intensive Treatment of Diabetes on the Development and Progression of Long-term Complications in Insulin-Dependent Diabetes Mellitus," *New England Journal of Medicine*, vol. 329, pp. 977–86, 1993.

[49] D. Nathan and for the DCCT/EDIC Research Group, "The Diabetes Control and Complications Trial/Epidemiology of Diabetes Interventions and Complications Study at 30 Years: Overview," *Diabetes Care*, vol. 37, pp. 9–16, 2014.

[50] UKPDS Group, "Intensive Blood-Glucose Control with Sulphonylureas or Insulin Compared with Conventional Treatment and Risk of Complications in Patients with Type 2 Diabetes," *Lancet*, vol. 352, pp. 837–53, 1998.

[51] The Diabetes Control and Complications Trial Research Group, "Hypoglycemia in the Diabetes Control and Complications Trial," *Diabetes*, vol. 46, no. 2, pp. 271–86, 1997.

[52] D. Nathan, F. Dunn, J. Bruch, C. McKitrick, M. Larkin, C. Haggan, J. Lavin-Tompkins, D. Norman, D. Rogers, and D. Simon, "Postprandial Insulin Profiles with Implantable Pump Therapy May Explain Decreased Frequency of Severe Hypoglycemia, Compared With Intensive Subcutaneous Regimens, in Insulin-Dependent Diabetes Mellitus Patients," *American Journal of Medicine*, vol. 100, no. 4, pp. 412–7, 1996.

[53] F. Dunn, D. Nathan, M. Scavini, J. Selam, and T. Wingrove, "Long-term Therapy of IDDM with an Implantable Insulin Pump. The Implantable Insulin Pump Trial Study Group," *Diabetes Care*, vol. 20, no. 1, pp. 59–63, 1997.

[54] J. Selam, P. Micossi, F. Dunn, and D. Nathan, "Clinical Trial of Programmable Implantable Insulin Pump for Type I Diabetes," *Diabetes Care*, vol. 15, no. 7, pp. 877–85, 1992.

[55] P. Oskarsson, P. Lins, H. Wallberg-Henriksson, and U. Adamson, "Metabolic and Hormonal Responses to Exercise in Type 1 Diabetic Patients During Continuous Subcutaneous as Compared to Continuous Intraperitoneal Insulin Infusion," *Diabetes & Metabolism*, vol. 25, no. 6, pp. 491–7, 1999.

[56] P. Oskarsson, P. Lins, L. Backman, and U. Adamson, "Continuous Intraperitoneal Insulin Infusion Partly Restores the Glucagon Response to Hypoglycemia in Type 1 Diabetic Patients," *Diabetes & Metabolism*, vol. 26, no. 2, pp. 118–24, 2000.

[57] V. Shah, A. Shoskes, B. Tawfik, and S. Garg, "Closed-Loop System in the Management of Diabetes: Past, Present, and Future," *Diabetes Technology & Therapeutics*, vol. 16, no. 8, pp. 477–90, 2014.

[58] J. Bondía, J. Vehí, C. Palerm, and P. Herrero, "El Páncreas Artificial: Control Automático de Infusión de Insulina en Diabetes Mellitus Tipo I," *Revista Iberoamericana de Automática e Informática Industrial*, vol. 7, no. 2, pp. 5–20, 2010.

[59] C. Cobelli, E. Renard, and B. Kovatchev, "Artificial Pancreas: Past, Present, Future," *Diabetes*, vol. 60, no. 11, pp. 2672–82, 2011.

[60] E. Atlas, A. Thorne, K. Lu, M. Phillip, and E. Dassau, "Closing the Loop," *Diabetes Technology & Therapeutics*, vol. 16 (Suppl. 1), pp. S23–S33, 2014.

[61] B. Bequette, "Challenges and Progress in the Development of a Closed-Loop Artificial Pancreas," in *American Control Conference*, Montreal, Canada, 2012, pp. 4065–71.

[62] A. Kadish, "Automation Control of Blood Sugar. A Servomechanism for Glucose Monitoring and Control," *American Society for Artificial Internal Organs*, vol. 9, no. 3, pp. 363–7, 1963.

[63] A. Albisser, B. Leibel, T. Ewart, Z. Davidovac, C. Botz, and W. Zingg, "An Artificial Endocrine Pancreas," *Diabetes*, vol. 23, no. 5, pp. 389–96, 1974.

[64] E. Marliss, F. Murray, E. Stokes, B. Zinman, A. Nakhooda, A. Denoga, B. Leibel, and A. Albisser, "Normalization of Glycemia in Diabetics During Meals with Insulin and Glucagon Delivery by the Artificial Pancreas," *Diabetes*, vol. 26, no. 7, pp. 663–72, 1977.

[65] P. Oskarsson, P. Lins, L. Backman, and U. Adamson, "Insulin Delivery Route for the Artificial Pancreas: Subcutaneous, Intraperitoneal, or Intravenous? Pros and Cons," *Journal of Diabetes Science and Technology*, vol. 2, no. 4, pp. 735–8, 2008.

[66] E. Dassau, H. Zisser, C. Palerm, B. Buckingham, L. Jovanovič, and F. Doyle III, "Modular Artificial β-Cell System: A Prototype for Clinical Research," *Journal of Diabetes Science and Technology*, vol. 2, no. 5, pp. 863–72, 2008.

[67] E. Dassau, H. Zisser, R. Harvey, M. Percival, B. Grosman, W. Bevier, E. Atlas, S. Miller, R. Nimri, L. Jovanovič, and F. Doyle III, "Clinical Evaluation of a Personalized Artificial Pancreas," *Diabetes Care*, vol. 36, no. 4, pp. 801–9, 2013.

[68] B. Kovatchev, E. Renard, C. Cobelli, H. Zisser, P. Keith-Hynes, S. Anderson, S. Brown, D. Chernavvsky, M. Breton, A. Farret, M. Pelletier, J. Place, D. Bruttomesso, S. Del Favero, R. Visentin, A. Filippi, R. Scotton, A. Avogaro, and F. Doyle III, "Feasibility of Outpatient Fully Integrated Closed-Loop Control: First Studies of Wearable Artificial Pancreas," *Diabetes Care*, vol. 36, no. 7, pp. 1851–8, 2013.

[69] M. Wilinska and R. Hovorka, "Simulation Models for In Silico Testing of Closed-Loop Glucose Controllers in Type 1 Diabetes," *Drug Discovery Today: Disease Models*, vol. 5, no. 4, pp. 289–98, 2008.

[70] A. Makroglou, J. Li, and Y. Kuang, "Mathematical Models and Software Tools for the Glucose-Insulin Regulatory System and Diabetes: An Overview," *Applied Numerical Mathematics*, vol. 56, pp. 559–73, 2006.

[71] F. Chee and T. Fernando, *Closed-Loop Control of Blood Glucose*. Springer, 2007, vol. 368.

[72] R. Bergman, Y. Ider, C. Bowden, and C. Cobelli, "Quantitative Estimation of Insulin Sensitivity," *American Journal of Physiology*, vol. 236, no. 6, pp. E667–77, 1979.

[73] G. Pacini and R. Bergman, "MINMOD: A Computer Program to Calculate Insulin Sensitivity and Pancreatic Responsivity from the Frequently Sampled Intravenous Glucose Tolerance Test," *Computer Methods and Programs in Biomedicine*, vol. 23, pp. 113–22, 1986.

[74] B. Kovatchev, M. Breton, C. Dalla Man, and C. Cobelli, "In Silico Preclinical Trials: A Proof of Concept in Closed-Loop Control of Type 1 Diabetes," *Journal of Diabetes Science and Technology*, vol. 3, no. 1, pp. 44–55, 2009.

[75] ——, "In Silico Model and Computer Simulation Environment Approximating the Human Glucose/Insulin Utilization," *Food and Drug Administration Master File MAF 1521*, 2008.

[76] M. Fisher, "A Semiclosed-Loop Algorithm for the Control of Blood Glucose Levels in Diabetics," *IEEE Transations on Biomedical Engineering*, vol. 38, pp. 57–61, 1991.

[77] G. Steil, K. Darwin, F. Hariri, and M. Saad, "Feasibility of Automating Insulin Delivery for the Treatment of Type 1 Diabetes," *Diabetes*, vol. 55, no. 12, pp. 3344–50, 2006.

[78] B. Grosman, E. Dassau, H. Zisser, L. Jovanovič, and F. Doyle III, "Zone Model Predictive Control: A Strategy to Minimize Hyper- and Hypoglycemic Events," *Journal of Diabetes Science and Technology*, vol. 4, no. 4, pp. 961–75, 2010.

[79] M. Breton, A. Farret, D. Bruttomesso, S. Anderson, L. Magni, S. Patek, C. Dalla Man, J. Place, S. Demartini, S. Del Favero, C. Toffanin, C. Hughes-Karvetski, E. Dassau, H. Zisser, F. Doyle III, G. De Nicolao, A. Avogaro, C. Cobelli, E. Renard, and B. Kovatchev on behalf of The International Artificial Pancreas Study Group, "Fully Integrated Artificial Pancreas in Type 1 Diabetes: Modular Closed-Loop Glucose Control Maintains Near Normoglycemia," *Diabetes*, vol. 61, no. 9, pp. 2230–37, 2012.

[80] B. Kovatchev, C. Cobelli, E. Renard, S. Anderson, M. Breton, S. Patek, W. Clarke, D. Bruttomesso, A. Maran, S. Costa, A. Avogaro, C. Dalla Man, A. Facchinetti, L. Magni, G. De Nicolao, J. Place, and A. Farret, "Multinational Study of Subcutaneous Model-Predictive Closed-Loop Control in Type 1 Diabetes Mellitus: Summary of the Results," *Journal of Diabetes Science and Technology*, vol. 4, no. 6, pp. 1374–81, 2010.

[81] C. Hughes, S. Patek, M. Breton, and B. Kovatchev, "Anticipating the Next Meal Using Meal Behavioral Profiles: A Hybrid Model-Based Stochastic Predictive Control Algorithm for T1DM," *Computer Methods and Programs in Biomedicine*, vol. 102, no. 2, pp. 138–48, 2011.

[82] K. Zarkogianni, A. Vazeou, S. Mougiakakou, A. Prountzou, and K. Nikita, "An Insulin Infusion Advisory System Based on Autotuning Nonlinear Model-Predictive Control," *IEEE Transactions on Biomedical Engineering*, vol. 58, no. 9, pp. 2467–77, 2011.

[83] K. Turksoy, E. Bayrak, L. Quinn, E. Littlejohn, and A. Cinar, "Multivariable Adaptive Closed-Loop Control of an Artificial Pancreas without Meal and Activity Announcement," *Diabetes Technology & Therapeutics*, vol. 15, no. 5, pp. 386–400, 2013.

[84] R. Sánchez-Peña, A. Ghersin, and F. Bianchi, "Time Varying Procedures for Diabetes Type I Control," *Journal of Electrical and Computer Engineering*, 2011, special Issue Electrical and Computer Technology for Effective Diabetes Management and Treatment.

[85] P. Colmegna and R. Sánchez-Peña, "Analysis of Three T1DM Simulation Models for Evaluating Robust Closed-Loop Controllers," *Computer Methods and Programs in Biomedicine*, vol. 113, no. 1, pp. 371–82, 2014.

[86] E. Ruiz-Velázquez, R. Femat, and D. Campos-Delgado, "Blood Blucose Control for Type I Diabetes Mellitus: A Robust Tracking $\mathcal{H}_\infty$ Problem," *Control Engineering Practice*, vol. 12, pp. 1179–95, 2004.

[87] R. Parker, F. Doyle III, J. Ward, and N. Peppas, "Robust $\mathcal{H}_\infty$ Glucose Control in Diabetes Using a Physiological Model," *A.I.Ch.E. Journal*, vol. 46, no. 12, pp. 2537–49, 2000.

[88] E. Atlas, R. Nimri, S. Miller, E. Grunberg, and M. Phillip, "MD-Logic Artificial Pancreas System. A Pilot Study in Adults with Type 1 Diabetes," *Diabetes Care*, vol. 33, no. 5, pp. 1072–76, 2010.

[89] R. Nimri, E. Atlas, M. Ajzensztejn, S. Miller, T. Oron, and M. Phillip, "Feasibility Study of Automated Overnight Closed-loop Glucose Control Under MD-Logic Artificial Pancreas in Patients with Type 1 Diabetes: The DREAM Project," *Diabetes Technology & Therapeutics*, vol. 14, no. 8, pp. 728–35, 2012.

[90] F. El-Khatib, J. Jiang, and E. Damiano, "A Feasibility Study of Bihormonal Closed-loop Blood Glucose Control Using Dual Subcutaneous Infusion of Insulin and Glucagon in Ambulatory Diabetic Swine," *Journal of Diabetes Science and Technology*, vol. 3, no. 4, pp. 789–803, 2009.

[91] F. El-Khatib, S. Russell, D. Nathan, R. Sutherlin, and E. Damiano, "A Bihormonal Closed-loop Artificial Pancreas for Type 1 Diabetes," *Science Translational Medicine*, vol. 2, no. 27, pp. 1–12, 2010.

[92] S. Russell, F. El-Khatib, D. Nathan, K. Magyar, J. Jiang, and E. Damiano, "Blood Glucose Control in Type 1 Diabetes with a Bihormonal Bionic Endocrine Pancreas," *Diabetes Care*, vol. 35, no. 11, pp. 2148–55, 2012.

[93] S. Weinzimer, J. Sherr, E. Cengiz, G. Kim, J. Ruiz, L. Carria, G. Voskanyan, A. Roy, and W. Tamborlane, "Effect of Pramlintide on Prandial Glycemic Excursions During Closed-Loop Control in Adolescents and Young Adults with Type 1 Diabetes," *Diabetes Care*, vol. 35, no. 10, pp. 1994–9, 2012.

[94] R. Sánchez-Peña and A. Ghersin, "LPV Control of Glucose for Diabetes Type I," in *Proceedings 32nd Annual International Conference*, IEEE EMBS, Ed., Buenos Aires, Argentina, 2010, pp. 680–83.

[95] E. Lehmann and T. Deutsch, "A Physiological Model of Glucose-Insulin Interaction in Type 1 Diabetes Mellitus," *Journal of Biomedical Engineering*, vol. 14, no. 3, pp. 235–42, 1992.

[96] P. Colmegna and R. Sánchez-Peña, "Insulin Dependent Diabetes Mellitus Control," *Latin American Applied Research*, vol. 43, no. 3, pp. 243–48, 2013.

[97] L. Kovács, B. Benyó, J. Bokor, and Z. Benyó, "Induced $\mathcal{L}_2$-norm Minimization of Glucose-Insulin System for Type I Diabetic Patients," *Computer Methods and Programs in Biomedicine*, vol. 102, pp. 105–18, 2011.

[98] L. Kovács and B. Kulcsár, "LPV Modeling of Type I Diabetes Mellitus," in *8th International Symposium of Hungarian Researchers*, 2007, pp. 163–73.

[99] L. Kovács, B. Kulcsár, J. Bokor, and Z. Benyó, "Model-Based Nonlinear Optimal Blood Glucose Control of Type I Diabetes Patients," in *30th Annual International IEEE EMBS Conference*, Vancouver, Canada, 2008, pp. 1607–10.

[100] M. Chamberlain and L. Stimmer, "The Renal Handling of Insulin," *J. Clin. Invest.*, vol. 46, no. 6, pp. 911–19, 1967.

[101] A. Haidar, L. Legault, M. Dallaire, A. Alkhateeb, A. Coriati, V. Messier, P. Cheng, M. Millette, B. Boulet, and R. Rabasa-Lhoret, "Glucose-Responsive Insulin and Glucagon Delivery (Dual-hormone Artificial Pancreas) in Adults with Type 1 Diabetes: A Randomized Crossover Controlled Trial," *Canadian Medical Association Journal*, vol. 185, no. 4, pp. 297–305, 2013.

[102] S. Steiner, M. Li, and R. Pohl, "Stabilized Glucagon Formulation for Bihormonal Pump Use," *Journal of Diabetes Science and Technology*, vol. 4, no. 6, pp. 1332–7, 2010.

[103] M. Jackson, N. Caputo, J. Castle, L. David, C. Roberts Jr, and W. Ward, "Stable Liquid Glucagon Formulations for Rescue Treatment and Bihormonal Closed-Loop Pancreas," *Current Diabetes Reports*, vol. 12, no. 6, pp. 705–10, 2012.

[104] R. Hovorka, F. Shojaee-Moradie, P. Carroll, L. Chassin, I. Gowrie, N. Jackson, R. Tudor, A. Umpleby, and R. Jones, "Partitioning Glucose Distribution/Transport, Disposal, and Endogenous Production During IVGTT," *Am. J. Physiology: Endocrinology Metabolism*, vol. 282, pp. 992–1007, 2002.

[105] R. Hovorka, V. Canonico, I. Chassin, U. Haueter, M. Massi-Benedetti, M. Federici, T. Pieber, H. Schaller, L. Schaupp, T. Vering, and M. Wilinska, "Nonlinear Model Predictive Control of Glucose Concentration in Subjects with Type 1 Diabetes," *Physiology Measurement*, vol. 25, no. 4, pp. 905–20, 2004.

[106] A. Revert, F. Garelli, J. Pico, H. De Battista, P. Rossetti, J. Vehí, and J. Bondía, "Safety Auxiliary Feedback Element for the Artificial Pancreas in Type 1 Diabetes," *IEEE Transactions on Biomedical Engineering*, vol. 60, no. 8, pp. 2113–22, 2013.

[107] P. Dua, F. Doyle III, and E. Pistikopoulos, "Model-Based Blood Glucose Control for Type 1 Diabetes via Parametric Programming," *IEEE Transactions on Biomedical Engineering*, vol. 53, no. 8, pp. 1478–91, 2006.

[108] S. Patek, B. Bequette, M. Breton, B. Buckingham, E. Dassau, F. Doyle III, J. Lum, L. Magni, and H. Zisser, "In Silico Preclinical Trials: Methodology and Engineering Guide to Closed-Loop Control in Type 1 Diabetes Mellitus," *Journal of Diabetes Science and Technology*, vol. 3, no. 2, pp. 269–82, 2009.

[109] L. Magni, D. Raimondo, C. Dalla Man, M. Breton, S. Patek, G. De Nicolao, C. Cobelli, and B. Kovatchev, "Evaluating the Efficacy of Closed-Loop Glucose Regulation via Control-Variability Grid Analysis," *Journal of Diabetes Science and Technology*, vol. 2, no. 4, pp. 630–5, 2008.

[110] G. Campetelli, M. Lombarte, M. Basualdo, and A. Rigalli, "Extended Adaptive Predictive Controller with Robust Filter to Enhance Blood Glucose Regulation in Type I Diabetic Subjects," *Computers & Chemical Engineering*, vol. 59, pp. 243–51, 2013.

[111] K. Zhou, J. Doyle, and K. Glover, *Robust and Optimal Control.* Prentice–Hall, 1996.

[112] R. Sánchez-Peña and M. Sznaier, *Robust Systems Theory and Applications.* John Wiley & Sons, Inc., 1998.

[113] M. Safonov, D. Limebeer, and R. Chiang, "Simplifying the $\mathcal{H}_\infty$ Theory via Loop Shifting, Matrix Pencil and Descriptor Concepts," *IJC*, vol. 50, no. 6, pp. 2467–88, 1989.

[114] P. Gahinet and P. Apkarian, "An LMI Approach to $\mathcal{H}_\infty$ Control," *International Journal of Robust and Nonlinear control*, vol. 4, no. 8, pp. 421–48, 1994.

[115] S. Patek, B. Bequette, M. Breton, B. Buckingham, E. Dassau, F. Doyle III, J. Lum, L. Magni, and H. Zisser, "In Silico Preclinical Trials: Methodology and Engineering Guide to Closed-Loop Control in Type 1 Diabetes Mellitus," *Journal of Diabetes Science and Technology*, vol. 3, no. 2, pp. 269–82, 2009.

[116] P. Colmegna and R. Sánchez-Peña, "Personalized Glucose Control Based on Patient Identification," in *Actas Reuniones de Procesamiento de la Información y Control*, Bariloche, Argentina, 2013, pp. 397–402.

[117] A. Laguna Sanz, "Uncertainty in Postprandial Model Identification in Type 1 Diabetes," Ph.D. dissertation, Universitat Politècnica de València, 2014.

[118] C. Ellingsen, E. Dassau, H. Zisser, B. Grosman, M. Percival, L. Jovanovič, and F. Doyle III, "Safety Constraints in an Artificial Pancreatic β Cell: An Implementation of Model Predictive Control with Insulin on Board," *Journal of Diabetes Science and Technology*, vol. 3, no. 3, pp. 536–44, 2009.

[119] H. Lee, B. Buckingham, D. Wilson, and B. Bequette, "A Closed-Loop Artificial Pancreas Using Model Predictive Control and a Sliding Meal Size Estimator," *Journal of Diabetes Science and Technology*, vol. 3, no. 5, pp. 1082–90, 2009.

[120] B. Kovatchev, S. Patek, E. Dassau, F. Doyle III, L. Magni, G. De Nicolao, and C. Cobelli, "Control to Range for Diabetes: Functionality and Modular Architecture," *Journal of Diabetes Science and Technology*, vol. 3, no. 5, pp. 1058–65, 2009.

[121] G. Steil, C. Palerm, N. Kurtz, G. Voskanyan, A. Roy, S. Paz, and F. Kandeel, "The Effect of Insulin Feedback on Closed-Loop Glucose Control," *The Journal of Clinical Endocrinology & Metabolism*, vol. 96, no. 5, pp. 1402–08, 2011.

[122] P. Herrero, P. Georgiou, N. Oliver, D. Johnston, and C. Toumazou, "A Bio-Inspired Glucose Controller Based on Pancreatic β-Cell Physiology," *Journal of Diabetes Science and Technology*, vol. 6, no. 3, pp. 606–16, 2012.

[123] R. Sánchez-Peña and F. Bianchi, "Model Selection: From LTI to Switched-LPV," in *American Control Conference*, Montreal, Canada, 2012, pp. 1561–66.

[124] K. van Heusden, E. Dassau, H. Zisser, D. Seborg, and F. Doyle III, "Control-Relevant Models for Glucose Control Using A Priori Patient Characteristics," *IEEE Transactions on Biomedical Engineering*, vol. 59, pp. 1839–49, 2012.

[125] P. Van Overschee and B. de Moor, "N4SID: Subspace Algorithms for the Identification of Combined Deterministic and Stochastic Systems," *Automatica*, vol. 30, no. 1, pp. 75–93, 1994.

[126] M. Cescon, F. Ståhl, M. Landin-Olsson, and R. Johansson, "Subspace-Based Model Identification of Diabetic Blood Glucose Dynamics," *15th IFAC Symposium on System Identification*, vol. 15, no. 1, pp. 233–8, 2009.

[127] J.Walsh and R. Roberts, *Pumping Insulin.* Torrey Pines Press, San Diego, CA, 2006.

[128] E. Dassau, F. Cameron, H. Lee, B. Bequette, H. Zisser, L. Jovanovič, H. Chase, D. Wilson, B. Buckingham, and F. Doyle III, "Real-Time Hypoglycemia Prediction Suite Using Continuous Glucose Monitoring," *Diabetes Care*, vol. 33, no. 6, pp. 1249–54, 2010.

[129] P. Colmegna, R. Sánchez-Peña, R. Gondhalekar, E. Dassau and F. J. Doyle III, "Reducing Risks in Type 1 Diabetes Using $\mathcal{H}_\infty$ Control," *IEEE Transactions on Biomedical Engineering*, vol. 61, no. 12, pp. 2939–47, 2014.

[130] P. Colmegna and R. Sánchez-Peña, "Linear Parameter-Varying Control to Minimize Risks in Type 1 Diabetes," in *Proc. 19th IFAC World Congress*, Cape Town, South Africa, 2014, pp. 9253–7.

[131] R. Gondhalekar, E. Dassau and F. Doyle III, "MPC Design for Rapid Pump-Attenuation and Expedited Hyperglycemia Response to Treat T1DM With an Artificial Pancreas," in *AACC American Control Conference*, Portland, OR, USA, 2014, pp. 4224–30.

[132] E. Dassau, B. Bequette, B. Buckingham and F. Doyle III, "Detection of a Meal Using Continuous Glucose Monitoring: Implications For An Artificial β-cell," *Diabetes Care*, vol. 31, no. 2, pp. 295–300, 2008.

[133] R. Harvey, E. Dassau, H. Zisser, D. Seborg and F. Doyle III, "Design of the Glucose Rate Increase Detector: A Meal Detection Module for the Health Monitoring System," *Journal of Diabetes Science and Technology*, vol. 8, no. 2, pp. 307–20, 2014.

[134] B. Kovatchev, M. Breton, C. Dalla Man and C. Cobelli, "*In Silico* Preclinical Trials: A Proof of Concept in Closed-Loop Control of Type 1 Diabetes," *Journal of Diabetes Science and Technology*, vol. 3, no. 1, pp. 44–55, 2009.

[135] A. Ghersin and R. Sánchez-Peña, "LPV control of a 6 DOF vehicle," *IEEE Transactions on Control Systems Technology*, 2002.

[136] ——, "Transient Shaping of LPV Systems," in *European Control Conference (Invited paper)*, Porto, Portugal, 2001, pp. 3080–5.

[137] R. Tóth, *Modeling and Identification of Linear Parameter-Varying Systems*, ser. Lecture Notes in Control and Information Sciences. Springer-Verlag, 2010, vol. 403.

[138] D. Liberzon, *Switching in Systems and Control*. Boston, MA: Birkhauser, 2003.

[139] G. Becker and A. Packard, "Robust Performance of LPV Systems Using Parametrically-Dependent Linear Feedback," *Systems and Control Letters*, vol. 23, pp. 205–15, 1994.

[140] L. DeJournett, "Essential Elements of the Native Glucoregulatory System, Which, If Appreciated, May Help Improve the Function of Glucose Controllers in the Intensive Care Unit Setting," *Journal of Diabetes Science and Technology*, vol. 4, no. 1, pp. 190–8, 2010.

[141] A. Savitzky and M. Golay, "Smoothing and Differentiation of Data by Simplified Least Squares Procedures," *Analytical Chemistry*, vol. 36, no. 8, pp. 1627–39, 1964.

[142] L. Magni, D. Raimondo, C. Dalla Man, M. Breton, S. Patek, G. De Nicolao, C. Cobelli and B. Kovatchev, "Evaluating the Efficacy of Closed-Loop Glucose Regulation via Control-Variability Grid Analysis," *Journal of Diabetes Science and Technology*, vol. 2, no. 4, pp. 630–5, 2008.

[143] M. Green and D. Limebeer, *Linear Robust Control*. Prentice-Hall, Englewood Cliffs, NJ, 1995.